



**HAL**  
open science

## Environmental forcing by submarine canyons: Evidence between two closely situated cold-water coral mounds (Porcupine Bank Canyon and Western Porcupine Bank, NE Atlantic)

Luke O'Reilly, Robin Fentimen, Felix Butschek, Jürgen Titschack, Aaron Lim, Niamh Moore, O J O'Connor, John Appah, Kimberley Harris, Torsten Vennemann, et al.

### ► To cite this version:

Luke O'Reilly, Robin Fentimen, Felix Butschek, Jürgen Titschack, Aaron Lim, et al.. Environmental forcing by submarine canyons: Evidence between two closely situated cold-water coral mounds (Porcupine Bank Canyon and Western Porcupine Bank, NE Atlantic). *Marine Geology*, 2022, 454, pp.106930. 10.1016/j.margeo.2022.106930 . hal-04278613

**HAL Id: hal-04278613**

**<https://univ-angers.hal.science/hal-04278613>**

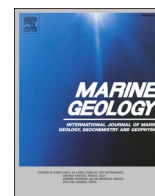
Submitted on 10 Nov 2023

**HAL** is a multi-disciplinary open access archive for the deposit and dissemination of scientific research documents, whether they are published or not. The documents may come from teaching and research institutions in France or abroad, or from public or private research centers.

L'archive ouverte pluridisciplinaire **HAL**, est destinée au dépôt et à la diffusion de documents scientifiques de niveau recherche, publiés ou non, émanant des établissements d'enseignement et de recherche français ou étrangers, des laboratoires publics ou privés.



Distributed under a Creative Commons Attribution 4.0 International License



## Environmental forcing by submarine canyons: Evidence between two closely situated cold-water coral mounds (Porcupine Bank Canyon and Western Porcupine Bank, NE Atlantic)

Luke O'Reilly<sup>a,b,\*</sup>, Robin Fentimen<sup>c</sup>, Felix Butschek<sup>a</sup>, Jürgen Titschack<sup>d,e</sup>, Aaron Lim<sup>f</sup>, Niamh Moore<sup>g,h</sup>, O.J. O'Connor<sup>g,h</sup>, John Appah<sup>a</sup>, Kimberley Harris<sup>i</sup>, Torsten Vennemann<sup>j</sup>, Andrew J. Wheeler<sup>a,k</sup>

<sup>a</sup> School of Biological, Earth & Environmental Sciences / Environmental Research Institute, Distillery Fields, North Mall Campus, University College Cork (UCC), Ireland

<sup>b</sup> Green Rebel, Crosshaven Boatyard, Crosshaven, Co. Cork, Ireland

<sup>c</sup> ENS Lyon, Dept of Earth Sciences, Ecole Normale Supérieure de Lyon, 46 allée d'Italie, 69364 Lyon cedex 07, France

<sup>d</sup> MARUM – Center for Marine Environmental Sciences, University of Bremen, Bremen, Germany

<sup>e</sup> Senckenberg am Meer, Marine Research Department, Wilhelmshaven, Germany

<sup>f</sup> Department of Geography, University College Cork

<sup>g</sup> Department of Radiology, Cork University Hospital (CUH), Wilton, Cork, Ireland

<sup>h</sup> Department of Radiology, University College Cork

<sup>i</sup> DP Energy Ireland Ltd, Mill House, Buttevant, P51 TN35, Co. Cork, Ireland

<sup>j</sup> IDYST – Institute of Earth Surface Dynamics, University of Lausanne, Switzerland

<sup>k</sup> Irish Centre for Research in Applied Geosciences - iCRAG / SFI Research Centre for Energy, Climate and Marine - MaREI, University College Cork, Ireland

### ARTICLE INFO

Editor: Michele Rebesco

#### Keywords:

Cold-water corals  
Benthic foraminifera assemblages  
Holocene  
NE Atlantic  
submarine canyon.

### ABSTRACT

Within the Porcupine Bank Canyon (NE Atlantic), cold-water coral (CWC) mounds are mostly found clustered along the canyon lip, with individual disconnected mounds occurring nearby on the western Porcupine Bank. Remotely operated vehicle-mounted vibrocoreing was utilized to acquire cores from both of these sites. This study is the first to employ this novel method when aiming to precisely sample two closely situated areas. Radiometric ages constrain the records from the early to mid-Holocene (9.1 to 5.6 ka BP). The cores were then subjected to 3D segmented computer tomography to capture mound formation stages. The cores were then further examined using stable isotopes and benthic foraminiferal assemblages, to constrain the paleoenvironmental variation that influenced CWC mound formation of each site. In total, mound aggradation rate in the Porcupine Bank Canyon and western Porcupine Bank was comparable to other Holocene CWC mounds situated off western Ireland. Results derived from multiproxy analysis, show that regional climatic shifts define the environmental conditions that allow positive coral mound formation. In addition, the aggradation rate of coral mounds is higher adjacent to the Porcupine Bank Canyon than on the western Porcupine Bank. Benthic foraminifera assemblages and planktic foraminiferal  $\delta^{13}\text{C}$  reveal that higher quality organic matter is more readily available closer to the canyon lip. As such, we hypothesize that coral mound formation in the region is likely controlled by an interplay between enhanced shelf currents and the existence of the Eastern North Atlantic Water-Mediterranean Outflow Water-Transition Zone. The geomorphology of the canyon promotes upwelling of these water masses that are enriched in particles, including food and sediment supply. The higher availability of these particles support the development and succession of ecological hotspots along the canyon lip and adjacent areas of the seafloor. These observations provide a glimpse into the role that submarine canyons play in influencing macro and micro benthic fauna distributions and highlights the importance of their conservation.

\* Corresponding author at: School of Biological, Earth & Environmental Sciences / Environmental Research Institute, Distillery Fields, North Mall Campus, University College Cork (UCC), Ireland.

E-mail address: [luke.oreilly@greenrebel.ie](mailto:luke.oreilly@greenrebel.ie) (L. O'Reilly).

<https://doi.org/10.1016/j.margeo.2022.106930>

Received 4 April 2022; Received in revised form 9 October 2022; Accepted 11 October 2022

Available online 29 October 2022

0025-3227/© 2022 The Authors. Published by Elsevier B.V. This is an open access article under the CC BY license (<http://creativecommons.org/licenses/by/4.0/>).

## 1. Introduction

Cold-water corals (CWCs) are widespread across the NE Atlantic and occupy a range of geomorphological settings, including open slope continental margins (Roberts et al., 2009; Hebbeln and Samankassou, 2015; Davies et al., 2017; Van Den Beld et al., 2017), seamounts (Roberts et al., 2008; Sakai et al., 2009; Wienberg et al., 2013; Davies et al., 2015), fjords (Roberts et al., 2009; Titschack et al., 2015) and submarine canyons (Huvenne et al., 2011; Davies et al., 2014; Stewart et al., 2014; Van Den Beld et al., 2017; Lim et al., 2018). Through geological time, they can grow to form mounds several kilometres across and exceeding 300 m in height (De Mol et al., 2002; Kenyon et al., 2003; Huvenne et al., 2005; Mienis et al., 2006; Wheeler et al., 2007). These mounds are composed mainly of the framework-building scleractinian corals *Demophyllum pertusum* (formerly named *Lophelia pertusa*; see Addamo et al., 2016) and *Madrepora oculata*. Coral mound development relies on the interplay between CWC growth and sediment input. The capacity of coral framework to baffle suspended sediment is an essential component of successful mound aggradation, whereby current-suspended sediments become entrapped, stabilizing the biogenic construction (Huvenne et al., 2009; Thierens et al., 2013; Titschack et al., 2015; Titschack et al., 2016). The accumulation and preservation of CWC framework and associated hemipelagic sediments can provide useful paleo-archives to monitor environmental change, especially in areas where stratigraphic records are lacking due to periods of non-deposition or prolonged erosion (Titschack et al., 2009; Frank et al., 2011; Thierens et al., 2013; Hebbeln et al., 2016). In intermediate water depths settings, CWC mounds offer insights into water mass characteristics (Fink et al., 2012; López Correa et al., 2012; Thierens et al., 2013; Stalder et al., 2014; Hebbeln et al., 2016; Fentimen et al., 2020b). However, CWCs mound formation is commonly discontinuous due to the absence of CWCs during periods of climatically unfavourable environmental conditions (Dorschel et al., 2005; Kano et al., 2007; Frank et al., 2009; Thierens et al., 2013; Stalder et al., 2018). As such, CWC mounds provide detailed records across restricted periods.

Submarine canyons are steep-sided valleys that incise continental margins (Shepard, 1981; Pratson et al., 2009; Amblas et al., 2018). Both topography and physical environment control the flow of water masses through these settings (Hall et al., 2014; Kämpf, 2018), which differs from the continental slope (Genin et al., 1986; Davies et al., 2008). High structural complexity and steep topographies elevate current velocities (Genin et al., 1986), creating stronger internal waves than along the surrounding slopes barren of canyons (Quaresma et al., 2007). These characteristics can drive turbulent mixing (Hall et al., 2014; Wilson et al., 2015; Aslam et al., 2018). Subsequently, this can provide a mechanism for shelf-slope particulate matter exchange (Quaresma et al., 2007; Arzola et al., 2008; García et al., 2008; Allen and Madron, 2009; Huvenne and Davies, 2014; Puig et al., 2014; Amaro et al., 2016; Fernandez-Arcaya et al., 2017; Saldías and Allen, 2020). Increased particulate organic matter (POM) concentrations and the formation of nepheloid layers are associated with this internal wave-driven turbulent mixing (Wilson et al., 2015; Hall et al., 2017; Aslam et al., 2018). These phenomena can generate environmental heterogeneity within canyons, and under certain circumstances, provide an ideal setting for enhanced biological diversity (Levin et al., 2001; De Leo et al., 2010; Levin et al., 2010; Schlacher et al., 2010), leading to deep-sea biodiversity hotspots (De Leo et al., 2010). In addition, topographically driven upwelling and downwelling (i.e. Allen and Madron, 2009) play a key role in enhancing shelf-slope exchanges of water masses (Connolly and Hickey, 2014). These processes are driven by surface winds and cross-shelf sea surface height gradients that cause Ekman effects (She and Klinck, 2000, Allen and Madron, 2009, Allen and Hickey, 2010). As a consequence, the cross-isobath exchange flow in a submarine canyon is stronger than that over a normal shelf-break (She and Klinck, 2000). Submarine canyons play a key role in many of the aforementioned processes, although there is still a need for a well-designed investigation of these systems, with a

focused assessment of their potential role for biodiversity.

CWCs are found within numerous submarine canyons along the NE Atlantic margin, forming isolated colonies, small patch reefs several metres across, large reef systems and living as dense accumulations on vertical walls (Roberts et al., 2006; Buhl-Mortensen et al., 2010; Morris et al., 2013; Wheeler et al., 2007; Lim et al., 2018; Corbera et al., 2019; Price et al., 2019). CWCs occupying the west Porcupine Bank (wPB) and Porcupine Bank Canyon (PBC) have recently received attention (Lim et al., 2018; Appah et al., 2020; Lim et al., 2020; de Oliveira et al., 2021; Appah et al., 2022; O'Reilly et al., 2022). Their present-day distribution is strongly influenced by POM supply, oceanographic and hydrographic processes, seabed terrain (depth and slope) and canyon morphological features (Mazzini et al., 2011; Appah et al., 2020; Lim et al., 2020). Strong currents within the PBC are further intensified locally by CWC mounds, suggesting they are critical in delivering food and nutrients to the reefs (Lim et al., 2020). Some studies also imply the dependence of CWCs on chemical nutrients (e.g., Findlay et al., 2014) and their ability to feed directly on dissolved organic carbon (e.g. Mueller et al., 2014). Despite the recent research into the spatial distribution and controls on CWC habitats within the PBC (i.e. Appah et al., 2020; Lim et al., 2020), their temporal distribution is still poorly understood. Furthermore, recent evidence suggests that submarine canyons provide a refuge for CWCs during periods of environmental stress caused by low oxygen availability during the Holocene (Wienberg et al., 2018). This highlights the need to assess CWCs in the wPB and PBC, to understand how canyon adjacent corals respond to periods of climate instability.

Benthic foraminifera can provide crucial insights into the lifecycle of CWCs (Margreth et al., 2009; Stalder et al., 2014; Spezzaferri et al., 2015; Stalder et al., 2015; Fentimen et al., 2018; Mojtahid et al., 2021). They link lower and higher levels of deep-sea food webs (Lipps and Valentine, 1970; Gooday, 1994; Gooday, 2019). Furthermore, they account for the connection between the biotic and abiotic factors that control CWC habitat distribution (i.e. nature of substrates, ecological demands, abundance of CWCs, microhabitat availability) and local physio-chemical processes (water mass properties, current speed variability, organic carbon fluxes) that influence foraminifera distributions (Margreth et al., 2009; Smeulders et al., 2014; Spezzaferri et al., 2015; Mojtahid et al., 2021). The flux of organic matter to the seafloor primarily controls the composition and diversity of benthic foraminiferal communities (e.g. De Rijk et al., 2000; Schmiel et al., 2000; Morigi et al., 2001; Fontanier et al., 2002). Regionally, assessments of recent (0–33 ka) benthic foraminiferal assemblages (BFAs) from CWCs in the Porcupine Seabight (Margreth et al., 2009; Schönfeld et al., 2011; Morigi et al., 2012; Smeulders et al., 2014; Fentimen et al., 2018; Fentimen et al., 2020b), the Rockall Bank (Morigi et al., 2012), northwest of Scotland (Mojtahid et al., 2021), offshore Norway (Mackensen et al., 1985; Cedhagen, 1994; Freiwald and Schönfeld, 1996; Spezzaferri et al., 2013; Stalder et al., 2014) and the Alboran Sea (Margreth et al., 2011; Stalder et al., 2015, 2018; Fentimen et al., 2020a) have been carried out. Of the studies that also aim to investigate CWC mound aggradation, interpretations are based on either a single core (Spezzaferri et al., 2013; Stalder et al., 2015, 2018; Fentimen et al., 2020a), or a number of cores acquired from distances located relatively far apart across the study area (Stalder et al., 2014). Furthermore, these studies typically rely on cores acquired using vessel-deployed coring instruments with little ground control on seabed conditions at great water depths. Consequently, the large distance between cores and the uncertainty of the exact core deposition might lead to uncertainties in the interpretation of coral mound development processes.

Therefore, the main aims of this study are to identify the environmental controls on CWC mound formation in the wPB and PBC using reliable sampling techniques. Computed tomography (CT) is becoming widely used in CWC mound studies, to reconstruct the three-dimensional architecture of coral bearing cores. This non-destructive method can be used to determine coral preservation patterns (CPP), that illustrate mound formation/cessation (see Titschack et al., 2015;



Wang et al., 2019). BFAs have not been used in conjunction with this advanced technology in any investigation of CWC mound history so far. Doing so can ascertain the environmental conditions that determine CPP type and thus mound development (Rüggeberg et al., 2007; Margreth et al., 2009; Margreth et al., 2011; Schönfeld et al., 2011; Fink et al., 2012; Stalder et al., 2014; Stalder et al., 2015; Fentimen et al., 2018; Fentimen et al., 2020a). Consequently, this enables a precise examination of local mound development variability. For this purpose, novel Remotely Operated Vehicle (ROV) vibrocores were collected from the mound summits of two sites of different proximity to the canyon to assess their development and environmental controls throughout the Early Holocene/mid-Holocene transition (i.e. 9.1 to 5.6 ka BP). ROV vibrocores allow to precisely identify and document coring sites, in contrast with the generally used vessel-deployed coring instruments that provide little ground control on seabed conditions at great water depths. Thus, ROV vibrocoreing is an ideal method to retrieve cores from two hard to access and closely located areas, such as the wPBC and PBC. In addition, this study builds on the findings of O'Reilly et al. (2022), where the geological history of the wPB ceases at 9.1 ka BP.

### 1.1. Regional setting

The wPB occupies the westernmost limits of the Porcupine Bank (Fig. 1a; see also 1c). Ice-rafted debris were deposited on the bank since at least 32.5 ka BP to 9.0 ka BP (O'Reilly et al., 2022), potentially providing suitable elevated substrates for CWC larvae to settle (Roberts et al., 2006). A single off-mound CWC barren vibrocore acquired from the region shows that since 9.7 ka, the study site has endured a period of non-deposition and/or erosion (O'Reilly et al., 2022). The incision of the bank by the PBC is tectonically steered through faulting (Shannon, 1991) and trends north-east to south-west (Shannon et al., 2007; Lim et al., 2020) with the addition of a smaller southern branch off the main canyon. The eastern canyon wall of the asymmetric canyon is dipping steeply (60 to 70 degrees) and is 800 m in height. At the base of this wall (>2800 m) exists the widest and deepest sinuous channels in the PBC system (Lim et al., 2020). Iceberg plough marks are visible along the upper canyon (Mazzini et al., 2011; O'Reilly et al., 2022).

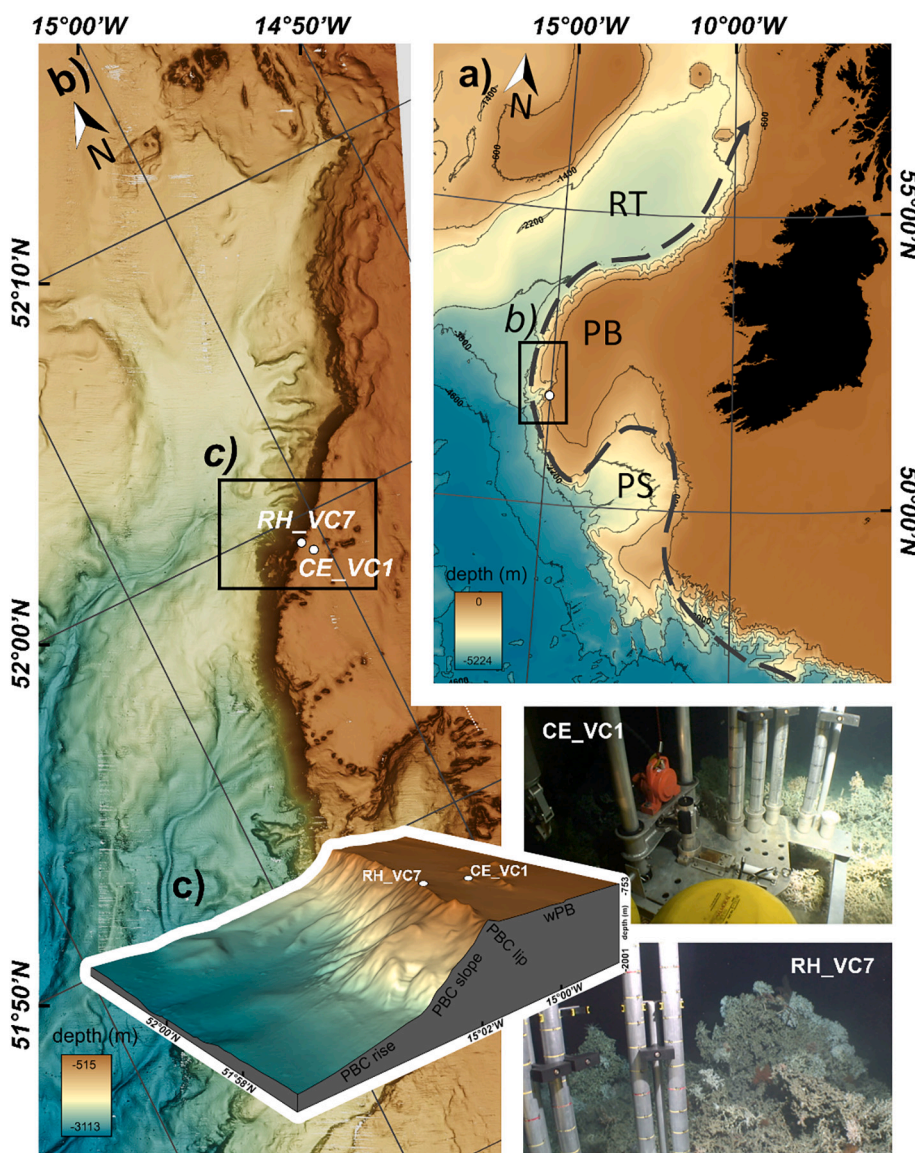


Fig. 1. (a) Location of the study site within the western Porcupine Bank (black rectangle) on the Irish continental margin (PB - Porcupine Bank, PS - Porcupine Seabight, RT - Rockall Trough) adapted from O'Reilly et al. 2022. Grey dashed line showing the flow direction of Eastern North Atlantic Water. (b) Bathymetry map of the upper Porcupine Bank Canyon modified after Lim et al. (2020). (c) Overview of coring sites used in this study. Insets on the bottom right from core site CE\_VC1 (top) and RH\_VC7 (bottom). Maps a) and b) were created using ArcGIS Desktop v10.6 ([www.arcgis.com](http://www.arcgis.com)). Map c) was created using AMIRA version 2018.36 (see Stalling et al., 2005; <http://amira.zib.de>); data sources – (a) - General Bathymetric Charts of the Oceans ([gebco.net](http://gebco.net)); (b and c) - additional bathymetry (10 m resolution) collected during CE18011 research cruise (Lim et al., 2018).



## 1.2. Hydrography

Eastern North Atlantic Water (ENAW) flows northerly at ~200–700 m water depth (White and Bowyer, 1997; Mazzini et al., 2011). This water mass forms in the Bay of Biscay and is advected northwards along the Porcupine Bank by the poleward Shelf-Edge Current (Ellett and Martin, 1973; Dickson and McCave, 1986; Pollard et al., 1996; White, 2007; Mazzini et al., 2011). The high salinity northward flowing Mediterranean Outflow Water (MOW) occurs at 800–1000 m water depth and underlays the ENAW (White, 2007; Mohn et al., 2014). The denser southerly following Labrador Sea Water occurs at 1100 m water depth (Appah et al., 2020; see also Appendix A).

Bedforms such as current-aligned scours in the lee of coral mounds reflect the long-term net effect of enhanced bottom currents shaping the seafloor (Lim et al., 2020). In situ acoustic doppler current profile measurements show that the wPB area is less hydrographically active than the area along the lip of the PBC (mean current velocity values of  $17.3 \text{ cm s}^{-1}$  and  $24 \text{ cm s}^{-1}$ , respectively; Lim et al., 2020). These measurements highlight the intensification of current speeds caused by the canyon geomorphology and local acceleration caused by mounds (Lim et al., 2020). Benthic water temperatures recorded from acoustic doppler current profile data vary minimally between the settings ( $\pm 0.4^\circ\text{C}$ ), with the wPB recording slightly warmer waters (summer mean  $-9.6^\circ\text{C}$ ; see Lim et al., 2020) than along the lip of the PBC (summer mean  $-9.2^\circ\text{C}$ ). Furthermore, the dominant current direction flowing over the wPB is orientated north-east (Lim et al., 2020) and represents the shelf-edge current (Huthnance, 1995) that transports the ENAW poleward (White, 2007). In contrast, the lip of the PBC is characterised by westerly current directions (Lim et al., 2020), likely as a result of exchange between open slope and canyon waters.

## 1.3. CWC distribution

Initial reports of the distribution of CWCs in the PBC are described by Mazzini et al. (2011). They observed that parallel to the lip (or the ridge between the wPB and PBC slope), steep-sided CWC mounds exist. On the eastern part of this canyon, mounds on the lip range from 30 to 50 m in height and extend for approximately 30 km (Lim et al., 2020). On the wPB, slightly larger (70 m in height) disconnected coral mounds are visible and follow a north-east to south-west distribution. More recently, Lim et al. (2020) identified the environmental window of CWC growth in the region. They found that current speeds determine living and dead (i.e. rubble) distributions, whereby slower current speeds (average  $25.4$  and  $9.4 \text{ cm s}^{-1}$ ) favour living corals and higher dead coral ratios are concurrent with elevated average current speeds ( $31.3 \text{ cm s}^{-1}$ ) which are subjected to periodic intensified pulses (max  $114 \text{ cm s}^{-1}$ ). High concentrations of resuspended POM ( $1330\text{--}3965 \mu\text{g l}^{-1}$ ) are recorded in the study area (Appah et al., 2020), representing an abundant food source for benthic communities. Phosphate rich authigenic deposits also indicate high biological productivity (Mazzini et al., 2011).

## 2. Methods

### 2.1. Vibrocoring

Cores (Table 1) were acquired using the Holland I ROV equipped

with a vibrocore rig from the PBC onboard the ILV Granuaile during the CoCoHaCa research cruise (cruise number RH17002; see Wheeler et al., 2017) for core RH17002\_VC7 (hereby shortened to RH\_VC7) and onboard the RV Celtic Explorer during the CoCoHaCa II research cruise (cruise number CE18011; see Lim et al., 2018) for core CE18011\_VC1 (hereby shortened to CE\_VC1). The novel use of the ROV granted the acquisition of precise samples from summits of coral mounds in the wPB and PBC with direct ground-truthing by live video footage following ROV video surveys (Wheeler et al., 2014; Wheeler et al., 2015; Wheeler et al., 2016, 2017; Lim et al., 2018) (see Fig. 1 inset). Cores acquired were 75 mm in diameter and were stored vertically at  $4^\circ\text{C}$  to minimize sediment deformation. Cores RH17002\_VC7 and CE18011\_VC1 were recovered with lengths of 81 and 130 cm, respectively (Table 1).

### 2.2. Core analysis

Non-destructive and destructive multiproxy analytical methods were performed on the CWC-bearing cores to assess relevant paleoenvironmental conditions.

#### 2.2.1. Computer tomography

All computed tomography images were acquired using the 64 section multi-slice scanner GE Healthcare Discovery CT 750 HD at Cork University Hospital, Cork, Ireland. A detailed overview of the methods applied in this study can be found in O'Reilly et al. (2022).

Core descriptions of coral-bearing cores are based on analysis of CT scan data (see Appendix B for detailed processing procedures). CWC preservation patterns were defined by quantifying macrofossil clast size and orientation following classification standards introduced by Titschack et al. (2015) and further defined by Wang et al. (2019). Three CPPs (A to C) were identified. CPP A represents coral framework in a living position, characterised by large  $> -4.7\Phi$  ( $>2.6 \text{ cm}$ ) average coral clast and variable orientations of up to  $90^\circ$ . CCP B represents a slightly collapsed coral framework, characterised by moderate clast sizes of  $-4.7$  to  $-4.4\Phi$  ( $\sim 2.6\text{--}2.1 \text{ cm}$ ) and orientations  $<60^\circ$ . CCP C represents coral rubble, characterised by small average clast sizes smaller than  $-4.4\Phi$  ( $\sim 2.1 \text{ cm}$ ) and orientations of  $<45^\circ$  or no obvious orientation. Facies classification and coral content cores CE\_VC1 and RH\_VC7 can be found in Fig. 2.

Variations to the aggradation rate (AR) and preservation state of CWC clasts can reflect fluctuations in environmental conditions (Titschack et al., 2015; Titschack et al., 2016; Wang et al., 2019). High AR is a function of rapid CWC growth and enhanced sediment supply that becomes entrapped in the framework. Coral framework produces low energy micro-environments in areas of relatively higher hydrodynamics (Wang et al., 2021). This rapid burial prevents CWC clasts from biodegradation and physical fragmentation, thus capturing corals in the living position (Titschack et al., 2015). In comparison, in periods of reduced CWC growth, or where dead coral framework remains exposed for a prolonged time, degradation and fragmentation of the coral skeleton may occur, leading to the formation of coral rubble. Using assigned CPP in combination with mound AR can give valuable insights into the temporal development of coral mounds (Titschack et al., 2015; Titschack et al., 2016; Wang et al., 2019).

**Table 1**

Summary of vibrocores collected from the west Porcupine Bank (wPB) and Porcupine Bank Canyon (PBC) during the CoCoHaCa I (RH17002) and CoCoHaCa II (CE18011) research cruises.

| Core ID | Acquisition Date | Geographical Setting | Latitude [DD] | Longitude [DD] | Water Depth [m] | Length [cm] |
|---------|------------------|----------------------|---------------|----------------|-----------------|-------------|
| CE_VC1  | 05.05.2018       | wPB CWC mound summit | 51.9829       | -14.9995       | 660             | 130         |
| RH_VC7  | 21.06.2017       | PBC CWC mound summit | 51.9892       | -15.0129       | 651             | 81          |

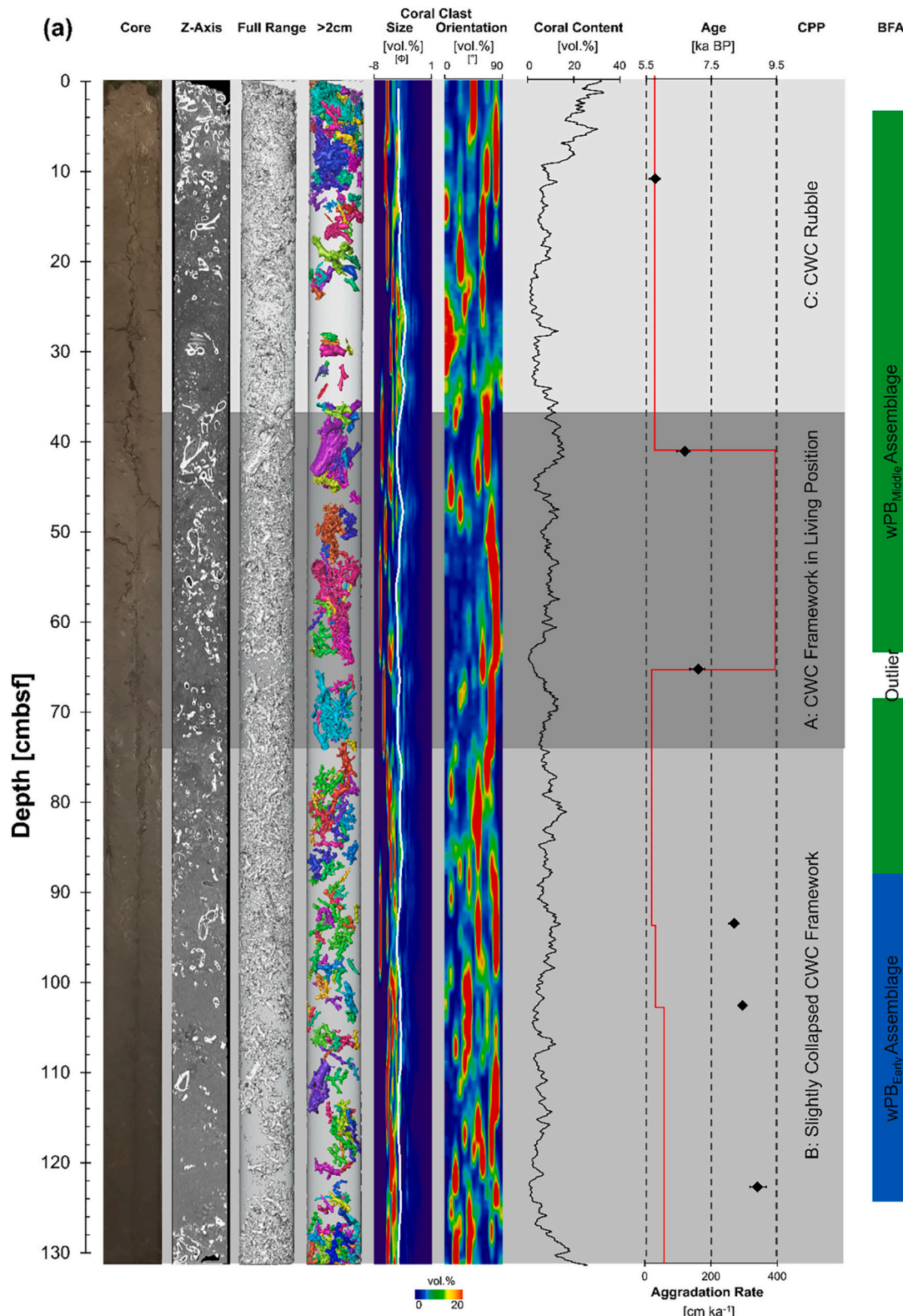


**Fig. 2.** Logs of cores CE\_VC1 from the wPB (a) and RH\_VC7 from the PBC (b). From left to right: True colour image of the core; orthogonal CT-image of core, with darkness a function of x-ray attenuation, a proxy for density; core CT 3D image of coral clasts in full-size range; coral clasts larger than >2 cm; coral clast size distribution where the white line indicates mean clast size (blue to red colour map denotes % volume of clasts on a scale of 0–20); coral clast orientation quantified coral content based on the CT data; coral content (black); <sup>14</sup>C ages were calibrated using IntCal20 (Reimer et al., 2020) with PaleoDataView (Langner and Mulitza, 2019) and determined with Bayesian statistics using the R-package BACON (Blaauw and Christen, 2011). Ages plotted as kilo-annum before present (ka BP) with 2σ calibrated age range (see Table 2) and calculated aggradation rates; cold-water coral preservation patterns CPPs; A-C; and benthic foraminifera assemblages (BFA). (For interpretation of the references to colour in this figure legend, the reader is referred to the web version of this article.)

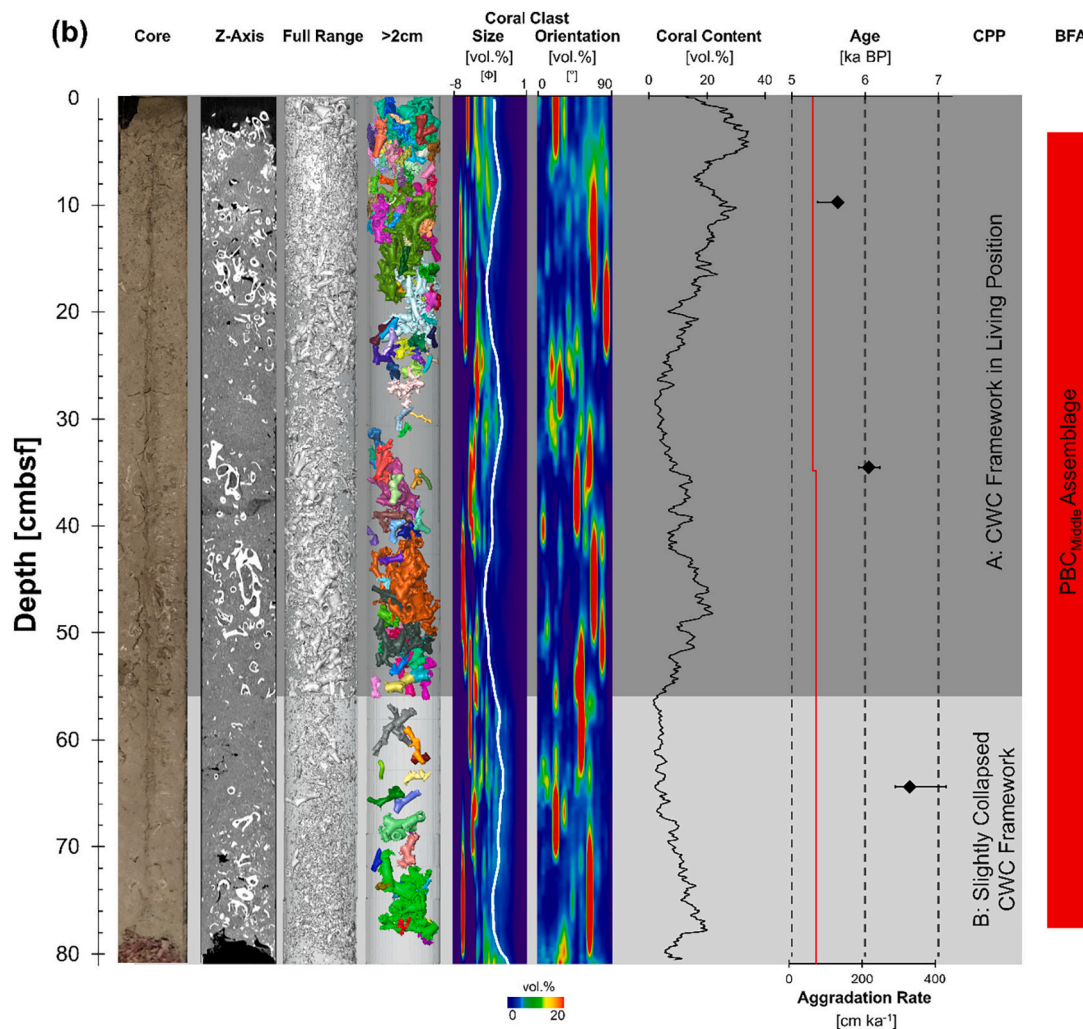


Fig. 2. (continued).

Table 2

AMS <sup>14</sup>C ages obtained from benthic and planktic foraminifera and CWC fragments collected from cores RH17002\_VC7 and CE18011\_VC1. Reservoir (res.) ages and error, calibrated (cal.) age determined from Paleo Data View (Langner and Mulitza, 2019) with the IntCal20 curve (Reimer et al., 2020). Age model (AM) age was determined using BACON (Blauw and Christen, 2011) and are visible in Appendix E. Aggradation rates (AR) are calculated through linear interpolation of acquired ages. ARs determined at 11 cm in core CE\_VC1 and 10 cm in core RH\_VC7 were also determined using BACON, whereby ages were interpolated beyond limits of each respective age model.

| Core   | Depth [cm] | Lab ID       | Dated Material      | Conventional Age [ka] |       | Cal. age [ka BP] |                |       |       |        | AR [cm ka <sup>-1</sup> ] |
|--------|------------|--------------|---------------------|-----------------------|-------|------------------|----------------|-------|-------|--------|---------------------------|
|        |            |              |                     | <sup>14</sup> C Age   | Error | Res. Age         | Res. Age Error | μ-2σ  | μ+2σ  | Median |                           |
| CE_VC1 | 11         | D-AMS 039278 | Mixed benthic       | 5.579                 | 0.03  | 0.53             | 0.051          | 5.602 | 5.923 | 5.779  | 30.4                      |
|        | 41         | D-AMS 039277 | Mixed benthic       | 6.461                 | 0.03  | 0.523            | 0.05           | 6.437 | 6.851 | 6.684  | 394.4                     |
|        | 65         | D-AMS 045772 | <i>M. oculata</i>   | 6.529                 | 0.03  | 0.534            | 0.05           | 6.838 | 7.295 | 7.101  | 20.4                      |
|        | 93         | D-AMS 037306 | Mixed benthic       | 7.900                 | 0.03  | 0.512            | 0.051          | 8.025 | 8.35  | 8.198  | 32.7                      |
|        | 102        | D-AMS 037307 | Mixed benthic       | 8.160                 | 0.03  | 0.475            | 0.05           | 8.33  | 8.586 | 8.455  | 58.7                      |
| RH_VC7 | 122        | D-AMS 034764 | <i>G. bulloides</i> | 8.486                 | 0.04  | 0.526            | 0.053          | 8.689 | 9.184 | 8.907  | -                         |
| RH_VC7 | 10         | D-AMS 043458 | <i>M. oculata</i>   | 5.429                 | 0.03  | 0.505            | 0.052          | 5.35  | 5.687 | 5.627  | 64.6                      |
|        | 35         | D-AMS 043459 | <i>M. oculata</i>   | 5.786                 | 0.03  | 0.518            | 0.051          | 5.911 | 6.203 | 6.050  | 74.4                      |
|        | 65         | D-AMS 034770 | <i>G. bulloides</i> | 6.194                 | 0.04  | 0.52             | 0.055          | 6.407 | 7.113 | 6.608  | -                         |



### 2.2.2. Grain size analysis

The cores were frozen at  $-20\text{ }^{\circ}\text{C}$  and split using an electric circular handsaw, photographed and lithologically described. The matrix sediment composition was determined every 5 cm by weight loss after the chemical dissolution of the organic matter and carbonate material by following the procedures outlined by Pirlet et al. (2011) (see Appendix C). The siliciclastic matrix fraction was then investigated for grain-size variations, using a Malvern Instruments Mastersizer 3000 (MS3000) at University College Cork with a refined standard operating procedure (see Appendix D). Grain-size distributions (GSD), median grain size ( $D_{x50}$ ), mean grain sizes (MGS), kurtosis and sorting were automatically calculated using GRADISTAT (Blott and Pye, 2001). The mean sortable silt (MSS) was calculated from the differential volume % of grains within the 10–63  $\mu\text{m}$  silt fraction, following McCave and Andrews (2019) approach. In this study, the MGS and MSS sizes are used to trace changes in near-bottom current strength (McCave et al., 1995). Stronger bottom-currents yield a coarser mean grain size of a non-cohesive silt fraction due to selective deposition and winnowing (McCave et al., 1995). A detailed overview of the methods applied in this study can be found in O'Reilly et al. (2022).

### 2.2.3. AMS radiocarbon measurements

A mixed sampling strategy was applied to CE\_VC1 and RH\_VC7 due to the narrowness of the vibrocores (75 mm) and varying abundances of dateable material. Where possible, monospecific planktic foraminifera (*Globigerina bulloides*) were used. If the sum weight of the material collected was inadequate (i.e.  $<15\text{ mg}$ ), the epibenthic foraminiferal species *Cibicides lobatulus*, *Cibicides refulgens* and *Discanomalina coronata* were picked. Finally, pristine-looking coral pieces (*M. oculata*) were dated if the sum weight of benthic foraminifera was still inadequate. The base of pristine-looking coral pieces was chosen from CCP A (coral in the living position; see Titschack et al., 2015, Wang et al., 2019).

As such, two monospecific planktic foraminifera and four mixed benthic foraminifera samples were taken from the cores by extracting 1  $\text{cm}^3$  of sediment at various depths and used for dating (see Table 2). Foraminifera samples were picked from a  $>150\text{ }\mu\text{m}$  aliquot size and cleaned in an ultrasonic bath for 180 s prior to submission. Three coral pieces were sampled from the cores (see Table 2). Each fragment was cleaned following the methods described by Adkins et al. (2002). Nine measurements were carried out at DirectAMS Laboratories, Washington, USA.

Water column stratification significantly impacts offsets between contemporary planktic and benthic foraminifera radiocarbon ages. The reliability of the acquired ages should thus be treated with caution when interpreting the developed chronology for the cores. To this end, age models were constructed using Paleo Data View (Langner and Mulitza, 2019) to allow applicability and consistency across synthesis. AMS  $^{14}\text{C}$  ages were converted to calendar years with the IntCal20 curve (Reimer et al., 2020) and reported as kiloyears before present (ka BP, Present = 1950 CE). The age model was developed in a Bayesian framework using BACON (Blaauw and Christen, 2011) in Paleo Data View (Appendix E).

### 2.2.4. Stable-isotope analysis

The planktic species *G. bulloides* was picked from the 150–250  $\mu\text{m}$  size fraction. It was chosen due to its abundance in the cores, sizeable geographic distribution in the North Atlantic, and its high abundance during different climatic periods (Chapman, 2010). The epibenthic foraminifera *C. lobatulus* was picked from the 212–250  $\mu\text{m}$  size fraction to avoid discrepancies in measurements due to ontogenic processes within this species (i.e. Schiebel and Hemleben, 2007). A minimum weight of 0.05 mg of sample was collected for each aliquot. Measurements were made in the Institute of Earth Surface Dynamics at the University of Lausanne on a ThermoFisher Scientific Delta V gas source mass spectrometer using a GasBench (Spötl and Vennemann, 2003). The normalized carbon and oxygen isotope values are expressed as per mil

deviation (‰) with respect to the international Vienna Pee Dee Belemnite standard (VPDB). The analytical standard deviation ( $1\sigma$ ) for  $\delta^{18}\text{O}$  and  $\delta^{13}\text{C}$  was  $\pm 0.07\text{‰}$ , and  $\pm 0.05\text{‰}$  for eight repeated measurements of the in-house standard carbonate (Carrara Marble) analysed in the same sequence as the planktic samples and  $\pm 0.05\text{‰}$  and  $\pm 0.02\text{‰}$  for the benthic samples, respectively. A correction of  $-1\text{‰}$  for *G. bulloides* was applied to account for a potential species-specific fractionation effect (vital effects) on the measured  $^{13}\text{C}$  isotopic compositions (Howard Spero, personal communication, 2021).

### 2.3. Benthic foraminiferal assemblages

BFA were first investigated at a 10 cm resolution throughout both cores from the  $>125\text{ }\mu\text{m}$  fraction. This data were then cross examined versus all other multiproxy data (i.e. CPP, grain size, stable isotopes) to assess paleoenvironmental signals. For intervals that warranted further investigation, a second sampling phase was conducted at a 5 cm resolution. As such, 31 BFA samples were investigated in this study. Foraminifera were picked under a light stereomicroscope at the Laboratory of Geology, University of Lyon (France). Taxonomic identification follows Margreth (2010) and Spezzaferri et al. (2015). The subsamples where foraminifera were very abundant were split with an Otto micro-splitter, and the whole splits were counted (see Appendix F). To help with the taxonomical identification Scanning Electron Microscope (SEM) photographs were acquired at the Department of Geosciences, University of Fribourg (Switzerland), using a Thermo Fischer SEM FEIXL30SFEG. A detailed description of the ecological preference of the dominant morphospecies is given in Appendix I.

To calculate expected species richness, samples were rarefied to  $n = 200$  in R, compensating for sample count differences between each assemblage. In addition, evenness was calculated using Hill's ratio  $E_{1,0}$  based on Shannon diversity, whereby high values (approaching 1) indicate more evenness between species (Hill, 1973; Alatalo, 1981). Abundance data were standardized to dry-weight ( $\text{n g}^{-1}$ ) to compensate for variable sub-samples sizes and used to compute a Hellinger distance matrix. Average agglomerative clustering was performed using the unweighted pair-group method using arithmetic averages. Tests of multivariate group dispersions were conducted to prevent the confusion of location and dispersion effects (Anderson et al., 2006) and returned insignificant differences in variance between sites and between species clusters but significant differences in group dispersion between facies. Therefore, only sites and species clusters were considered as group factors along with continuous environmental data and the age model (see section 3.1.3). To test for significance of the selected environmental factors on species assemblages, distance-based redundancy analysis (db-RDA) was implemented using 10,000 permutations as a non-parametric method for multivariate analysis of variance (Legendre and Anderson, 1999; McArdle and Anderson, 2001). These methods were implemented using the packages *vegan* (Oksanen et al., 2020) and *adespatial* (Dray et al., 2022) in the statistical programming environment R (R Core Team, 2021).

## 3. Results

### 3.1. Core CE\_VC1

Core CE\_VC1 contains well-preserved CWC fragments (mainly *D. pertusum* and *M. oculata*) embedded in a homogenous matrix of predominantly medium to fine brown silts (Fig. 2). CPP A (representing coral framework in a living position) occurs between 36 and 73 cm (Fig. 2). CCP B (representing a slightly collapsed coral framework) occurs between 73 and 130 cm. Coral rubble (CCP C) occurs between 0 and 36 cm. MGS recorded in core CE\_VC1 are between 7.1 and 15.5  $\mu\text{m}$  (see Appendix G). MSS fluctuates between 17.1 and 25.3  $\mu\text{m}$ . Core CE18011\_VC1 has relatively low planktic  $\delta^{13}\text{C}$  (range:  $-0.48$  to  $0.03\text{‰}$ ; see Appendix G).

### 3.2. Core RH\_VC7

Core RH\_VC7 contains well-preserved CWC fragments (mainly *D. pertusum* and *M. oculata*) embedded in a homogenous matrix of predominately medium to fine brown silts (Fig. 2). CPP A occurs between 0 and 56 cm (Fig. 2). CCP B occurs between core depths of 56–80 cm. MGS recorded in core RH\_VC7 are between 8.2 and 12.4  $\mu\text{m}$  (see Appendix G). MSS fluctuates between 17.9 and 21.4  $\mu\text{m}$ . Core RH\_VC7 has a relatively low planktic  $\delta^{13}\text{C}$  (range:  $-0.84$  to  $-0.33\text{‰}$ ; see Appendix G).

### 3.3. Chronology and coral mound aggradation rates

Six AMS  $^{14}\text{C}$  ages ranging from 8.9 to 5.8 ka BP (see Table 2) were obtained from core CE\_VC1, using planktic foraminifera (at 122 cmbsf), benthic foraminifera (at 102, 93, 41 and 11 cmbsf) and coral pieces (at 65 cmbsf). Three ages (8.9, 8.5 and 8.2 ka BP) date back to the early Holocene and three ages (7.1, 6.7 and 5.8 ka BP) are from the mid-Holocene (see Table 2). During the early Holocene, the coral mound AR fluctuates between 58.7 and 32.7  $\text{cm ka}^{-1}$  (see Table 2). During the mid-Holocene, the AR decreases to 20.4  $\text{cm ka}^{-1}$  and increases rapidly to

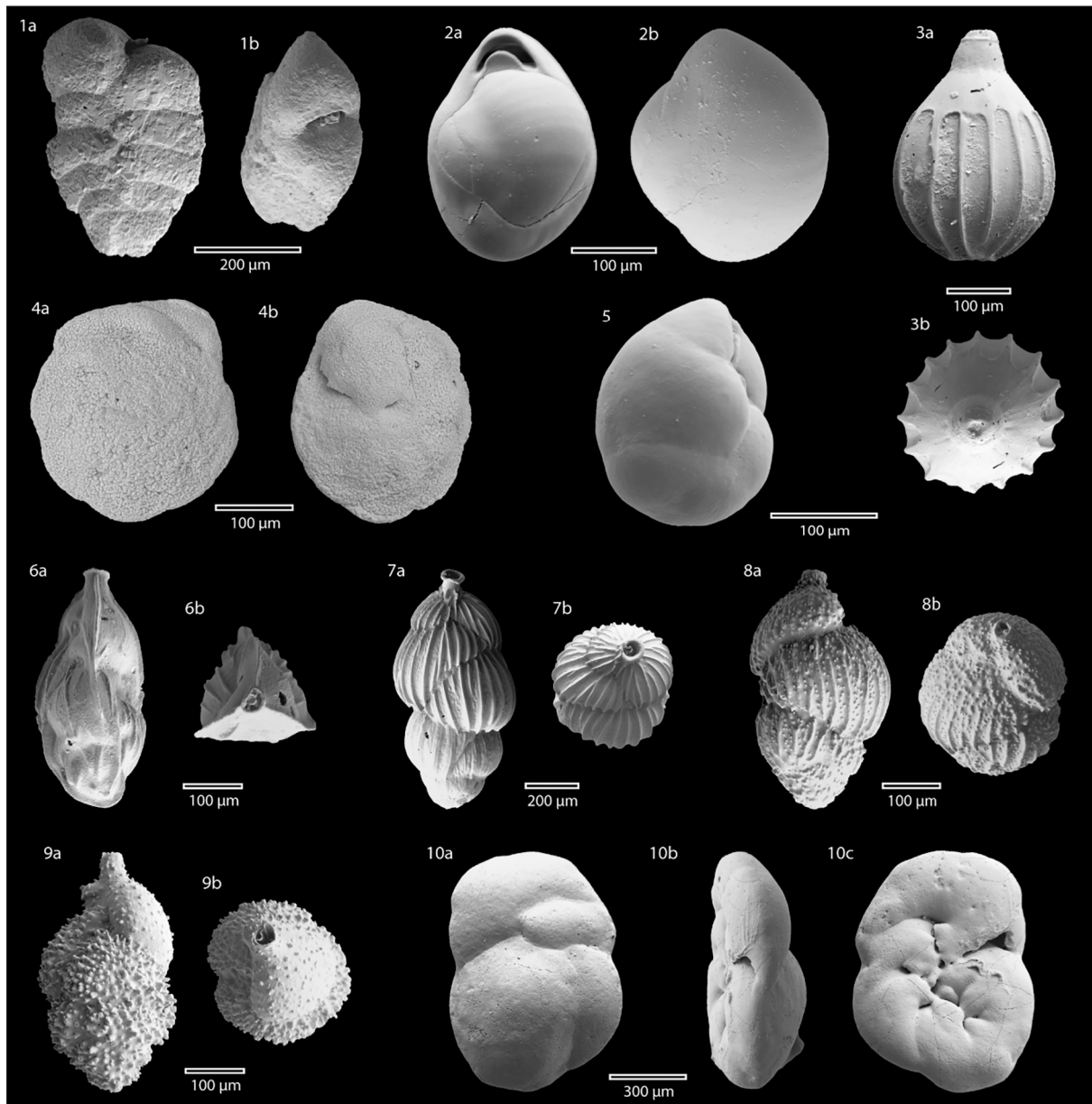


**Fig. 3.** Dominant benthic foraminifera species across this study. Plate 1.1 - *Spiroplectammina sagittula* (Defrance, 1824) a. side view, b. apertural view; 2. *Biloculinella globula* (Bomemann, 1855) a. apertural view, b. side view; 3. *Homalohedra borealis* (Loeblich and Tappan, 1954) a. side view, b. apertural view; 4. *Nuttallides umbonifera* (Cushman, 1933) a. spiral side; b. umbilical side; 5. *Globocassidulina subglobosa* (Brady, 1881) side view; 6. *Trifarina angulosa* (Williamson, 1858) a. lateral view, b. apertural view; 7. *Uvigerina mediterranea* (Hofker, 1932) a. lateral view, b. apertural view; 8. *Uvigerina pygmae* (d'Orbigny, 1826) a. lateral view, b. apertural view; 9. *Uvigerina auberiana* (d'Orbigny, 1839) a. lateral view, b. apertural view; 10. *Hyrrokin sarcophaga* (Cedhagen, 1994) a. spiral side, b. peripheral view, c. umbilical side.

Plate 2. 1. *Melonis barleeanum* (Williamson, 1858) a. side view, b. apertural view; 2. *Discanomalina coronata* (Parker and Jones, 1865) a. spiral side, b. peripheral view, c. umbilical side; 3. *Pullenia subcarinata* (d'Orbigny, 1839) a. side view 1, b. side view 2; 4. *Cibicides refulgens* (Montfort, 1808) a. spiral side, b. peripheral view, c. umbilical side; 5. *Planulina ariminensis* (d'Orbigny, 1826) a. spiral side, b. peripheral view; 6. *Cibicides lobatulus* (Rzehak, 1886) a. spiral side, b. peripheral view, c. umbilical side.

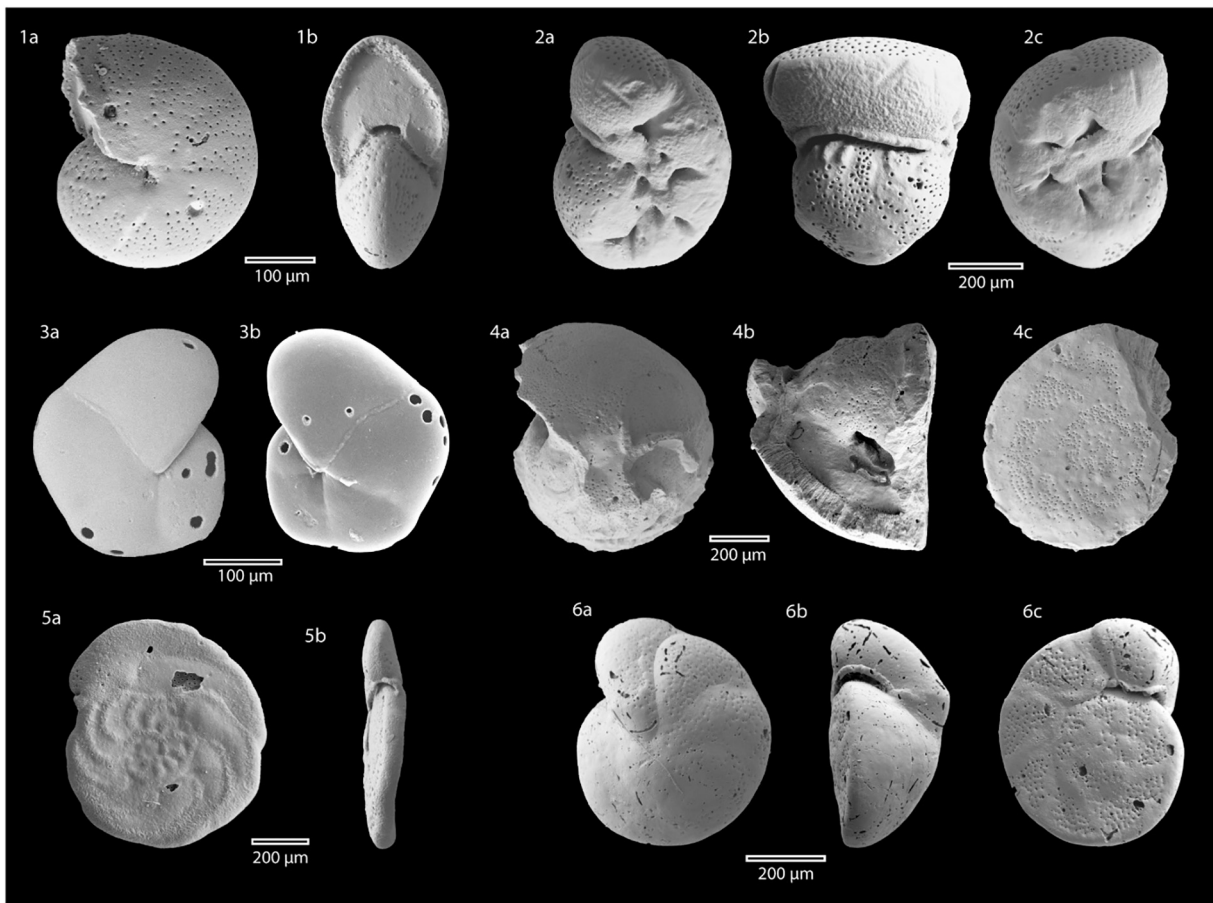
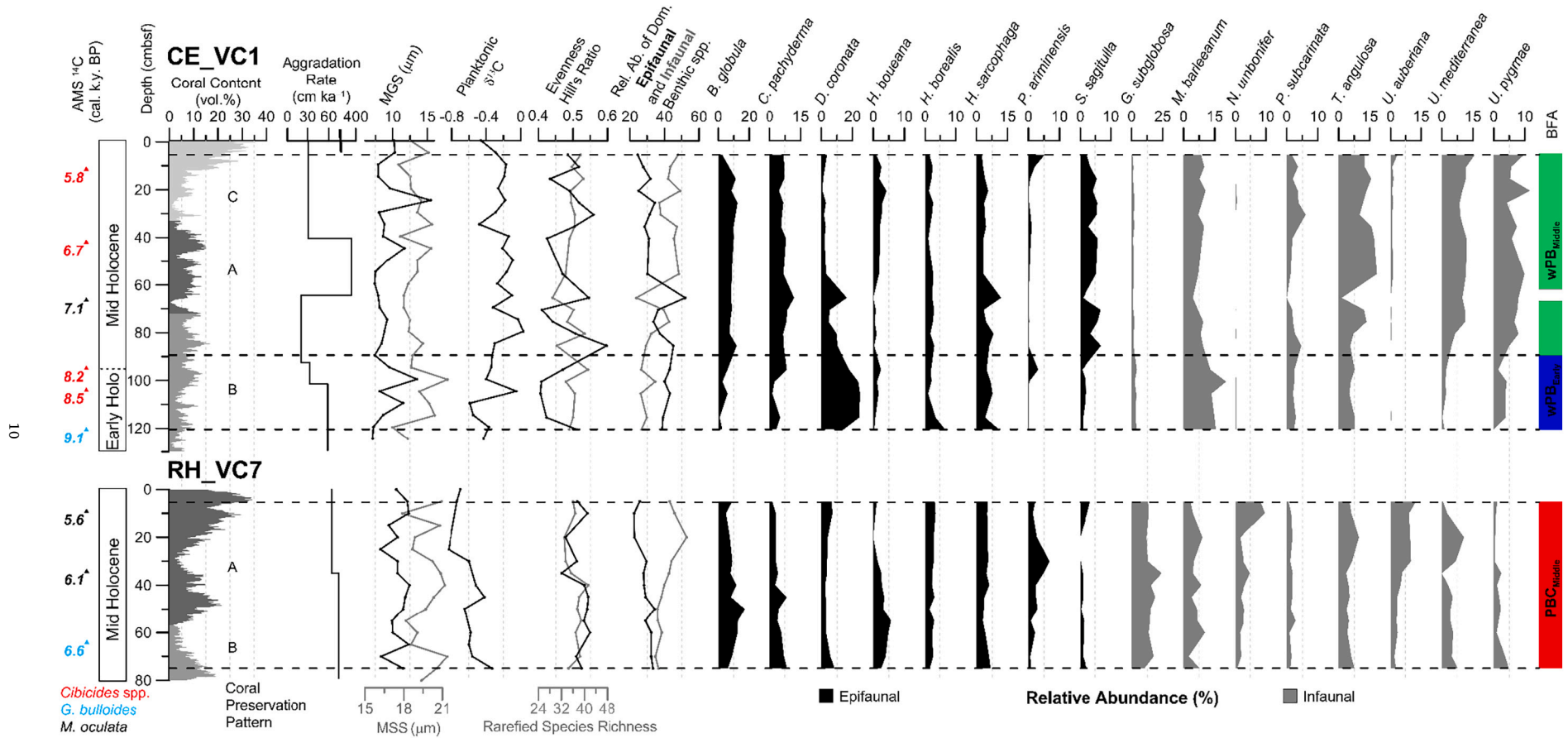


Fig. 3. (continued).





**Fig. 4.** Multiproxy data used in this study for cores CE\_VC1 (top) and RH\_VC7 (bottom). From left to right: The chronology of the core is based on AMS <sup>14</sup>C ages of the planktic foraminifera species *G. bulloides*, the benthic foraminifera genus *Cibicides* and the cold-water coral species *M. oculata* (Note: that in core CE\_VC1 the boundary between the Early Holocene and mid Holocene may be tied by the near absence of coral at 68 cmbsf); Distribution of cold-water coral content with associated CPP (see Fig. 2); aggradation rates interpolated from AMS <sup>14</sup>C ages; mean grain size (MGS – black) and mean sortable silt size (MSS – grey), planktic δ<sup>13</sup>C; evenness Hill's Ratio (black) and rarefied species richness (grey) of the entire benthic foraminifera population; relative abundance of dominant benthic foraminifera species (epifaunal – black, infaunal – grey); relative abundance of individual dominant benthic foraminifera species (epifaunal – black, infaunal – grey); and associated benthic foraminifera assemblages (BFA).

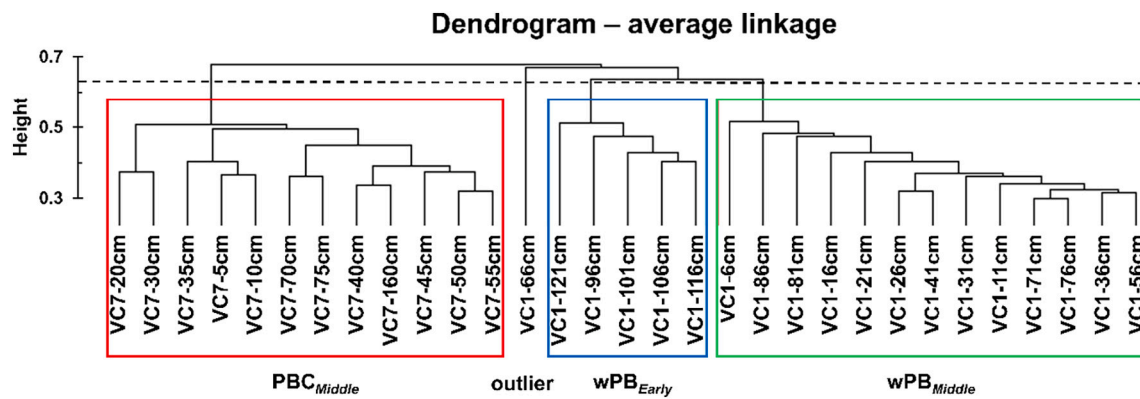


Fig. 5. Agglomerative dendrogram based on the Hellinger dissimilarity matrix of the benthic foraminiferal community dataset from cores CE\_VC1 and RH\_VC1. Cut at a dissimilarity of 64%, three clusters (PBC<sub>Middle</sub>, wPB<sub>Middle</sub> and wPB<sub>Early</sub>) and an outlier can be recognized.

Table 3

Percentage relative abundance of dominant benthic foraminifera from each BFAs. Also shown is the mean relative abundance across the whole study.

| Species                | PBC <sub>Middle</sub> (%) | wPB <sub>Middle</sub> (%) | wPB <sub>Early</sub> (%) | Mean (%) |
|------------------------|---------------------------|---------------------------|--------------------------|----------|
| <i>D. coronata</i>     | 5.5                       | 5.5                       | 20.7                     | 10.5     |
| <i>M. barleeanum</i>   | 6.5                       | 8.9                       | 15.4                     | 10.3     |
| <i>T. angulosa</i>     | 6.1                       | 12.1                      | 6.9                      | 8.4      |
| <i>B. globula</i>      | 8.8                       | 8.4                       | 4.1                      | 7.1      |
| <i>G. subglobosa</i>   | 14                        | 1.9                       | 3.6                      | 6.5      |
| <i>C. lobatulus</i>    | 5.5                       | 7.3                       | 4.9                      | 5.9      |
| <i>H. sarcophaga</i>   | 5.5                       | 4.7                       | 6.5                      | 5.6      |
| <i>U. mediterranea</i> | 5.2                       | 9.9                       | 1.6                      | 5.6      |
| <i>U. pygmae</i>       | 2.6                       | 6.9                       | 2.5                      | 4        |
| <i>H. borealis</i>     | 2.4                       | 2.3                       | 2.8                      | 2.5      |
| <i>S. sagittula</i>    | 1.5                       | 4.7                       | 1.3                      | 2.5      |
| <i>P. subcarinata</i>  | 1.4                       | 2.6                       | 2.4                      | 2.2      |
| <i>H. boueana</i>      | 2.8                       | 1.5                       | 1.5                      | 1.9      |
| <i>U. auberiana</i>    | 4.8                       | 0.7                       | 0                        | 1.8      |
| <i>P. ariminensis</i>  | 2                         | 0.9                       | 1.2                      | 1.3      |
| <i>N. umbonifer</i>    | 2.8                       | 0.1                       | 0.2                      | 1        |

394.4 cm ka<sup>1</sup> (see Table 2) and then decreases to 30.4 cm ka<sup>-1</sup>. The AR for the entire constrained core is 35.9 cm ka<sup>-1</sup>. Three AMS <sup>14</sup>C ages ranging from 6.6 to 5.6 ka BP were obtained from core RH\_VC7 (Table 2) using benthic foraminifera (at 65 cmbsf) and coral pieces (at 35 and 10 cmbsf). All ages (6.6 ka BP, 6.1 ka BP and 5.6 ka BP) occur in the mid-Holocene. During this period, the coral mound aggradation rates (AR) fluctuate between 74.4 and 64.6 cm ka<sup>-1</sup>. The AR for the entire constrained core is 56.1 cm ka<sup>-1</sup>.

#### 3.4. 4.3 Benthic foraminifera

A total of 109 benthic foraminiferal taxa were observed across the two cores in this study (see Appendix F). 16 taxa were noted as dominant (i.e. showing relative abundances ≥5% in at least one sample; see also Figs. 3 and 4 and Appendix F). The ecological preferences of these species can be found in Appendix I. 101 taxa were represented in CE\_VC1 and 83 in RH\_VC1. Twelve dominant species were observed in each core, of which eight were identical in both cores.

##### 3.4.1. Multivariate analysis and species diversity

Multivariate analysis performed on the complete and standardized dataset reveals variations in the relative number of individuals (n g<sup>-1</sup>) from one sample to another. Listed in Appendix I are species contributing to average dissimilarity/similarity and abundance. According to their associated BFA, information on diversity (rarefied species richness and evenness Hill's ratio) will also be discussed.

The agglomerative cluster analysis distinguished 3 clusters (blue, red and green, composed of 5, 12 and 13 samples, respectively; see Fig. 5;

Table 4

Results of the db-RDA test. R<sup>2</sup> represents the proportion of variance in the dependent variable explained by the respective explanatory variables. Pseudo F represents the ratio of total dissimilarities among groups to within group dissimilarity, each divided by their respective degrees of freedom. The p-value reports the proportion of random permutations exceeding the observed pseudo-F statistic, determining the significance codes (\*\*\*) for highly significant p-values <0.001 and \*\* for significance at an α of 0.01).

| Explanatory variable | R <sup>2</sup> | pseudo-F | p-value (>F) |
|----------------------|----------------|----------|--------------|
| Site                 | 0.29135        | 14.1325  | 0.0001***    |
| Age                  | 0.13812        | 6.6996   | 0.0001***    |
| Sortable Silt        | 0.02515        | 1.2199   | 0.2409       |
| Grain size           | 0.01526        | 0.7405   | 0.6603       |
| Organic content      | 0.01473        | 0.7144   | 0.6921       |
| Site-Age Interaction | 0.05682        | 2.9735   | 0.0057**     |

see also Fig. 2a and b) and an outlier sample at 64% similarity. Each cluster relates to a specific BFA. The blue cluster groups all samples in CE\_VC1 from 96 to 121 cmbsf and will be hereafter referred to as the “Early Holocene wPB Assemblage” (abbreviated to wPB<sub>Early</sub>; see Fig. 5). The green cluster groups samples in CE\_VC1 from 6 to 86 cmbsf, except for 66 cmbsf, representing the outlier. The green cluster will be hereafter referred to as the “mid-Holocene wPB Assemblage” (abbreviated to wPB<sub>Middle</sub>). The red cluster groups all samples in RH\_VC7 and will be hereafter referred to as the “Middle Holocene PBC Assemblage” (abbreviated to PBC<sub>Middle</sub>). The assemblages are plotted versus depth in Fig. 2a and b.

The wPB<sub>Early</sub> Assemblage is characterised by *D. coronata* (20.7 relative %; hereby abbreviated to %; Table 3; see also Appendix H) and *Melonis barleeanum* (15.4%). Less contributing species are *Trifarina angulosa* (6.9%), *Hyrrokin sarcophagi* (6.5%), *Cibicides lobatulus* (4.9%), *Biloculinella globula* (4.1%) and *Globocassidulina subglobosa* (3.6%). An average of 37 expected species (max – 41, min – 34) is present throughout this assemblage according to rarefied species richness, with an average evenness Hill's ratio E<sub>1,0</sub> = 0.45 (max – 0.51, min – 0.41).

The wPB<sub>Middle</sub> assemblage is characterised by *T. angulosa* (12.1%; Table 3; see Appendix H) and *Uvigerina mediterranea* (9.9%). Less contributing species are *M. barleeanum* (8.9%), *B. globula* (8.4%), *C. lobatulus* (7.3%), *Uvigerina pygmae* (6.9%), *D. coronata* (5.5%) and *H. sarcophaga* (4.7%). An average of 35 expected species (max – 40, min – 30) is present throughout this assemblage according to rarefied species richness, with an average evenness of E<sub>1,0</sub> = 0.49 (max – 0.60, min – 0.41).

The PBC<sub>Mid</sub> assemblage is characterised by *G. subglobosa* (14.0%; Table 3; see Appendix H) and *B. globula* (8.8%). Less contributing species are *M. barleeanum* (6.5%), *T. angulosa* (6.1%), *C. lobatulus* (5.5%), *H. sarcophaga* (5.5%), *D. coronata* (5.5%), and *U. mediterranea* (5.2%).

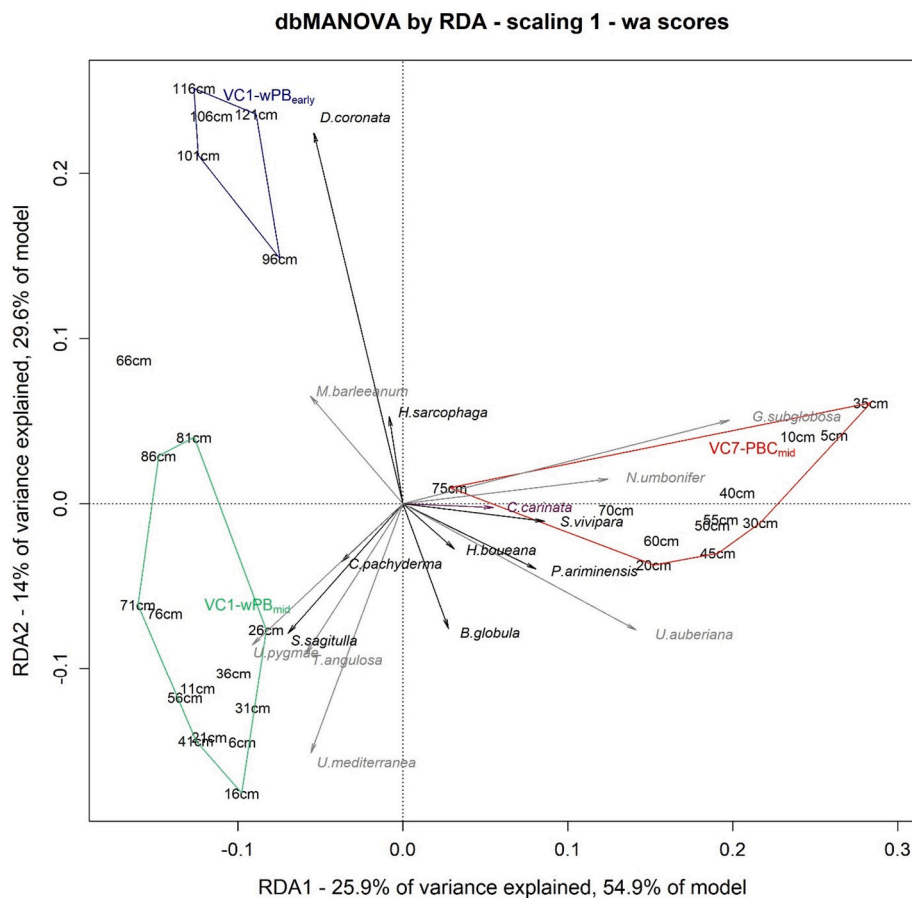


Fig. 6. Scaling one triplot representation of the redundancy analysis (RDA) ordination on Hellinger-transformed data constrained by the three groups identified through average agglomerative clustering in the same colour-coding as Fig. 5. RDA1–3 are highly significant, RDA 1 separating the wPB assemblages from the PBC, and RDA 2 differentiating between the early and mid-Holocene assemblage at wPB. With an adjusted  $R^2$  value of 0.434, the model explains a large proportion of variation in the data. Grey arrows represent species scores for infaunal foraminifera, and black arrows are for epibenthic species. The purple species has a shallow infaunal to epifaunal lifestyle. Only the species that contribute most to reduced space are shown to avoid overplotting. (For interpretation of the references to colour in this figure legend, the reader is referred to the web version of this article.)

An average of 37 expected species (max – 41, min – 33) is present throughout this assemblage according to rarefied species richness, with an average evenness of  $E_{1,0} = 0.52$  (max – 0.55, min – 0.47).

### 3.4.2. Distance-based redundancy analysis (dbRDA)

Testing environmental variables significance in shaping foraminiferal community composition through dbRDA showed that site was a highly significant parameter ( $p < 0.001$ , pseudo- $F_{1,25} = 14.29$ ; see Table 4; see also Fig. 6). In addition, site explained the greatest variation in the species composition data ( $R^2 = 0.29$ ; see Table 4). The age model was the second-most-important variable, explaining 14% of the variation ( $p < 0.001$ , pseudo- $F_{1,25} = 6.77$ ; see Table 4). Other factors, such as mean sediment grain size, mean sortable silt (a proxy for current velocity) and organic content (based on planktic  $\delta^{13}C$ ), were insignificant. A significant ( $p < 0.01$ ) interaction effect between the site and age model was detected. This accounted for 5.7% of the variance (Table 4) and indicated that periodic differences in community change between the two sites occurred. Space-time interaction confounds ecological interpretation (Legendre et al., 2010) and thus, the two sites were tested for temporal effects independently. The age model remained highly significant ( $p < 0.001$ ) at both sites with  $F_{1,7} = 3.09$  and  $R^2 = 0.24$  for VC7 at the PBC and  $F_{1,14} = 7.35$  and  $R^2 = 0.31$  for VC1 at the wPB.

## 4. Discussion

### 4.1. The controls of mound development in the wPB

#### 4.1.1. Early Holocene (9.1–8.2 ka BP)

Mean ARs determined from core CE\_VC1 suggest that relatively low mound formation occurs on the wPB during the early Holocene (mean  $40.9 \text{ cm ka}^{-1}$ ; see Table 2) where rates are comparable to mound

formation on the Rockall Bank ( $60 \text{ cm ka}^{-1}$ ; see Frank et al., 2009). In comparison, higher ARs are captured in the Norwegian fjords during the Holocene ( $1500 \text{ cm ka}^{-1}$ , see Titschack et al., 2015), suggesting that the wPB provided rather unfavourable environmental conditions for positive mound formation during the Early Holocene. The BFA wPB<sub>Early</sub> (dominated by *D. coronata* and *M. barleeianum*) characterises the period and is consistent with other BFAs observed at the surface of CWC mounds from the Rockall (567–657 m water depth) and Porcupine (567–820 m water depth) Banks (Morigi et al., 2012; Smeulders et al., 2014). These similarities are confirmed by the abundance of epifaunal species including *B. globula*, *H. sarcophagi*, and *C. lobatulus* (Fig. 4). These species live on elevated substrates (e.g. coral frameworks, coral rubble and dropstones), feeding on food particles transported by strong bottom currents (Hald and Vorren, 1987; Linke and Lutze, 1993; Schönfeld, 1997; Schönfeld, 2002a; Schönfeld, 2002b; Hawkes and Scott, 2005).

During the early Holocene, the northern migration of the polar front possibly triggered enhanced surface ocean productivity (Rüggeberg et al., 2007; Frank et al., 2011). Concurrently, the return of the MOW to the region (e.g. Dorschel et al., 2005; Øvrebo et al., 2006; Rüggeberg et al., 2007), created a stratified water column with the ENAW that instigated the generation of internal tides (Wienberg et al., 2020). This resulted in a strengthening of bottom waters in the region, that enhanced food transport to the seafloor. Enhanced currents are evident along the shelf edge (see Howe et al., 1994; Howe, 1996; Armishaw et al., 2000; Knutz et al., 2001; Knutz et al., 2002a; Knutz et al., 2002b; Øvrebo et al., 2006). High MGS and MSS values were also recorded ( $13.5 \mu\text{m}$  and  $21.4 \mu\text{m}$ , respectively; see Fig. 4), further supporting the idea that elevated bottom currents were present in the region. High current speeds likely resulted in mass wasting, exposing the dead coral framework, ultimately reducing mound formation (see also Dorschel



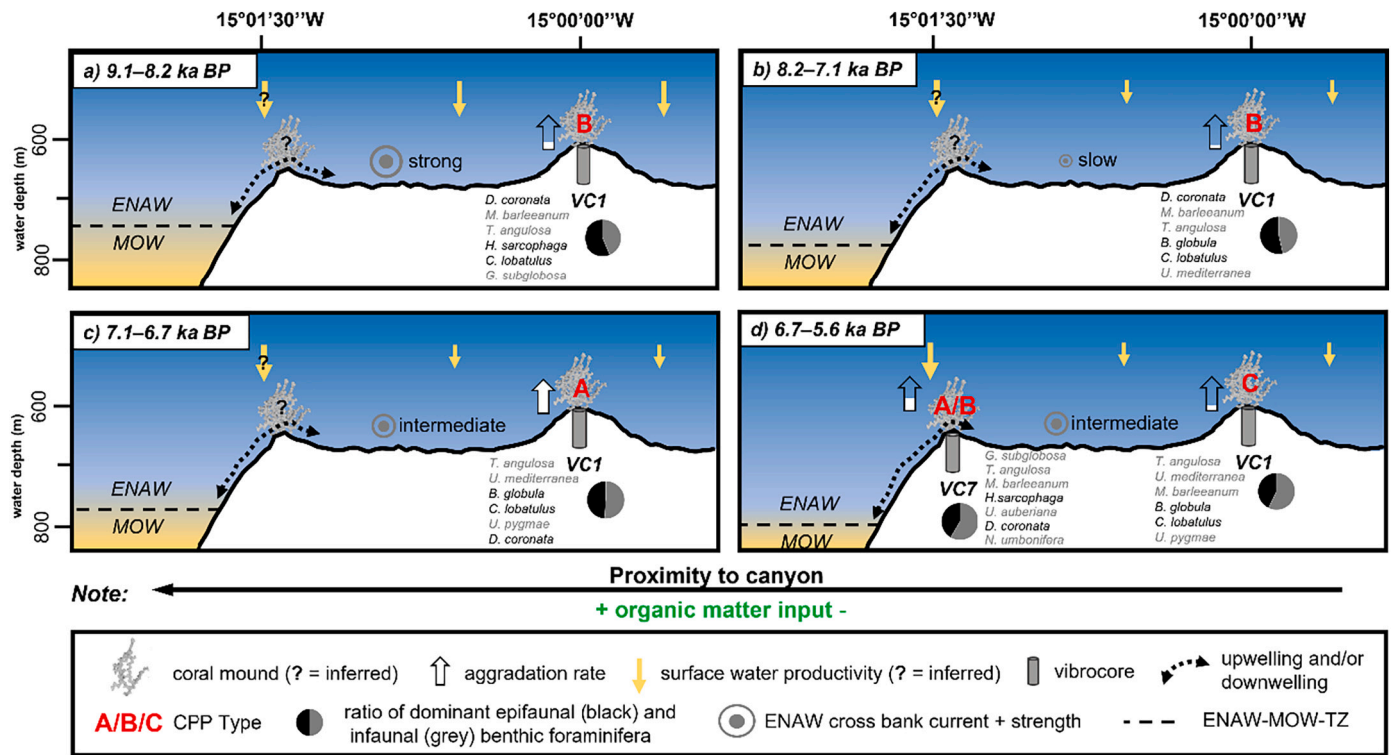


**Fig. 7.** Summary of environmental factors controlling wPB and PBC mounds during the Holocene. Aggradation rates (white arrow) and coral preservation pattern (CPP; red) describe environmental variability. Benthic foraminifera at each core locality are listed by decreasing dominance alongside the ratio of dominant epifaunal (black) and infaunal (grey) species. Bottom currents strength (grey circle) are inferred from mean grain size, mean sortable silt size and benthic foraminiferal distribution. Surface water productivity (orange arrow) reflected by variations in  $\delta^{13}\text{C}$  from planktic foraminifera (Note: it likely remains more enriched over the lip of canyon from Ekman driven downwelling of surface waters (see Granata et al., 1999, Palanques et al., 2005, Raimeyer et al., 2006, Allen and Madron, 2009), and is annotated with black question marks). Upwelling (black arrow) remains prominent throughout each period. (a) 9.1–8.2 ka BP; (b) 8.2–7.1 ka BP; (c) 7.1–6.7 ka BP; and (d) 6.7–5.6 ka BP. (For interpretation of the references to colour in this figure legend, the reader is referred to the web version of this article.)

et al., 2009). The resulting low AR, combined with high MSS are testament to persistently elevated bottom currents during the Early Holocene. In addition, the high relative abundances of *D. coronata* are possibly linked to the suitable substrate availability provided by the available coral skeletons. This supports regional findings, where higher abundances of *D. coronata* are associated with coral rubble/coral debris facies in the Porcupine and Rockall Banks (Schönfeld et al., 2011; Smeulders et al., 2014).

Food from surface waters is in high supply throughout the early Holocene, as indicated by the mean trend in the planktic  $\delta^{13}\text{C}$  signal (Fig. 4; see also Appendix G). Furthermore, the relative abundance of *M. barleeanum* is high during this period (20.49%; see Fig. 4 and Appendix F at 101 cmbsf). This infaunal species is typical of productive waters high in POM (Corliss, 1985, Genin et al., 1986, Caralp, 1989, Loubere, 1998, Murray, 2006a, Koho et al., 2008; see Fig. 4) and has been observed in early Holocene CWC mounds in the Porcupine Seabight (Schönfeld et al., 2011; Morigi et al., 2012; Smeulders et al., 2014). Accordingly, the re-organization of the regional water column structure, combined with this enrichment in water productivity, increased food supply to the corals during the Holocene (Frank et al., 2011).

#### 4.1.2. Early – mid-Holocene transition (8.2 ka BP)

ARs decrease during the early – mid-Holocene transition (20.4 cm ka<sup>-1</sup>; see Table 2 and Fig. 4), suggesting a slowing of mound formation. Concurrently, a steady decrease is observed in MGS and MSS (7.4 and 18.7 mm, respectively; Fig. 4). A decelerated hydrodynamic regime would cause a depleted food supply to the corals, which might have resulted in the reduced coral content at this time interval. This generates a small accommodation space, that limits the on-mound

deposition of current-transported sediments (Wang et al., 2021), temporarily slowing mound formation. Climate simulations show that large parts of the Northern Hemisphere, including the NE Atlantic, were affected by periods of abrupt cooling of 1–3 °C at 8.2 ka (Barber et al., 1999; Thomas et al., 2007; Morrill et al., 2013), caused by the centennial meltwater pulse from the collapse of the Hudson Bay ice saddle (Carlson et al., 2008; Carlson et al., 2009; Gregoire et al., 2012; Wagner et al., 2013; Matero et al., 2017; Appah et al., 2020). Regionally, this short climatic shift has been observed in CWC mound records from the Porcupine Seabight and Rockall Trough, where mound formation slows due to decelerated bottom current speeds (O'Reilly et al., 2004; Frank et al., 2009). A freshwater discharge of this magnitude during the 8.2 ka climate reversal may have also slowed the northern flowing ENAW along the wPB.

Concurrently, an increase in Hill's Ratio (0.47 to 0.61) and a simultaneous decrease in rarefied species richness (41 to 20; see Fig. 4; see also Appendix F from 96 to 86 cmbsf, respectively) suggest that conditions favour fewer benthic foraminifera species across this period. Additionally, a decrease in the relative abundances of *D. coronata* is observed (from 18 to 10%). *D. coronata* has been used as an indicator species for living Irish CWC mounds (Margreth et al., 2009). In the case of the wPB however, it is more likely better suited as a proxy to determine the availability of suitable substrates (i.e. dead coral/coral rubble; Schönfeld et al., 2011, Smeulders et al., 2014; Fentimen et al., 2021). The benthic and planktonic  $\delta^{18}\text{O}$  remain relatively constant throughout this phase (Appendix G), potentially suggesting that water mass temperature and/or salinity on this part of the continental margin remained somewhat unaffected. Therefore, changes to current speed are likely the primary driver for slowing mound formation. Subsequently, this

alteration to the available ecological niches for benthic foraminifera markedly impacted community structure.

#### 4.1.3. Mid-Holocene (8.2–6.7 ka BP)

Between 8.2 and 7.1 ka BP, mound AR on the wPB remains low ( $20.4 \text{ cm ka}^{-1}$ ). Mounds from the Rockall Bank and Porcupine Seabight record similar estimations ( $15 \text{ cm ka}^{-1}$ ; see Frank et al., 2009), suggesting a regional reduction in mound AR in the NE Atlantic. The coral clasts throughout this phase become progressively more aligned parallel to the seafloor (i.e.  $<60^\circ$ ; see Fig. 2a between 93 and 63 cmbsf). Furthermore, low MGS and MSS (average 8.3 and  $18.5 \mu\text{m}$ , respectively; see Appendix G) indicate that current speeds on the wPB were sluggish throughout this phase. Collectively, these pieces of evidence capture the control of hydrodynamic forcing on mound formation by regulating food and suspended sediment supply. In this case, the coral skeleton is exposed to degradation processes for a longer duration resulting from decelerated currents and thus lower framework supporting sediment infill (Titschack et al., 2015; Titschack et al., 2016; Wang et al., 2019). More exposed to bioerosion, the framework eventually breaks and becomes deposited on the seafloor. This change in macrohabitats appears to have a knock-on effect on microhabitats. A distinct difference is visible between the early and mid-Holocene foraminiferal assemblage at the wPB. The shift from the wPB<sub>Early</sub> to the wPB<sub>Middle</sub> Assemblage may constitute a re-structuring of the benthic community after environmental conditions had become unfavourable for numerous rarer species occupying ecosystem niches dependent on more upright coral clasts.

Between 7.1 and 6.7 ka BP, mound formation on the wPB becomes more favourable, as indicated by the shift to CPP A (defined as “coral in living position”). In this instance, the framework generates coral-derived accommodation space (Pomar, 2001, see also Wang et al., 2021), creating a local low energy environment for current-transported sediments to settle (Flügel, 2004; Titschack et al., 2009). When combined with a high sediment supply, this entrapment mechanism results in high mound aggradation ( $394.4 \text{ cm ka}^{-1}$ ). This window of favourable mound development correlates with a decrease in abundances of *D. coronata* (from 16 to 3%), presuming its ecological niche is dependent on the availability of coral rubble (Schönfeld et al., 2011; Smeulders et al., 2014). Instead, the wPB<sub>Middle</sub> assemblage is abundant with infaunal benthic foraminifera, mostly *M. barleeianum*, *T. angulosa* and *Uvigerina* spp. (Fig. 4). *Uvigerina* spp. represent high fluxes of organic C and labile organic matter (Altenbach et al., 1999; Fontanier et al., 2002; Murray, 2006a), whilst *T. angulosa* is commonly associated with shelf-edge-upper-slope areas under strong bottom currents (Hald and Vorren, 1984; Mackensen et al., 1985; Qvale and Weering, 1985; Austin and Evans, 2000; Schönfeld, 2002a; Mojtahid et al., 2021) and occurs in coarser sediment (Mackensen et al., 1995; Schönfeld, 2002b). The development of this infaunal community infers high food availability, delivered by strong bottom currents. Typically, enhanced hydrodynamism causes mass wasting, slowing mound formation. In this case, the coral framework granted sufficient accommodation space (Wang et al., 2021), ensuring that mound formation outpaces the rate of erosion. This results in a faster burial of CWC pieces, reducing the likelihood of biodegradation processes. This interplay is widely documented in CWC mound literature (De Mol et al., 2002; De Haas et al., 2009; Dorschel et al., 2009; Mienis et al., 2013).

#### 4.2. Proximity to the canyon – an essential driver for coral growth

The topmost 40 cm of CE\_VC1 is contemporaneous with the entirety of RH\_VC7 and is constrained between 6.7 and 5.6 ka BP (Fig. 4). As such, site-specific mound development across this period can be compared. In core CE\_VC1, CPP is represented entirely by coral rubble (CPP C; see Fig. 4). In contrast, the bottommost 24 cm and the topmost 56 cm of core RH\_VC7 are respectively represented by slightly collapsed coral framework (defined as CPP B) and coral framework in living position (defined as CPP A). Mean mound AR in core RH\_VC7 is greater by

a factor of two when compared to core CE\_VC1 (see Table 2 and Fig. 4). Isotopic data show that lighter planktic  $\delta^{13}\text{C}$  occurs in core RH\_VC7 (range:  $-0.84$  to  $-0.33\text{‰}$ ) than in core CE\_VC1 (range:  $-0.46$  to  $-0.19\text{‰}$ ; Fig. 4 and Appendix G), suggesting that proximity of mounds to the canyon is a crucial factor for food supply.

The incising geomorphology of submarine canyons result in complex patterns of hydrography, sediment transport and accumulation (Shepard et al., 1974; Oliveira et al., 2007; García et al., 2008), that can increase suspended particulate matter concentrations and transport of organic matter (Genin, 2004; Canals et al., 2006; Company et al., 2008). They intercept the path of slope currents flowing along isobaths (Font et al., 1988) and can entrain particles (including POM) travelling along the margin (Huthnance, 1995). Upwelling has been observed on the continental slope of the Porcupine Bank at  $51^\circ 41' \text{N}$  and  $14^\circ 39' \text{W}$  in 464 m water depth (Dickson and Mccave, 1986) and has since been corroborated in the PBC by Wheeler et al. (2021). Downwelling above canyons commonly occur, further intensifying the ability of canyons to trap particles transported by long-shore currents (Granata et al., 1999; Palanques et al., 2005; Allen and Madron, 2009). In the PBC, Ekman downwelling may be induced by northerly gales combined with the northward flow of the slope current (e.g. Ratmeyer et al., 2006). These processes can enrich benthic productivity within canyons resulting in increased biodiversity (Rowe et al., 1982; Ryan et al., 2005; Schiebel and Hemleben, 2007; Vetter et al., 2010). Thus, adjacent to the margins of the surveyed submarine canyon where large mounds occur, resides a diverse interplay of downwelling and upwelling currents. These water masses are rich in particles including organic matter. For benthic sessile filter feeders, such as CWCs, this enrichment mechanism on the continental margin provides essential food and sediment supply.

Several studies have captured the important role of water mass boundaries on CWC mound formation in the NE Atlantic (e.g. Freiwald, 2002; Dullo et al., 2008; Flügel et al., 2014). The re-initiation of CWCs at the Porcupine Seabight during the Holocene is likely linked to the strengthening of the Eastern North Atlantic Water-Mediterranean Outflow Water-Transition Zone (ENAW-MOW-TZ; Wienberg et al., 2020). Within this boundary, explorative ROV surveys have observed dense and diverse populations of CWCs growing upright on the slopes of the PBC, providing clear evidence that food is readily available (Wheeler et al., 2017; Lim et al., 2018; Appah et al., 2020). A limiting factor for mound development on the slopes of the PBC is the steep topography, which in parts exceeds  $70^\circ$ . Instead, mounds favour the shallower adjacent banks of the continental margin (Fig. 1b), a few hundred metres above the ENAW-MOW boundary. This suggests that the PBC plays a pivotal role in upwelling and acts as a conduit for enhanced particulate organic matter resuspension and supply. Conversely, these currents may also have a degradative control on CWC mound formation. Where coral rubble is the dominant facies type, current speeds reach up to  $114 \text{ cm s}^{-1}$  (Lim et al., 2020). In comparison, where live coral framework dominates, current speeds fail to exceed  $66 \text{ cm s}^{-1}$ . In this instance, flows which may originate from upwelling or downwelling merely provide food and nutrients to corals, rather than having an erosive impact.

Coral framework functions as a sediment trap for lateral and vertical advected sediments, thus higher ARs coincide with favourable growth conditions that have a sufficient sediment supply (Genin et al., 1986; Mienis et al., 2007; Davies et al., 2009; Frank et al., 2009; Mienis et al., 2009; Douarin et al., 2013; Wang et al., 2021). A comparison of AR the wPB and PBC across a comparable timescale (in this instance between 6.7 and 5.6 ka BP; see Fig. 4) shows that advantageous conditions are present adjacent to the canyon ( $68 \text{ cm ka}^{-1}$  in the PBC versus  $31.5 \text{ cm ka}^{-1}$  in the wPB). Corals from core RH\_VC7 (i.e. from the PBC; see Fig. 1) are mainly observed in the living position (Fig. 2), whereas corals from core CE\_VC1 (i.e. from the wPB) are rather found as coral rubble. This suggests that proximity to the canyon results in faster mound development due to higher food and sediment availability.

Moreover, the PBC<sub>Middle</sub> Assemblage of RH\_VC7 is characteristic of higher organic matter flux than both the wPB<sub>Early</sub> and wPB<sub>Middle</sub>

assemblages in core CE\_VC1. Indeed, the infaunal *G. subglobosa* and *N. umbonifera*, which are regarded as indicator species for positive fluxes in organic matter in response to bloom events in the NE Atlantic (Corliss, 1979; Gooday, 1994; Mackensen et al., 1995; Fariduddin and Loubere, 1997; Altenbach et al., 1999; Fontanier et al., 2002; Suhr et al., 2003; Fontanier et al., 2005; Murray, 2006a; Alve, 2010), are more abundant in the PBC<sub>Middle</sub> Assemblage of RH\_VC7 and are identified as suitable discriminating species between assemblages (see Appendix H). The PBC<sub>Middle</sub> Assemblage also reveals higher proportions of the shallow infaunal *U. auberiana* (Fig. 4), a species associated with steady to episodic labile organic content (higher protein and phytopigment content; see Gooday and Hughes, 2002, Suhr et al., 2003, Gooday, 2019). The high abundance of this species is strong evidence that higher quality organic matter is more available within closer proximity to the canyon. Thus, increased food supply seems to be the most important ecological parameter controlling the BFAs on the mound summits.

Multivariate analysis confirms that site and age account for 43% of the variance within the BFAs across both sites. These two factors are highly significant, with a  $p$ -value of  $<0.0001$  (Table 4). Site is the single most significant contributor to the model, indicating that the distance from the canyon plays an important role, perhaps along with other site-specific abiotic factors. Interestingly, the site contribution to variance over a short distance of 1 km between the two coral mound summits outweighs the temporal contribution to variance for 2–4 thousand years. Respectively, the environmental differences between the canyon lip and 1 km onto the shelf as evidenced by the foraminiferal assemblages present is much greater than the environmental change experienced at both sites over the last few thousand years. However, the age model still explains 14% of the variation in the community data of the global model and is highly significant (Table 4). The error introduced through the Bayesian age model and shorter core record captured in core VC7 may affect this. Nevertheless, its significance among multiple abiotic factors highlights the observable shift in BFAs across time, specifically at the 8.2 ka boundary. The higher temporal contribution at the longer wPB core site when temporal effects are tested for each core independently ( $R^2_{VC1} = 0.31$  compared to  $R^2_{VC7} = 0.24$  at the PBC) stresses the importance of the 8.2 ka event as a tipping point. Planktic  $d^{13}C$  could only be tested on a smaller subset of the data because there were insufficient foraminifera to obtain stable isotope ratios in all core subsamples (see Appendix G). However, the variable was selected for at a 0.1  $\alpha$ -level and corresponds with the BFA in core RH\_VC7 (Fig. 4), suggesting a more enriched organic signal is seen along the PBC canyon lip compared to the wPB. These findings, alongside higher AR, show that the canyon's lip is a highly favourable location for CWC development in the wPB and PBC region. This indicates that areas adjacent to submarine canyons, such as the PBC, may act as refuges for CWCs, providing habitable conditions throughout periods of stress. These findings are summarised below in Fig. 7.

## 5. Conclusion

Strong bottom currents resulted in slow mound development in the wPB during the Early Holocene. Regional climate-driven processes reduced sediment supply to the wPB during the Early Holocene–mid-Holocene transition, which further slowed mound development. Between 7.1 and 6.7 ka BP, a rapid formation phase in the wPB mound was observed and is likely linked with the major oceanographic reorganisation in the NE Atlantic. Finally, between 6.7 and 5.6 ka BP, the wPB mound formation reduces rapidly, although the contemporaneous PBC

mound formed at least twice as fast as the wPB mound. The succession of CWCs in the region can be linked with enhanced shelf currents, the existence of the ENAW-MOW-TZ and crucially, upwelling and downwelling caused by canyon topography. These mechanisms collectively create an ideal setting for CWC habitats, such as along the lip of the PBC. Furthermore, proximity to the canyon results in higher sediment supply and food availability.

Methods used in this study (i.e. ROV-vibrocoring) offer convincing results when aiming to compare two closely situated sites and should be considered in future endeavours. Furthermore, we recommend the use of wider vibrocores, which would alleviate any preferential alignment of coral pieces during coring acquisition, that may affect CPP classification. Open questions remain regarding a) the initial colonization of CWCs in the region and b) their ability to survive during glacial intervals. Both questions would be rectified through the acquisition of longer cores that extend further back in time.

To date, no CWCs have been found living during glacial periods along the margin. Evidence provided in this study suggests that submarine canyons offer likely habitable conditions for CWCs, as they are an enriched source of food and sediment. Coring coral occupied canyons in the NE Atlantic, such as the PBC, could thus test and substantiate the hypothesis that they offer a refuge for CWCs during glacial periods. Furthermore, a detailed hydrodynamic model of the canyon would greatly improve our understanding of upwelling/downwelling processes that control nutrient supply to the mounds.

## Declaration of Competing Interest

The authors declare that they have no known competing financial interests or personal relationships that could have appeared to influence the work reported in this paper.

## Data availability

Data used in this article can be found online at <https://doi.org/10.1594/PANGAEA.945476>.

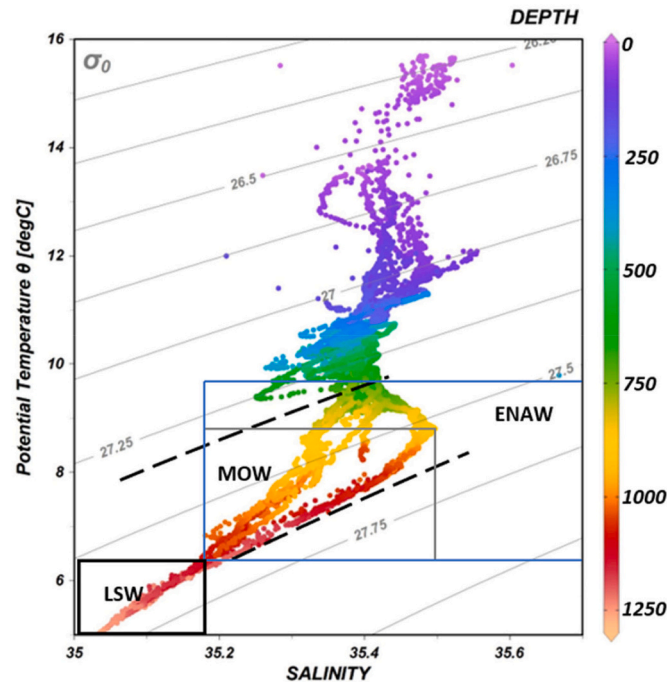
## Acknowledgements

The authors would like to thank Mr. Paddy O'Driscoll (Marine Institute) for his assistance in developing the vibrocoring unit used in this study. Luke O'Reilly would like to thank the comments and suggestions provided by two anonymous reviewers, which greatly improved the quality of the manuscript. All shiptime is funded under the National Development Plan (2019), National Grant-aided Shiptime Programme. Luke O'Reilly is funded by Science Foundation Ireland project "MMMonKey\_Pro" ([grant number: 16/IA/4528]), which is co-funded by the Geological Survey, Ireland and Marine Institute. Felix Butschek is funded from the European Union's Horizon 2020 research and innovation program under grant agreement No 818123 (iAtlantic). Jürgen Titschack received funding from the Cluster of Excellence "The Ocean Floor—Earth's Uncharted Interface" (Germany's Excellence Strategy—EXC-2077-390741603 of the DFG). The authors would like to thank the University of Lyon and the University of Fribourg for access to the optical microscope and SEM. Luke O'Reilly would like to thank the MMonKey\_Pro team members and members of the Marine Geosciences Research Group at UCC and scientific parties, officers, and crew of cruise RH17002 and CE18011.



## Appendix A. Appendices

### A.1. Water mass properties



Taken from Appah et al. (2020): T-S plot of CTD data with density contours to characterise the water mass properties through a 1200 m depth from the surface water in the PBC: ENAW (Eastern North Atlantic Water), MOW (Mediterranean Outflow Water), LSW (Labrador Sea Water). Space between broken lines reveal the predicted density envelope for NE Atlantic CWCs (Dullo et al., 2008).

### A.2. Computed tomography processing procedures

The raw DICOM data were processed with the ZIB edition of Amira software (version 2018.36; Stalling et al., 2005; <http://amira.zib.de>). Within Amira, the CT scans of the cores liners, including approx. 2 mm of the core rims, were removed from the data set (using a combination of the segmentation editor and the Arithmetic tool) to remove density artefacts resulting from the coring process. Isotropic voxels were generated by reducing each voxel size to 0.2 mm in all dimensions, correcting for partial volume averaging errors. An isosurface was created to visualise the dataset in 3D space, which was then re-positioned interactively through the live module in the software to account for any offsets during scanning. The resampled dataset was reformatted using the Lanczos interpolation method, which tries to approximate a low-pass filter that is in accordance with the sampling theorem, thus sharpening images (see Amira Reference Guide, Visage Imaging). The macroscopic sediment components (>ca 1 mm) were quantified in each CT-slice with the segmentation editor (Threshold 1370 value: 1400) and the MaterialStatistics module (volume per slice). Further evaluation of these components was performed with the ContourTreeSegmentation algorithm (Threshold: 1400; Persistence Value: 1100), which is based on the concept of contour trees and functions similar to hierarchical watershed segmentation and topological persistence (see (Titschack et al., 2015) and references therein). This created an automatic segmentation of the 3D macroscopic components. At this stage, the CT results were visually checked to assess if the 3D segmentation was correctly applied. The ShapeAnalysis module and GrainSizeDistribution module were used to characterise each component. Clast length [unit:  $\phi = \log_2 [\text{length (mm)}/1 \text{ mm}]$ ] was used to analyse clast size. Therefore, every clast within a window of 51 CT-slices (about 1 cm) was counted and the result was added to a spreadsheet. The analysing window was moved slice by slice. Furthermore, the ShapeAnalysis module and GrainAngleDistribution module were used to characterise the z-orientation of the major axis of each clast in a similar manner, whereby horizontal =  $0^\circ$  and vertical =  $90^\circ$ . Additionally, X-ray density of the matrix sediment was determined by calculating the mean value and its standard deviation of the matrix sediment per slice. The final results were exported to a spreadsheet.

### A.3. Carbonate dissolution and organic matter removal procedures

Subsamples of roughly 1 cm<sup>3</sup> of sediment were taken from the core at 5 cm intervals. Each sample was assigned to a beaker and oven-dried at 60 °C for 24 h. When dry, the sample was left cool for 30 min. At this stage, any large bioclasts (>2 mm) which may have been extracted in the initial sampling stage were removed. 200 ml of distilled water and 10 ml of 10% HCl were added to each beaker and heated to 90 °C for 2 h to dissolve the carbonate fraction of the sample. If an incomplete reaction occurred, extra heat and HCl were added. The samples were given 1 h to settle. Any remaining solution was removed with a syringe, taking care not to disturb any sediment on the bottom of the beaker. The samples were then oven dried at 60 °C for 24 h. The aforementioned steps were then repeated, using a solution of 10 ml of 10% H<sub>2</sub>O<sub>2</sub> to oxidise organic matter from the samples. When complete, the samples were dried at 60 °C for 24 h. Each sample was sieved through a 2 mm sieve, removing larger lithoclasts 1402 from the sample. These clasts were weighed and stored in individual containers. The sieved samples were stored in individual test tubes with 30 ml of distilled water and a solution of 5.51404 g/l sodium tetraphosphate for at least 24 h. This chemical dispersant prevented grains from aggregating during the grain-size measurements as well as after sonication.

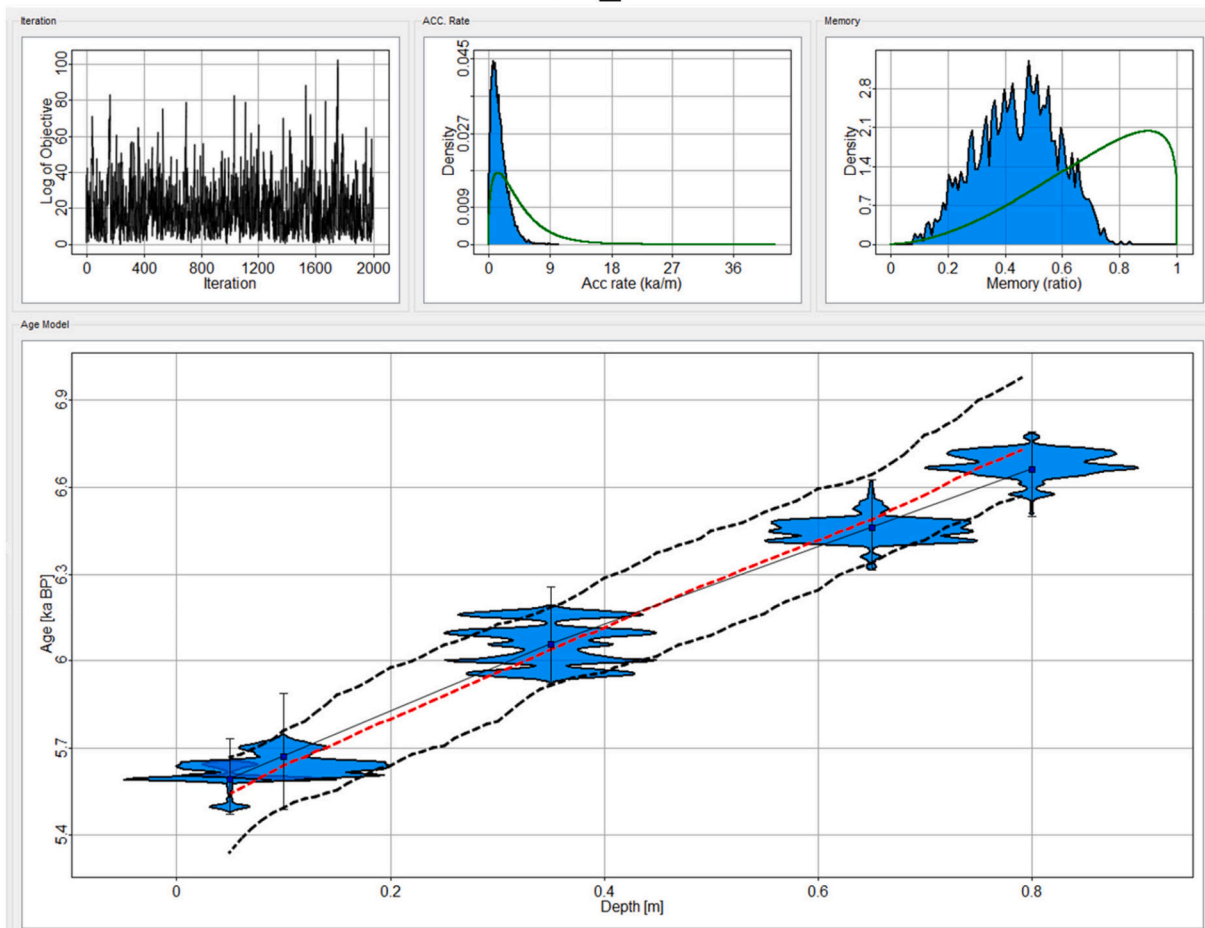
### A.4. Grain size analysis and operating procedures

Prior to analysis, method building was required to ensure the best representative results were retrieved with the MS3000 by optimising the machine parameters. Variations on obscuration %, stirrer speed and ultrasonic duration were determined using a fine and coarse sediment fraction, insuring a representative control on the experiment. When a consistent relative standard deviation (RSD) value <2% was yielded, these parameters constructed standard operating procedures for the study (see table below). All samples showed stability using these methods. The measurement procedure in the MS3000 was carried out with deionized water. Prior to adding the sample to the MS3000 wet dispersion unit, the sample was shaken by hand for approximately 10 s to minimize flocculation of particles. The sample was then introduced into the wet dispersion unit using a 1 ml pipette, allowing the addition to occur in a controlled manner. Before accepting a grain size value, the data was first inspected for anomalous results which could be attributed to air bubbles or operational errors.

| PSA Operating Procedures              |                                   |                                      |
|---------------------------------------|-----------------------------------|--------------------------------------|
| <b>Particle Type</b>                  |                                   |                                      |
| Non-spherical                         |                                   |                                      |
| <b>Material Properties</b>            |                                   |                                      |
| Quartz                                |                                   |                                      |
| <i>Refractive Index: 1.543</i>        | <i>Absorption Index: 0.01</i>     | <i>Density (g/cm<sup>3</sup>): 1</i> |
| <b>Dispersant Properties</b>          |                                   |                                      |
| Water                                 |                                   |                                      |
| <i>Refractive Index: 1.33</i>         | <i>Level Sensor threshold: 75</i> |                                      |
| <b>Measurement Duration (seconds)</b> |                                   |                                      |
| Red                                   |                                   |                                      |
| <i>Background: 10</i>                 | <i>Sample: 10</i>                 |                                      |
| Blue                                  |                                   |                                      |
| <i>Background: 10</i>                 | <i>Sample: 10</i>                 |                                      |
| <b>Number of measurements</b>         |                                   |                                      |
| 5                                     |                                   |                                      |
| <b>Clean Type</b>                     |                                   |                                      |
| Normal (3 clean cycles)               |                                   |                                      |
| <b>Analysis settings</b>              |                                   |                                      |
| General purpose                       |                                   |                                      |
| <b>Stirrer Speed (rpm)</b>            |                                   |                                      |
| Fine: 2400                            | Coarse: up to 3400                |                                      |
| <b>Obscuration%</b>                   |                                   |                                      |
| Fine: 10–15%                          | Coarse: 15–20%                    |                                      |
| <b>Ultrasonication (seconds)</b>      |                                   |                                      |
| Fine: 120                             | Coarse: up to 240                 |                                      |

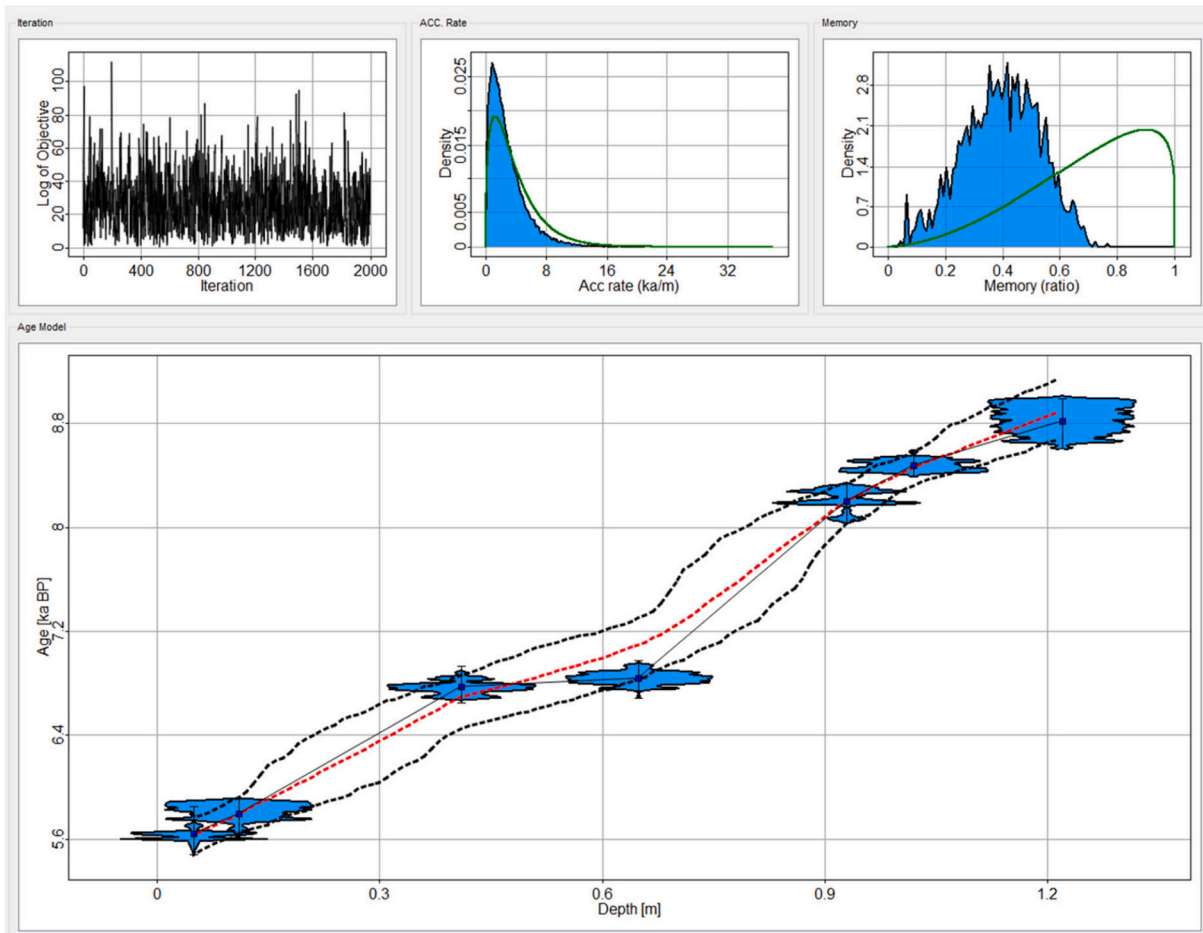
A.5. Age models parameters RH\_VC7 and CE\_VC1

### RH\_VC7





# CE\_VC1



## A.6. Multiproxy environmental data

| Core   | Depth [cmbfs] | MGS [mm] | MSS [mm] | Planktic $\delta^{13}\text{C}$ [‰] | Planktic $\delta^{18}\text{O}$ [‰] | Benthic $\delta^{13}\text{C}$ [‰] | Benthic $\delta^{18}\text{O}$ [‰] | CPP            |
|--------|---------------|----------|----------|------------------------------------|------------------------------------|-----------------------------------|-----------------------------------|----------------|
|        | 0             | 10.2     | 18.5     | -0.46                              | 1.03                               | 1.17                              | 1.45                              | A1             |
|        | 5             | 10.3     | 19.9     | -0.29                              | 0.79                               | 1.36                              | 1.53                              | A1             |
|        | 10            | 7.9      | 17.6     | -0.17                              | 1.19                               | 1.44                              | 1.81                              | A1             |
|        | 15            | 7.9      | 18.5     | -0.19                              | 1.24                               | 1.5                               | 1.68                              | A1             |
|        | 20            | 9.6      | 18.5     | -0.26                              | 1.24                               | 1.52                              | 1.6                               | A1             |
|        | 25            | 15.5     | 19.4     | -0.18                              | 1.15                               | 1.48                              | 1.56                              | A1             |
|        | 30            | 8.0      | 19.1     | -0.29                              | 1.31                               | 1.51                              | 1.54                              | B1             |
|        | 35            | 8.8      | 20.2     | -0.48                              | 1.2                                | 1.39                              | 1.75                              | A2             |
|        | 40            | 8.6      | 17.7     | -0.14                              | 1.63                               | 1.49                              | 1.6                               | A2             |
|        | 45            | 11.7     | 20.1     | -0.21                              | 1.12                               | 1.51                              | 1.64                              | A2             |
|        | 50            | 9.3      | 19.1     | -0.09                              | 1.14                               | 1.57                              | 1.66                              | A2             |
|        | 55            | 7.5      | 19.1     | -0.16                              | 1.09                               | 1.47                              | 1.64                              | A2             |
|        | 60            | 7.4      | 18.4     | -0.27                              | 1.34                               | 1.65                              | 1.63                              | A2             |
|        | 65            | 7.9      | 18.0     | -0.1                               | 1.33                               | 1.55                              | 1.67                              | B2             |
|        | 70            | 8.1      | 18.0     | -0.32                              | 1.05                               | 2.08                              | 2.11                              | B2             |
|        | 75            | 9.2      | 18.5     | -0.03                              | 1.24                               | 1.7                               | 1.65                              | B2             |
|        | 80            | 8.8      | 18.4     | 0.03                               | 1.27                               | 1.47                              | 1.63                              | A <sub>1</sub> |
|        | 85            | 8.4      | 19.5     | -0.3                               | 1.03                               | 1.41                              | 1.61                              | A <sub>1</sub> |
|        | 90            | 7.4      | 18.7     | -0.33                              | 1.28                               | 1.44                              | 1.65                              | A <sub>1</sub> |
|        | 95            | 9.5      | 18.6     | -0.34                              | 1.16                               | 1.46                              | 1.83                              | A <sub>1</sub> |
|        | 100           | 13.5     | 21.4     | -0.4                               | 0.82                               | -                                 | -                                 | A <sub>1</sub> |
|        | 105           | 8.1      | 19.2     | -0.05                              | 1.06                               | -                                 | -                                 | C <sub>1</sub> |
|        | 110           | 11.5     | 20.0     | -0.59                              | 1.19                               | -                                 | -                                 | C <sub>1</sub> |
|        | 115           | 8.6      | 20.4     | -0.55                              | 1.43                               | -                                 | -                                 | C <sub>1</sub> |
|        | 120           | 7.2      | 17.1     | -0.37                              | 1.14                               | -                                 | -                                 | A <sub>2</sub> |
| CE_VC1 | 125           | 7.1      | 18.3     | -0.43                              | 0.96                               | -                                 | -                                 | A <sub>2</sub> |

(continued on next page)

(continued)

| Core   | Depth [cmbsf] | MGS [mm] | MSS [mm] | Planktic $\delta^{13}\text{C}$ [‰] | Planktic $\delta^{18}\text{O}$ [‰] | Benthic $\delta^{13}\text{C}$ [‰] | Benthic $\delta^{18}\text{O}$ [‰] | CPP            |
|--------|---------------|----------|----------|------------------------------------|------------------------------------|-----------------------------------|-----------------------------------|----------------|
|        | 0             | 10.5     | 19.4     | -0.70                              | 0.90                               | 1.10                              | 1.60                              | A <sub>2</sub> |
|        | 5             | 12.1     | 20.5     | -0.74                              | 0.84                               | 1.43                              | 1.37                              | A <sub>2</sub> |
|        | 10            | 12.3     | 21.4     | -                                  | -                                  | -                                 | -                                 | A <sub>2</sub> |
|        | 15            | 9.4      | 18.6     | -                                  | -                                  | -                                 | -                                 | A <sub>2</sub> |
|        | 20            | 10.7     | 19.1     | -                                  | -                                  | -                                 | -                                 | A <sub>2</sub> |
|        | 25            | 8.2      | 18.2     | -0.84                              | 0.87                               | 1.47                              | 1.75                              | B <sub>1</sub> |
|        | 30            | 10.7     | 19.7     | -0.60                              | 1.11                               | 1.53                              | 1.79                              | B <sub>1</sub> |
| RH_VC7 | 35            | 10.7     | 20.3     | -                                  | -                                  | -                                 | -                                 | B <sub>1</sub> |
|        | 40            | 12.4     | 21.2     | -0.52                              | 1.32                               | 1.61                              | 1.71                              | B <sub>1</sub> |
|        | 45            | 11.8     | 20.9     | -0.42                              | 1.25                               | 1.52                              | 1.73                              | B <sub>1</sub> |
|        | 50            | 11.5     | 20.2     | -0.65                              | 1.17                               | 1.64                              | 1.84                              | C <sub>2</sub> |
|        | 55            | 9.9      | 18.7     | -                                  | -                                  | -                                 | -                                 | C <sub>2</sub> |
|        | 60            | 10.0     | 18.9     | -0.58                              | 1.16                               | 1.51                              | 1.73                              | A <sub>3</sub> |
|        | 65            | 12.3     | 20.8     | -0.60                              | 1.33                               | 1.62                              | 1.93                              | A <sub>3</sub> |
|        | 70            | 8.3      | 17.9     | -0.56                              | 1.17                               | 1.48                              | 1.80                              | A <sub>3</sub> |
|        | 75            | 11.5     | 20.9     | -0.33                              | 1.11                               | 1.53                              | 1.77                              | A <sub>3</sub> |

## A.7. Relative abundance of all benthic foraminifera in BFAs

| Species                            | PBC <sub>Middle</sub> rel. Abundance (%) | WPB <sub>Middle</sub> rel. Abundance (%) | WPB <sub>Early</sub> rel. Abundance (%) | Mean rel. Abundance (%) |
|------------------------------------|--|--|---|-------------------------|
| <i>Discanomalina coronata</i>      | 5.49                                     | 5.48                                     | 20.65                                   | 10.54                   |
| <i>Melonis barleeianum</i>         | 6.50                                     | 8.94                                     | 15.43                                   | 10.29                   |
| <i>Trifarina angulosa</i>          | 6.07                                     | 12.11                                    | 6.91                                    | 8.36                    |
| <i>Biloculina globula</i>          | 8.82                                     | 8.41                                     | 4.06                                    | 7.10                    |
| <i>Globocassidulina subglobosa</i> | 14.04                                    | 1.88                                     | 3.56                                    | 6.49                    |
| <i>Cibicides lobatulus</i>         | 5.55                                     | 7.31                                     | 4.88                                    | 5.91                    |
| <i>Hyrrokin sarcophaga</i>         | 5.49                                     | 4.71                                     | 6.49                                    | 5.56                    |
| <i>Uvigerina mediterranea</i>      | 5.15                                     | 9.87                                     | 1.65                                    | 5.56                    |
| <i>Uvigerina pygmae</i>            | 2.57                                     | 6.88                                     | 2.53                                    | 3.99                    |
| <i>Homalohedra williamsoni</i>     | 2.43                                     | 2.35                                     | 2.80                                    | 2.53                    |
| <i>Spiroplectinella sagitulla</i>  | 1.51                                     | 4.66                                     | 1.26                                    | 2.48                    |
| <i>Cassidulina teretis</i>         | 2.88                                     | 1.86                                     | 1.90                                    | 2.22                    |
| <i>Pullenia subcarinata</i>        | 1.45                                     | 2.64                                     | 2.43                                    | 2.17                    |
| <i>Hanzawaia boueana</i>           | 2.75                                     | 1.52                                     | 1.52                                    | 1.93                    |
| <i>Uvigerina auferiana</i>         | 4.76                                     | 0.70                                     | 0.04                                    | 1.83                    |
| <i>Spiroplectinella wrightii</i>   | 1.54                                     | 2.64                                     | 1.23                                    | 1.80                    |
| <i>Eggerella humboldti</i>         | 2.13                                     | 1.49                                     | 0.53                                    | 1.38                    |
| <i>Cassidulina reniforme</i>       | 0.58                                     | 1.66                                     | 1.83                                    | 1.36                    |
| <i>Planulina ariminensis</i>       | 2.01                                     | 0.86                                     | 1.16                                    | 1.34                    |
| <i>Globulina minuta</i>            | 0.71                                     | 0.78                                     | 1.94                                    | 1.14                    |
| <i>Nuttalides umbonifer</i>        | 2.85                                     | 0.08                                     | 0.19                                    | 1.04                    |
| <i>Glandulina ovula</i>            | 0.38                                     | 0.72                                     | 1.53                                    | 0.88                    |
| <i>Oolina melo</i>                 | 0.50                                     | 1.15                                     | 0.88                                    | 0.84                    |
| <i>Bulimina marginata</i>          | 0.66                                     | 1.00                                     | 0.67                                    | 0.78                    |
| <i>Gyroldina soldanii</i>          | 0.75                                     | 0.65                                     | 0.91                                    | 0.77                    |
| <i>Lenticulina orbicularis</i>     | 0.29                                     | 0.59                                     | 1.44                                    | 0.77                    |
| <i>Astrononion stelligerum</i>     | 0.43                                     | 0.49                                     | 1.27                                    | 0.73                    |
| <i>Astrononion tumidum</i>         | 0.82                                     | 0.43                                     | 0.72                                    | 0.66                    |
| <i>Gaudryna rudis</i>              | 0.50                                     | 0.72                                     | 0.63                                    | 0.62                    |
| <i>Spirillina vivipara</i>         | 1.47                                     | 0.12                                     | 0.00                                    | 0.53                    |
| <i>Cibicides refulgens</i>         | 0.77                                     | 0.50                                     | 0.15                                    | 0.47                    |
| <i>Amphycorina scalaris</i>        | 0.13                                     | 0.31                                     | 0.80                                    | 0.41                    |
| <i>Homalohedra eucoata</i>         | 0.34                                     | 0.28                                     | 0.60                                    | 0.41                    |
| <i>Robertinoides bradyi</i>        | 0.12                                     | 0.36                                     | 0.71                                    | 0.40                    |
| <i>Rosalina globularis</i>         | 0.39                                     | 0.23                                     | 0.57                                    | 0.40                    |
| <i>Trifarina bradyi</i>            | 1.13                                     | 0.01                                     | 0.00                                    | 0.38                    |
| <i>Quinqueloculina semiluna</i>    | 0.41                                     | 0.30                                     | 0.40                                    | 0.37                    |
| <i>Oolina globosa</i>              | 0.36                                     | 0.34                                     | 0.39                                    | 0.36                    |
| <i>Globulina rotundata</i>         | 0.10                                     | 0.12                                     | 0.82                                    | 0.35                    |
| <i>Pyrgo sarsi</i>                 | 0.29                                     | 0.39                                     | 0.35                                    | 0.34                    |
| <i>Lenticulina gibba</i>           | 0.54                                     | 0.20                                     | 0.19                                    | 0.31                    |
| <i>Palliolatella semimarginata</i> | 0.52                                     | 0.21                                     | 0.12                                    | 0.29                    |
| <i>Cassidulina carinata</i>        | 0.78                                     | 0.06                                     | 0.00                                    | 0.28                    |
| <i>Hyalinea balthica</i>           | 0.32                                     | 0.23                                     | 0.24                                    | 0.27                    |
| <i>Gavelinopsis praegeri</i>       | 0.28                                     | 0.34                                     | 0.16                                    | 0.26                    |
| <i>Fissurina eburnea</i>           | 0.38                                     | 0.16                                     | 0.12                                    | 0.22                    |
| <i>Oolina lineata</i>              | 0.08                                     | 0.13                                     | 0.29                                    | 0.17                    |
| <i>Karrerella bradyi</i>           | 0.01                                     | 0.25                                     | 0.22                                    | 0.16                    |
| <i>Pyrgo elongata</i>              | 0.01                                     | 0.10                                     | 0.34                                    | 0.15                    |
| <i>Cibicides mundulus</i>          | 0.13                                     | 0.15                                     | 0.16                                    | 0.15                    |
| <i>Quinqueloculina viennensis</i>  | 0.02                                     | 0.18                                     | 0.22                                    | 0.14                    |
| <i>Dentalina sp identified</i>     | 0.07                                     | 0.04                                     | 0.28                                    | 0.13                    |

(continued on next page)

(continued)

| Species                             | PBC <sub>Middle</sub> rel. Abundance (%) | wPB <sub>Middle</sub> rel. Abundance (%) | wPB <sub>Early</sub> rel. Abundance (%) | Mean rel. Abundance (%) |
|-------------------------------------|--|--|---|-------------------------|
| <i>Gaudryna pseudotrochus</i>       | 0.01                                     | 0.11                                     | 0.24                                    | 0.12                    |
| <i>Cycloforina laevigata</i>        | 0.11                                     | 0.07                                     | 0.17                                    | 0.12                    |
| <i>Siphonina reticulata</i>         | 0.17                                     | 0.18                                     | 0.00                                    | 0.12                    |
| <i>Discorbina bertheloti</i>        | 0.01                                     | 0.09                                     | 0.24                                    | 0.12                    |
| <i>Elphidium excavatum</i>          | 0.02                                     | 0.07                                     | 0.25                                    | 0.11                    |
| <i>Cibicides ungerianus</i>         | 0.04                                     | 0.23                                     | 0.06                                    | 0.11                    |
| <i>Bulimina pupoides</i>            | 0.00                                     | 0.06                                     | 0.26                                    | 0.11                    |
| <i>Fissurina annectens</i>          | 0.13                                     | 0.15                                     | 0.04                                    | 0.10                    |
| <i>Bolivina pseudopunctata</i>      | 0.18                                     | 0.04                                     | 0.09                                    | 0.10                    |
| <i>Lagena squamosalata</i>          | 0.03                                     | 0.21                                     | 0.04                                    | 0.09                    |
| <i>Alabaminella weddellensis</i>    | 0.17                                     | 0.00                                     | 0.09                                    | 0.09                    |
| <i>Pyrgo comata</i>                 | 0.18                                     | 0.02                                     | 0.04                                    | 0.08                    |
| <i>Anomalina globulosa</i>          | 0.00                                     | 0.11                                     | 0.12                                    | 0.08                    |
| <i>Glandulonodosaria calomorpha</i> | 0.00                                     | 0.10                                     | 0.12                                    | 0.07                    |
| <i>Triloculina trigonula</i>        | 0.04                                     | 0.14                                     | 0.00                                    | 0.06                    |
| <i>Sigmoilopsis schlumbergeri</i>   | 0.00                                     | 0.12                                     | 0.00                                    | 0.04                    |
| <i>Nonionella turgida</i>           | 0.05                                     | 0.07                                     | 0.00                                    | 0.04                    |
| <i>Spiroloculina dilatata</i>       | 0.02                                     | 0.10                                     | 0.00                                    | 0.04                    |
| <i>Pattellina corrugata</i>         | 0.11                                     | 0.00                                     | 0.00                                    | 0.04                    |
| <i>Dentalina cuvieri</i>            | 0.10                                     | 0.01                                     | 0.00                                    | 0.04                    |
| <i>Cassidulina laevigata</i>        | 0.01                                     | 0.04                                     | 0.04                                    | 0.03                    |
| <i>Quinqueloculina bosciana</i>     | 0.03                                     | 0.04                                     | 0.00                                    | 0.02                    |
| <i>Parafissurina lateralis</i>      | 0.00                                     | 0.07                                     | 0.00                                    | 0.02                    |
| <i>Bolivina dilatata</i>            | 0.06                                     | 0.00                                     | 0.00                                    | 0.02                    |
| <i>Fissurina agassizi</i>           | 0.06                                     | 0.00                                     | 0.00                                    | 0.02                    |
| <i>Homalohedra apiopleura</i>       | 0.01                                     | 0.05                                     | 0.00                                    | 0.02                    |
| <i>Textularia agglutinans</i>       | 0.03                                     | 0.02                                     | 0.00                                    | 0.02                    |
| <i>Chilostomella oolina</i>         | 0.03                                     | 0.02                                     | 0.00                                    | 0.02                    |
| <i>Oolina acuticosta</i>            | 0.00                                     | 0.05                                     | 0.00                                    | 0.02                    |
| <i>Siphonotextularia obesa</i>      | 0.00                                     | 0.04                                     | 0.00                                    | 0.01                    |
| <i>Fissurina sp 1</i>               | 0.02                                     | 0.02                                     | 0.00                                    | 0.01                    |
| <i>Favulina squamosa</i>            | 0.00                                     | 0.04                                     | 0.00                                    | 0.01                    |
| <i>Spiroloculina tenuisepta</i>     | 0.00                                     | 0.03                                     | 0.00                                    | 0.01                    |
| <i>Bulimina aculeata</i>            | 0.01                                     | 0.02                                     | 0.00                                    | 0.01                    |
| <i>Sphaeroidina bulloides</i>       | 0.01                                     | 0.02                                     | 0.00                                    | 0.01                    |
| <i>Globobulimina affinis</i>        | 0.03                                     | 0.00                                     | 0.00                                    | 0.01                    |
| <i>Gyroldina lamarckiana</i>        | 0.00                                     | 0.03                                     | 0.00                                    | 0.01                    |
| <i>Quinqueloculina laevigata</i>    | 0.03                                     | 0.00                                     | 0.00                                    | 0.01                    |
| <i>Triloculina tricarinata</i>      | 0.02                                     | 0.00                                     | 0.00                                    | 0.01                    |
| <i>Discanomalina japonica</i>       | 0.02                                     | 0.00                                     | 0.00                                    | 0.01                    |
| <i>Cornuspira involvens</i>         | 0.01                                     | 0.00                                     | 0.00                                    | 0.00                    |

### A.8. Ecological preferences

Ecological preferences (when known) of dominant benthic foraminiferal species identified in this study. In alphabetical order based on species dominant at both sites, then species dominant only in CE\_VC1, then species dominant only in RH\_VC7.

| Species                       | Living strategy    | Feeding strategy   | Energy  | Other ecological preferences   | References  |
|-------------------------------|--------------------|--|---|--|---|
| <i>Biloculinella globula</i>  | epifaunal          | ?  | ?   | identified in the Mediterranean Sea, the Alboran Sea and the Porcupine Seabight  | (Kaminski et al., 2002, Stalder et al., 2015, Fentimen et al., 2018)  |
| <i>Cibicides lobatulus</i>    | epifaunalattached  | passive suspension feeder, prefers labile components of organic matter | high  | characteristic for the mixed water assemblage, indicative of relatively cold well ventilated benthic environment             | (Sejrup et al., 1981, Williamson et al., 1984, Martins et al., 2006, Murray, 2006b, Margreth et al., 2009, Stalder et al., 2018)  |
| <i>Discanomalina coronata</i> | epifaunal attached | ?  | strong bottom currents up to 26–50 cm s <sup>-1</sup> | attached on hydroids and octocorals, possibly shows preference to coral rubble/dead coral                                    | (Schönfeld, 1997, Schönfeld, 2002a, Schönfeld, 2002b, Hawkes and Scott, 2005, Smeulders et al., 2014)   |
| <i>Hyrrokkin sarcophaga</i>   | epifaunal          | parasitic  | high  | found in aphotic environments, attaches to large suspension feeders living in deep water, even where metabolic rates are low | (Cedhagen, 1994)  |
| <i>Melonis barleeanum</i>     | infaunal           | may feed on low and intermediate quality organic matter                | ?   | found in waters <10 °C which are high in POM, lives in high productivity waters, lives on the redox front                    | (Corliss, 1985, Genin et al., 1986, Caralp, 1989, Loubere, 1991, Fontanier et al., 2005, Murray, 2006a, Fontanier et al., 2008, Koho et al., 2008, Morigi et al., 2012) |
| <i>Planulina ariminensis</i>  | epifaunal attached | suspension feeder  | high  | live on elevated substrates directly exposed to the water masses and flourish where strong currents                          | (Corliss, 1985, Lutze and Thiel, 1989, Schönfeld, 1997, Schönfeld, 2002a, Schönfeld, 2002b)   |

(continued on next page)



(continued)

| Species                            | Living strategy    | Feeding strategy   | Energy | Other ecological preferences  | References  |
|------------------------------------|--------------------|--|--------|---|---|
| <i>Trifarina angulosa</i>          | infaunal           | ?  | high   | mobilize suspended food particles associated with shelf-edge-upper-slope areas under the influence of strong bottom currents  | (Sejrup et al., 1981, Hald and Vorren, 1984, Mackensen et al., 1985, Qvale and Weering, 1985, Austin and Evans, 2000, Schönfeld, 2002a, Mojtahid et al., 2021)  |
| <i>Uvigerina mediterranea</i>      | shallow, infaunal  | ?  | ?      | Dominantly eutrophic. More abundant in the pelagic sediments overlying coral-fragment rich horizons                           | (De Stigter et al., 1998, Altenbach et al., 1999, Fontanier et al., 2002, Murray, 2006a)  |
| <i>Hanzawaia boueana</i>           | epifaunal attached | epiphytic  | high   | identified in the Alboran Sea and Porcupine Seabight  | (Spezzaferri and Coric, 2001, Murray, 2006a, Stalder et al., 2015, Fentimen et al., 2018)   |
| <i>Pullenia subcarinata</i>        | infaunal           | ?  | ?      | ?   |   |
| <i>Spiroplectinella sagittula</i>  | epifaunal          | ?  | ?      | ?   |   |
| <i>Uvigerina pygmae</i>            | infaunal           | ?  | ?      | very tolerant of low oxygen levels  | (Phleger and Soutar, 1973, Boltovskoy and Wright, 1976, Brotsma, 1978, Streeter and Shackleton, 1979, Woodruff and Douglas, 1981, Van Der Zwaan, 1982)  |
| <i>Globocassidulina subglobosa</i> | infaunal           | phytodetritus feeder, preferentially ingests fresh diatoms | ?      | oligotrophic; organic matter rich sediments, indicative of organic matter fluxes of 0.8–60 g m <sup>-2</sup> yr <sup>-1</sup> | (Corliss, 1979, Gooday, 1993, Mackensen et al., 1995, Fariduddin and Loubere, 1997, Altenbach et al., 1999, Fontanier et al., 2002, Suhr et al., 2003, Fontanier et al., 2005, Murray, 2006a, Alve, 2010) |
| <i>Homalohedra borealis</i>        |                    | ?  | ?      | trace amounts identified in the Porcupine Seabight  | (Fentimen et al., 2018)   |
| <i>Nuttalides umbonifer</i>        | infaunal           | ?  | ?      | ?   | (Corliss, 1979, Schnitker, 1980, Corliss, 1985, Corliss and Chen, 1988)   |
| <i>Uvigerina auberiana</i>         | infaunal           | ?  | ?      | very tolerant of low oxygen levels and indicates high organic matter  | (Phleger and Soutar, 1973, Boltovskoy and Wright, 1976, Brotsma, 1978, Streeter and Shackleton, 1979, Woodruff and Douglas, 1981, Van Der Zwaan, 1982, Singh et al., 2021)                                |

## Appendix A. Supplementary data

Supplementary data to this article can be found online at <https://doi.org/10.1016/j.margeo.2022.106930>.

## References

- Addamo, A.M., Vertino, A., Stolarski, J., García-Jiménez, R., Taviani, M., Machordom, A., 2016. Merging Scleractinian genera: the overwhelming genetic similarity between solitary Desmophyllum and colonial Lophelia. *BMC Evol. Biol.* 16 <https://doi.org/10.1186/s12862-016-0654-8>.
- Adkins, J.F., Griffin, S., Kashgarian, M., Cheng, H., Druffel, E.R.M., Boyle, E.A., Lawrence Edwards, R., Shen, C.-C., 2002. Radiocarbon dating of deep-sea corals. *Radiocarbon* 44, 567–580. <https://doi.org/10.1017/S0033822200031921>.
- Alatalo, R.V., 1981. Problems in the measurement of evenness in ecology. *Oikos* 37, 199–204. <https://doi.org/10.2307/3544465>.
- Allen, S.E., Madron, X.D.D., 2009. A review of the role of submarine canyons in deep-ocean exchange with the shelf. *Ocean Sci.* 5, 607–620. <https://doi.org/10.5194/os-5-607-2009>.
- Allen, S.E., Hickey, B.M., 2010. Dynamics of advection-driven upwelling over a shelf break submarine canyon. *J. Geophys. Res.* 115 <https://doi.org/10.1029/2009JC005731>.
- Altenbach, A.V., Pflaumann, U., Schiebel, R., Thies, A., Timm, S., Trauth, M.H., 1999. Scaling percentages and distributional patterns of benthic foraminifera with flux rates of organic carbon. *J. Foraminif. Res.* 29, 173–185.
- Alve, E., 2010. Benthic foraminiferal responses to absence of fresh phytodetritus: A two-year experiment. *Mar. Micropaleontol.* 76, 67–75. <https://doi.org/10.1016/j.marmicro.2010.05.003>.
- Amaro, T., Huvenne, V., Allcock, A.L., Aslam, T., Davies, J.S., Danovaro, R., Stigter, H.C. D., Duineveld, G., Gambi, C., Gooday, A.J., Gunton, L.M., Hall, R.A., Howell, K.L., Ingels, J., Kiriakoulakis, K., Kershaw, C.E., Lavaleye, M.S.S., Robert, K., Stewart, H. A., Rooij, D.V., White, M., Wilson, A.M., 2016. The Whittard canyon: A case study of submarine canyon processes. *Prog. Oceanogr.* 146, 38–57. <https://doi.org/10.1016/j.pocean.2016.06.003>.
- Amblas, D., Ceramicola, S., Gerber, T.P.D., Canals, M., Chiocci, F.L., Dowdeswell, J.A., Harris, P.T., Huvenne, V., Lai, S.Y.J., Lastras, G., Iacono, C.L., Micallef, A., Mountjoy, J.J., Paull, C.K., Puig, P., Sánchez-Vidal, A., 2018. Submarine canyons and gullies. *Submarine Geomorphol.* 251–272 [https://doi.org/10.1007/978-3-319-57852-1\\_14](https://doi.org/10.1007/978-3-319-57852-1_14).
- Anderson, M.J., Ellingsen, K.E., McArdle, B.H., 2006. Multivariate dispersion as a measure of beta diversity. *Ecol. Lett.* 9, 683–693. <https://doi.org/10.1111/j.1461-0248.2006.00926.x>.
- Appah, J., Lim, A., Harris, K., O'Riordan, R., O'Reilly, L., Wheeler, A., 2020. Are non-reef habitats as important to benthic diversity and composition as coral reef and rubble habitats in submarine canyons? Analysis of controls on benthic megafauna distribution in the porcupine Bank canyon, NE Atlantic. *Front. Mar. Sci.* 7 <https://doi.org/10.3389/fmars.2020.571820>.
- Appah, J.K.M., Killeen, O., Lim, A., O'Riordan, R., O'Reilly, L., Wheeler, A.J., 2022. Accumulation of Marine Litter in Cold-Water Coral Habitats: A Comparative Study of Two Irish Special Areas of Conservation, NE Atlantic. *Marine Pollution Bulletin*. <https://doi.org/10.1016/j.marpolbul.2022.113764>.
- Armishaw, J.E., Holmes, R.L., Stow, D., a. V., 2000. The Barra fan: A bottom-current reworked, glacially-fed submarine fan system. *Mar. Pet. Geol.* 17, 219–238. [https://doi.org/10.1016/S0264-8172\(99\)00049-5](https://doi.org/10.1016/S0264-8172(99)00049-5).
- Arzola, R.G., Wynn, R.B., Lastras, G., Masson, D.G., Weaver, P.P.E., 2008. Sedimentary features and processes in the Nazaré and Setúbal submarine canyons, west Iberian margin. *Mar. Geol.* 250, 64–88. <https://doi.org/10.1016/j.margeo.2007.12.006>.
- Aslam, T., Hall, R.A., Dye, S.R., 2018. Internal tides in a dendritic submarine canyon. *Prog. Oceanogr.* 169, 20–32. <https://doi.org/10.1016/j.pocean.2017.10.005>.
- Austin, W.E.N., Evans, J.R., 2000. Ne Atlantic benthic foraminifera: modern distribution patterns and palaeoecological significance. *J. Geol. Soc.* 157, 679–691. <https://doi.org/10.1144/jgs.157.3.679>.
- Barber, D.C., Dyke, A., Hillaire-Marcel, C., Jennings, A.E., Andrews, J.T., Kerwin, M.W., Bilodeau, G., Mcneely, R., Southon, J., Morehead, M.D., Gagnon, J.-M., 1999. Forcing of the cold event of 8,200 years ago by catastrophic drainage of Laurentide Lakes. *Nature* 400, 344–348. <https://doi.org/10.1038/22504>.
- Blaauw, M., Christen, J.A., 2011. Flexible paleoclimate age-depth models using an autoregressive gamma process. *Bayesian Anal.* 6, 457–474. <https://doi.org/10.1214/11-BA618>.
- Blott, S.J., Pye, K., 2001. Gradstat: a grain size distribution and statistics package for the analyses of unconsolidated sediments. *Earth Surf. Process. Landf.* 26, 1237–1248. <https://doi.org/10.1002/esp.261>.
- Boltovskoy, E., Wright, R.C., 1976. *Recent Foraminifera*.

- Brolmsa, M.J., 1978. Quantitative Foraminiferal Analysis and Environmental Interpretation of the Pliocene and Topmost Miocene on the South Coast of Sicily. *Buhl-Mortensen, L., Vanreusel, A., Gooday, A.J., Levin, L.A., Priede, I.G., Buhl-Mortensen, P., Gheerardyn, H., King, N.J., Raes, M.*, 2010. Biological structures as a source of habitat heterogeneity and biodiversity on the Deep Ocean margins. *Mar. Ecol. Prog. Ser.* 31, 21–50. <https://doi.org/10.1111/j.1439-0485.2010.00359.x>.
- Canals, M., Puig, P., Durrieu De Madron, A., Leu, S., Palanques, A., Fabres, J., 2006. Flushing submarine canyons. *Nature* 444, 354–357. <https://doi.org/10.1038/nature05271>.
- Caralp, M.H., 1989. Size and morphology of the benthic foraminifer *Melonis Barleeanum*; relationships with marine organic matter. *J. Foraminif. Res.* 19, 235–245. <https://doi.org/10.2113/gsfjr.19.3.235>.
- Carlson, A.E., Legrande, A.N., Oppo, D.W., Came, R.E., Schmidt, G.A., Anslow, F.S., Licciardi, J.M., Obbink, E.A., 2008. Rapid Early Holocene deglaciation of the Laurentide ice sheet. *Nat. Geosci.* 1, 620–624. <https://doi.org/10.1038/ngeo285>.
- Carlson, A.E., Anslow, F.S., Obbink, E.A., Legrande, A.N., Ullman, D.J., Licciardi, J.M., 2009. Surface-melt driven Laurentide ice sheet retreat during the Early Holocene. *Geophys. Res. Lett.* 36 <https://doi.org/10.1029/2009GL040948>.
- Cedhagen, T., 1994. Taxonomy and biology of *Hyrrokkinn Sarcophaga* gen. Et Sp. N., a parasitic Foraminiferan (Rosalinidae). *Sarsia* 79, 65–82. <https://doi.org/10.1080/00364827.1994.10413549>.
- Chapman, M., 2010. Seasonal production patterns of planktonic foraminifera in the Atlantic Ocean: implications for Paleotemperature and hydrographic reconstructions. *Paleoceanography* 25. <https://doi.org/10.1029/2008PA001708>.
- Company, J.B., Puig, P., Sardà, F., Palanques, A., Latasa, M., Scharek, R., 2008. Climate influence on deep sea populations. *PLoS One* 3, e1431. <https://doi.org/10.1371/journal.pone.0001431>.
- Connolly, T.P., Hickey, B.M., 2014. Regional impact of submarine canyons during seasonal upwelling. *J. Geophys. Res.* 119, 953–975. <https://doi.org/10.1002/2013JC009452>.
- Corbera, G., Lo Iacono, C., Gràcia, E., Grinyó, J., Pierdomenico, M., Huvenne, V., a, I., Aguilar, R., Gili, J.M., 2019. Ecological characterisation of a Mediterranean cold-water coral reef: Cabliers coral Mound Province (Alboran Sea, Western Mediterranean). *Prog. Oceanogr.* 175, 245–262. <https://doi.org/10.1016/j.pocan.2019.04.010>.
- Corliss, B.H., 1979. Quaternary Antarctic bottom-water history: deep-sea benthonic foraminiferal evidence from the Southeast Indian Ocean – inferred bottom-water routes and ecological implications. *Quat. Res.* 12, 271–289. [https://doi.org/10.1016/0033-5894\(79\)90062-0](https://doi.org/10.1016/0033-5894(79)90062-0).
- Corliss, B.H., 1985. Microhabitats of benthic foraminifera within deep-sea sediments. *Nature* 314, 435–438. <https://doi.org/10.1038/314435a0>.
- Corliss, B.H., Chen, C., 1988. Morphotype patterns of Norwegian Sea deep-sea benthic foraminifera and ecological implications. *Geology* 16, 716–719. [https://doi.org/10.1130/0091-7613\(1988\)016%3C0716:MPONSD%3E2.3.CO;2](https://doi.org/10.1130/0091-7613(1988)016%3C0716:MPONSD%3E2.3.CO;2).
- Davies, A.J., Wisshak, M., Orr, J.C., Roberts, J.M., 2008. Predicting suitable habitat for the cold-water coral *Lophelia Pertusa* (Scleractinia). *Deep-Sea Res. I* 55, 1048–1062. <https://doi.org/10.1016/j.dsr.2008.04.010>.
- Davies, A.J., Duineveld, G.C., Lavaleye, M.S., Bergman, M.J., Van Haren, H., Roberts, J.M., 2009. Downwelling and deep-water bottom currents as food supply mechanisms to the cold-water coral *Lophelia Pertusa* (Scleractinia) at the Mingulay reef complex. *Limnol. Oceanogr.* 54, 620–629. <https://doi.org/10.4319/lo.2009.54.2.0620>.
- Davies, J.S., Howell, K.L., Stewart, H.A., Guinan, J., Golding, N., 2014. Defining biological assemblages (biotopes) of conservation interest in the submarine canyons of the south west approaches (offshore United Kingdom) for use in marine habitat mapping. *Deep-Sea Res. II Top. Stud. Oceanogr.* 104, 208–229. <https://doi.org/10.1016/j.dsr2.2014.02.001>.
- Davies, J.S., Stewart, H.A., Narayanaswamy, B.E., Jacobs, C.L., Spicer, J.I., Golding, N., Howell, K.L., 2015. Benthic assemblages of the Anton Dohrn seamount (ne Atlantic): defining deep-sea biotopes to support habitat mapping and management efforts with a focus on vulnerable marine ecosystems. *PLoS One* 10. <https://doi.org/10.1371/journal.pone.0124815>.
- Davies, J., Guillaumont, B., Tempora, F., Vertino, A., Beuck, L., Olafsdottir, S.H., Smith, C.J., Fosså, J., Beld, I.V.D., Savini, A., Rengstorf, A.M., Bayle, C., Bourillet, J., Arnaud-Haond, S., Grehan, A., 2017. A new classification scheme of European cold-water coral habitats: implications for ecosystem-based management of the deep sea. *Deep-Sea Res. Part II* 145, 102–109. <https://doi.org/10.1016/j.dsr2.2017.04.014>.
- De Haas, H., Mienis, F., Frank, N., Richter, T.O., Steinacher, R., De Stigter, H.C., Van Der Land, C., Van Weering, T.C.E., 2009. Morphology and sedimentology of (clustered) cold-water coral mounds at the south Rockall trough margins, ne Atlantic Ocean. *Facies* 55, 1–26. <https://doi.org/10.1007/s10347-008-0157-1>.
- De Leo, F.C., Smith, C.R., Rowden, A.A., Bowden, D.A., Clark, M.R., 2010. Submarine canyons: hotspots of benthic biomass and productivity in the deep sea. *Proc. R. Soc. B Biol. Sci.* 277, 2783–2792. <https://doi.org/10.1098/rspb.2010.0462>.
- De Mol, B., Van Rensbergen, P., Pillen, S., Van Herreweghe, K., Van Rooij, D., McDonnell, A., Huvenne, V., Ivanov, M.K., Swennen, R., Henriot, J.-P., 2002. Large deep-water coral banks in the Porcupine Basin, southwest of Ireland. *Mar. Geol.* 188, 193–231. [https://doi.org/10.1016/S0025-3227\(02\)00281-5](https://doi.org/10.1016/S0025-3227(02)00281-5).
- De Rijk, S., Jorissen, F.J., Rohling, E.J., Troelstra, S.R., 2000. Organic flux control on bathymetric zonation of Mediterranean benthic foraminifera. *Mar. Micropaleontol.* 40, 151–166. [https://doi.org/10.1016/S0377-8398\(00\)00037-2](https://doi.org/10.1016/S0377-8398(00)00037-2).
- De Stigter, H.C., Jorissen, F.J., Zwaan, G.J.V.D., 1998. Bathymeric distribution and microhabitat partitioning of live (rose Bengal stained) benthic foraminifera along a shelf to bathyal transect in the southern Adriatic Sea. *J. Foraminif. Res.* 28, 40–65.
- Dickson, R.R., Mccave, I.N., 1986. Nephroid layer on the continental slope west of porcupine Bank. *Deep-Sea Res. Part A* 33, 791–818. [https://doi.org/10.1016/0198-0149\(86\)90089-0](https://doi.org/10.1016/0198-0149(86)90089-0).
- Dorschel, B., Hebbeln, D., Rüggeberg, A., Dullo, W.-C., Freiwald, A., 2005. Growth and erosion of a cold-water coral covered carbonate mound in the Northeast Atlantic during the Late Pleistocene and Holocene. *Earth Planet. Sci. Lett.* 233, 33–44. <https://doi.org/10.1016/j.epsl.2005.01.035>.
- Dorschel, B., Wheeler, A.J., Huvenne, V., De Haas, H., 2009. Cold-water coral mounds in an erosive environmental setting: Tobi side-scan sonar data and Rov video footage from the northwest porcupine Bank, ne Atlantic. *Mar. Geol.* 264, 218–229. <https://doi.org/10.1016/j.margeo.2009.06.005>.
- Douarin, M., Elliot, M., Noble, S.R., Sinclair, D., Henry, L.-A., Long, D., Moreton, S.G., Murray Roberts, J., 2013. Growth of north-East Atlantic cold-water coral reefs and mounds during the Holocene: a high resolution U-series and 14c chronology. *Earth Planet. Sci. Lett.* 375, 176–187. <https://doi.org/10.1016/j.epsl.2013.05.023>.
- Dray, S., Bauman, D., Blanchet, G., Borcard, D., Clappe, S., Guénard, G., Jombart, T., Larocque, G., Legandre, P., Madi, N., Wagner, H.H., 2022. ADESPATIAL: Multivariate multiscale spatial analysis. 0.3-20. <https://CRAN.R-project.org/package=adespatial>.
- Dullo, W.C., Flögel, S., Rüggeberg, A., 2008. Cold-water coral growth in relation to the hydrography of the Celtic and Nordic European continental margin. *Mar. Ecol. Prog. Ser.* 371, 165–176. <https://doi.org/10.3354/meps07623>.
- Ellett, D.J., Martin, J.H.A., 1973. The physical and chemical oceanography of the Rockall channel. *Deep-Sea Res. Oceanogr. Abstr.* 20, 585–625. [https://doi.org/10.1016/0011-7471\(73\)90030-2](https://doi.org/10.1016/0011-7471(73)90030-2).
- Fariduddin, M., Loubere, P.W., 1997. The surface ocean productivity response of deeper water benthic foraminifera in the Atlantic Ocean. *Mar. Micropaleontol.* 32, 289–310. [https://doi.org/10.1016/S0377-8398\(97\)00026-1](https://doi.org/10.1016/S0377-8398(97)00026-1).
- Fentimen, R., Rüggeberg, A., Lim, A., Kateb, A.E., Foubert, A., Wheeler, A.J., Spezzaferrì, S., 2018. Benthic foraminifera in a deep-sea high-energy environment: the Moira mounds (porcupine Seabight, Sw of Ireland). *Swiss J. Geosci.* 111, 561–572. <https://doi.org/10.1007/s00015-018-0317-4>.
- Fentimen, R., Feenstra, E.J., Rüggeberg, A., Vennemann, T.W., Hajdas, I., Adatte, T., Van Rooij, D., Foubert, A., 2020a. Cold-water coral mound archive provides unique insights into intermediate water mass dynamics in the Alboran Sea during the last deglaciation. *Front. Mar. Sci.* 7 <https://doi.org/10.3389/fmars.2020.00354>.
- Fentimen, R., Lim, A., Rüggeberg, A., Wheeler, A.J., Van Rooij, D., Foubert, A., 2020b. Impact of bottom water currents on benthic foraminiferal assemblages in a cold-water coral environment: the Moira mounds (ne Atlantic). *Mar. Micropaleontol.* 154, 101799. <https://doi.org/10.1016/j.marmicro.2019.101799>.
- Fentimen, R., Schmiedl, G., Rüggeberg, A., Foubert, A., 2021. Benthic foraminiferal faunas associated with cold water coral environments in the North Atlantic realm. *Deposit. Record* 7, 223–255. <https://doi.org/10.1002/dep2.149>.
- Fernandez-Arcaya, U., Ramirez-Llodra, E., Aguzzi, J., Allcock, A.L., Davies, J.S., Dissanayake, A., Harris, P.T., Howell, K.L., Huvenne, V., Macmillan-Lawler, M., Martín, J., Menot, L., Nizinski, M.S., Puig, P., Rowden, A.A., Sanchez, F., Van Den Beld, I.M.J., 2017. Ecological role of submarine canyons and need for canyon conservation: a review. *Front. Mar. Sci.* 4, 1–26. <https://doi.org/10.3389/fmars.2017.00005>.
- Findlay, H.S., Hennige, S., Wicks, L.C., Navas, J.M., Woodward, E.M.S., Roberts, J.M., 2014. Fine-scale nutrient and carbonate system dynamics around cold-water coral reefs in the Northeast Atlantic. *Sci. Rep.* 4 <https://doi.org/10.1038/srep03671>.
- Fink, H.G., Wienberg, C., Hebbeln, D., Mcgregor, H.V., Schmiedl, G., Taviani, M., Freiwald, A., 2012. Oxygen control on Holocene cold-water coral development in the eastern Mediterranean Sea. *Deep-Sea Res. I Oceanogr. Res. Pap.* 62, 89–96. <https://doi.org/10.1016/j.dsr.2011.12.013>.
- Flögel, S., Dullo, W.C., Pfannkuche, O., Kiriakoulakis, K., Rüggeberg, A., 2014. Geochemical and physical constraints for the occurrence of living cold-water corals. *Deep-Sea Res. Part II* 99, 19–26. <https://doi.org/10.1016/j.dsr2.2013.06.006>.
- Flügel, E.A., 2004. *Microfacies of Carbonate Rocks: Analysis. Interpretation and Application*. Springer, Berlin, Heidelberg.
- Font, J., Salat, J., Tintoré, J., 1988. Permanent features of the circulation in the Catalan Sea. *Oceanol. Acta Spec. Issue* 16–20 (<https://archimer.ifremer.fr/doc/00267/37808/>).
- Fontanier, C., Jorissen, F.J., Licari, L., Alexandre, A., Anschutz, P., Carbonel, P., 2002. Live benthic foraminiferal faunas from the Bay of Biscay: faunal density, composition, and microhabitats. *Deep-Sea Res. I Oceanogr. Res. Pap.* 49, 751–785. [https://doi.org/10.1016/S0967-0637\(01\)00078-4](https://doi.org/10.1016/S0967-0637(01)00078-4).
- Fontanier, C., Jorissen, F.J., Chaillou, G., Anschutz, P., Grémare, A., Griveaud, C., 2005. Live foraminiferal faunas from a 2800 M deep lower Canyon Station from the Bay of Biscay: faunal response to focusing of refractory organic matter. *Deep-Sea Res. I Oceanogr. Res. Pap.* 52, 1189–1227. <https://doi.org/10.1016/j.dsr.2005.01.006>.
- Fontanier, C., Jorissen, F.J., Lansard, B., Mouret, A., Buscail, R., Schmidt, S., Kerhervé, P., Buron, F.F., Zaragosi, S., Hunault, G., Ernoult, E., Artero, C., Anschutz, P., Rabouille, C., 2008. Live foraminifera from the open slope between grand Rhône and petit Rhône canyons (gulf of lions, Nw Mediterranean). *Deep-Sea Res. I Oceanogr. Res. Pap.* 55, 1532–1553. <https://doi.org/10.1016/j.dsr.2008.07.003>.
- Frank, N., Ricard, E., Lutringer-Paquet, A., Van Der Land, C., Colin, C., Blamart, D., Foubert, A.T.G., Van Rooij, D., Henriot, J.-P., De Haas, H., Van Weering, T.C.E., 2009. The Holocene occurrence of cold water corals in the ne Atlantic: implications for coral carbonate mound evolution. *Mar. Geol.* 266, 129–142. <https://doi.org/10.1016/j.margeo.2009.08.007>.
- Frank, N., Freiwald, A., López Correa, M., Wienberg, C., Eisele, M., Hebbeln, D., Van Rooij, D., Henriot, J.-P., Colin, C., Van Weering, T.C.E., De Haas, H., Buhl-Mortensen, P., Roberts, J.M., De Mol, B., Douville, E., Blamart, D., Hatté, C., 2011. Northeastern Atlantic cold-water coral reefs and climate. *Geology* 39, 743–746. <https://doi.org/10.1130/G31825.1>.
- Freiwald, A., 2002. Reef-forming cold-water corals. In: Wefer, G., Billett, D.S.M., Hebbeln, D., Jørgensen, B.B., Van Weering, T.C.E. (Eds.), *Ocean Margin Systems*.

- Hanse Conference on Ocean Margin Systems (2000: Delmenhorst, Germany). Springer, Berlin Heidelberg New York.
- Freiwald, A., Schönfeld, J., 1996. Substrate pitting and boring pattern of *Hyrokkina Sarcophaga* Cedhagen, 1994 (foraminifera) in a modern deep-water coral reef mound. *Mar. Micropaleontol.* 28, 199–207. [https://doi.org/10.1016/0377-8398\(96\)00002-3](https://doi.org/10.1016/0377-8398(96)00002-3).
- García, R., Evelen, D.V., Soetaert, K., Thomsen, L., Stigter, H.C.D., Epping, E., 2008. Deposition rates, mixing intensity and organic content in two contrasting submarine canyons. *Prog. Oceanogr.* 76, 192–215. <https://doi.org/10.1016/j.pcean.2008.01.001>.
- Genin, A., 2004. Bio-physical coupling in the formation of zooplankton and fish aggregations over abrupt topographies. *J. Mar. Syst.* 50, 3–20. <https://doi.org/10.1016/j.jmarsys.2003.10.008>.
- Genin, A., Dayton, P.K., Lonsdale, P.F., Spiess, F.N., 1986. Corals on seamount peaks provide evidence of current acceleration over deep-sea topography. *Nature* 322, 59–61. <https://doi.org/10.1038/322059a0>.
- Gooday, A.J., 1993. The biology of deep-sea foraminifera; a review of some advances and their applications in paleoceanography. *PALAIOS* 9, 14–31. <https://doi.org/10.2307/3515075>.
- Gooday, A.J., 1994. The biology of deep-sea foraminifera; a review of some advances and their applications in paleoceanography. *PALAIOS* 9, 14–31. <https://doi.org/10.2307/3515075>.
- Gooday, A.J., 2019. Encyclopedia of Ocean Sciences Deep-Sea Benthic Foraminifera, pp. 684–705. <https://doi.org/10.1016/B978-0-12-409548-9.09071-0>.
- Gooday, A.J., Hughes, J., 2002. Foraminifera associated with Phytodetritus deposits at a bathyal site in the northern Rockall trough (ne Atlantic): seasonal contrasts and a comparison of stained and dead assemblages. *Mar. Micropaleontol.* 46, 83–110. [https://doi.org/10.1016/S0377-8398\(02\)00050-6](https://doi.org/10.1016/S0377-8398(02)00050-6).
- Granata, T., Vidondo, B., Duarte, C.M., Satta, M.P., García, M.A., 1999. Hydrodynamics and particle transport associated with a submarine canyon off Blanes (Spain), Nw Mediterranean Sea. *Cont. Shelf Res.* 19, 1249–1263. [https://doi.org/10.1016/S0278-4343\(98\)00118-6](https://doi.org/10.1016/S0278-4343(98)00118-6).
- Gregoire, L.J., Payne, A.J., Valdes, P.J., 2012. Deglacial Rapid Sea level rises caused by ice-sheet saddle collapses. *Nature* 487, 219–222. <https://doi.org/10.1038/nature11257>.
- Hald, M., Vorren, T.O., 1984. Modern and Holocene foraminifera and sediments on the continental shelf off Troms, North Norway. *Boreas* 13, 133–154. <https://doi.org/10.1111/j.1502-3885.1984.tb00067.x>.
- Hald, M., Vorren, T.O., 1987. Foraminiferal stratigraphy and environment of late Weichselian deposits on the continental shelf off Troms, northern Norway. *Mar. Micropaleontol.* 12, 129–160. [https://doi.org/10.1016/0377-8398\(87\)90018-1](https://doi.org/10.1016/0377-8398(87)90018-1).
- Hall, R.A., Alford, M.H., Carter, G.S., Gregg, M.C., Lien, R.C., Wain, D.J., Zhao, Z.K., 2014. Transition from partly standing to progressive internal tides in Monterey submarine canyon. *Deep-Sea Res. Part II* 104, 164–173. <https://doi.org/10.1016/j.dsr2.2013.05.039>.
- Hall, R.A., Aslam, T., Huvenne, V., 2017. Partly standing internal tides in a dendritic submarine canyon observed by an ocean glider. *Deep-Sea Res. I Oceanogr. Res. Pap.* 126, 73–84. <https://doi.org/10.1016/j.dsr.2017.05.015>.
- Hawkes, A.D., Scott, D.B., 2005. Attached Benthic Foraminifera as Indicators of Past and Present Distribution of the Coral *Primnoa Resedaeformis* on the Scotian Margin. Springer, Berlin, Heidelberg.
- Hebbeln, D., Samankassou, E., 2015. Where did ancient carbonate mounds grow — in bathyal depths or in shallow shelf waters? *Earth Sci. Rev.* 145, 56–65. <https://doi.org/10.1016/j.earscirev.2015.03.001>.
- Hebbeln, D., Van Rooij, D., Wienberg, C., 2016. Good Neighbours shaped by vigorous currents: cold-water coral mounds and Contourites in the North Atlantic. *Mar. Geol.* 378, 171–185. <https://doi.org/10.1016/j.margeo.2016.01.014>.
- Hill, M.O., 1973. Diversity and evenness: A unifying notation and its consequences. *Ecology* 54, 427–432. <https://doi.org/10.2307/1934352>.
- Howe, J.A., 1996. Turbidite and Contourite sediment waves in the northern Rockall trough, North Atlantic Ocean. *Sedimentology* 43, 219–234. <https://doi.org/10.1046/j.1365-3091.1996.d01-1.x>.
- Howe, J.A., Stoker, M.S., Stow, D., 1994. Late Cenozoic sediment drift complex, northeast Rockall trough, North Atlantic. *Paleoceanography* 9, 989–999. <https://doi.org/10.1029/94PA01440>.
- Huthnance, J.M., 1995. Circulation, exchange and water masses at the ocean margin: the role of physical processes at the shelf edge. *Prog. Oceanogr.* 35, 353–431. [https://doi.org/10.1016/0079-6611\(95\)80003-C](https://doi.org/10.1016/0079-6611(95)80003-C).
- Huvenne, V., Davies, J.S., 2014. Towards a new and integrated approach to submarine canyon research. *Deep-Sea Res. Part II* 104, 1–5. <https://doi.org/10.1016/j.dsr2.2013.09.012>.
- Huvenne, V.A.L., Beyer, A., De Haas, H., Dekindt, K., Henriot, J.-P., Kozachenko, M., Olu-Le Roy, K., Wheeler, A.J., Participants, T.P.C., Participants, C.C., Freiwald, A., Roberts, J.M., 2005. The seabed appearance of different Coral Bank provinces in the porcupine Seabight, Ne Atlantic: results from Sidescan sonar and Rov seabed mapping. In: *Cold-Water Corals and Ecosystems*. Springer-Verlag, Berlin Heidelberg.
- Huvenne, V., Masson, D.G., Wheeler, A.J., 2009. Sediment dynamics of a Sandy Contourite: the sedimentary context of the Darwin cold-water coral mounds, northern Rockall trough. *Int. J. Earth Sci.* 98, 865–884. <https://doi.org/10.1007/s00531-008-0312-5>.
- Huvenne, V.A., Tyler, P.A., Masson, D.G., Fisher, E.H., Hauton, C., Huhnerbach, V., Le Bas, T.P., Wolff, G.A., 2011. A picture on the wall: innovative mapping reveals cold-water coral refuge in submarine canyon. *PLoS One* 6, e28755. <https://doi.org/10.1371/journal.pone.0028755>.
- Kaminski, M.A., Aksu, A.E., Box, M.R., Hiscott, R.N., Filipescu, S., Al-Salameen, M., 2002. Late glacial to Holocene benthic foraminifera in the Marmara Sea: implications for Black Sea Mediterranean Sea connections following the last deglaciation. *Mar. Geol.* 190, 165–202. [https://doi.org/10.1016/S0025-3227\(02\)00347-X](https://doi.org/10.1016/S0025-3227(02)00347-X).
- Kämpf, J., 2018. On the dynamics of canyon flow interactions. *J. Marine Sci. Eng.* 6, 129. <https://doi.org/10.3390/jmse6040129>.
- Kano, A., Ferdelman, T.G., Williams, T., Henriot, J.-P., Ishikawa, T., Kawagoe, N., Takashima, C., Kakizaki, Y., Abe, K., Sakai, S., Browning, E.L., Li, X., Andres, M.S., Bjerager, M., Cragg, B.A., De Mol, B., Dorschel, B., Foubert, A.T.G., Frank, T.D., Fuwa, Y., Gaillot, P., Gharib, J.J., Gregg, J.M., Huvenne, V., Léonide, P., Mangelsdorf, K., Monteys, X., Novosel, I., O'Donnell, R., Rüggeberg, A., Samarkin, V. A., Sasaki, K., Spivack, A.J., Tanaka, A., Titschack, J., Van Rooij, D., Wheeler, A.J., 2007. Age constraints on the origin and growth history of a deep-water coral mound in the Northeast Atlantic drilled during integrated ocean drilling program expedition 307. *Geology* 35, 1051–1054. <https://doi.org/10.1130/G23917A>.
- Kenyon, N.H., Akhmetzhanov, A.M., Wheeler, A.J., Van Weering, T.C.E., De Haas, H., Ivanov, M.K., 2003. Giant carbonate mounds in the southern Rockall trough. *Mar. Geol.* 195, 3–50. [https://doi.org/10.1016/S0025-3227\(02\)00680-1](https://doi.org/10.1016/S0025-3227(02)00680-1).
- Knutz, P.C., Austin, W.E.N., Jones, E.J.W., 2001. Millennial-scale depositional cycles related to British ice sheet variability and North Atlantic Paleocirculation since 48 Kyr B.P., Barra fan, U.K. Margin. *Paleoceanography* 16, 53–64. <https://doi.org/10.1029/1999PA000483>.
- Knutz, P.C., Jones, E.J.W., Austin, W.E.N., Weering, T.C.E.V., 2002a. Glacimarine slope sedimentation, Contourite drifts and bottom current pathways on the Barra fan, UK North Atlantic margin. *Mar. Geol.* 188, 129–146. [https://doi.org/10.1016/S0025-3227\(02\)00278-5](https://doi.org/10.1016/S0025-3227(02)00278-5).
- Knutz, P.C., Jones, E.J.W., Howe, J.E., Van Weering, T.C.E., Stow, D., a. V., 2002b. Wave-form sheeted Contourite drift on the Barra fan, NW UK continental margin. *Geol. Soc. Lond. Mem.* 22, 85–97. <https://doi.org/10.1144/GSL.MEM.2002.022.01.08>.
- Koho, K.A., García, R., Stigter, H.C.D., Epping, E., Koning, E., Kouwenhoven, T.J., Zwaan, G.J.V.D., 2008. Sedimentary labile organic carbon and pore water redox control on species distribution of benthic foraminifera: a case study from Lisboá Setúbal canyon (southern Portugal). *Prog. Oceanogr.* 79, 55–82. <https://doi.org/10.1016/j.pcean.2008.07.004>.
- Langner, M., Mulitza, S., 2019. Technical note: Paleodataview@ A software toolbox for the collection, homogenization and visualization of marine proxy data. *Clim. Past* 15, 2067–2072. <https://doi.org/10.5194/cp-15-2067-2019>.
- Legendre, P., Anderson, M.J., 1999. Distance based redundancy analysis: testing multispecies Responses in multifactorial ecological experiments. *Ecol. Monogr.* 69, 1–24. [https://doi.org/10.1890/0012-9615\(1999\)069%5B0001:DBRATM%5D2.0.CO;2](https://doi.org/10.1890/0012-9615(1999)069%5B0001:DBRATM%5D2.0.CO;2).
- Legendre, P., De Cáceres, M., Borcard, D., 2010. Community surveys through space and time: testing the space-time interaction in the absence of replication. *Ecology* 91, 262–272. <https://doi.org/10.1890/09-0199.1>.
- Levin, L.A., Etter, R.J., Rex, M., Gooday, A.J., Smith, C.R., Pineda, J., Stuart, C.T., Hessler, R.R., Pawson, D.L., 2001. Environmental influences on regional deep-sea species diversity. *Annu. Rev. Ecol. Syst.* 32, 51–93. <https://doi.org/10.1146/annurev.ecolsys.32.081501.114002>.
- Levin, L.A., Sibuet, M., Gooday, A.J., Smith, C.R., Vanreusel, A., 2010. The roles of habitat heterogeneity in generating and maintaining biodiversity on continental margins: an introduction. *Mar. Ecol.* 31, 1–5. <https://doi.org/10.1111/j.1439-0485.2009.00358.x>.
- Lim, A., O'Reilly, L., Burke, S., Wheeler, A., Appah, J., Summers, G., Harris, K., Shine, A., Booloukos, C., McAleer, A., Conti, L., Holland I Rov Technical Team, Officers and Crew of the Rv Celtic Explorer, 2018. Controls of Cold-Water Coral Habitats in Submarine Canyons, Survey (Cocohaca II) of the Porcupine Bank Canyon, Cruise Report (<http://marinegeology.ucc.ie/wp-content/uploads/sites/87/2018/08/Cruise-Report-CoCoHaCa-II.pdf>).
- Lim, A., Wheeler, A., Price, D., O'Reilly, L., Harris, K., Conti, L., 2020. Influence of benthic currents on cold-water coral habitats: A combined benthic monitoring and 3d photogrammetric investigation. *Sci. Rep.* 10, 19433. <https://doi.org/10.1038/s41598-020-76446-y>.
- Linke, P., Lutze, G.F., 1993. Microhabitat preferences of benthic foraminifera—a static concept or a dynamic adaptation to optimize food acquisition? *Mar. Micropaleontol.* 20, 215–234. [https://doi.org/10.1016/0377-8398\(93\)90034-U](https://doi.org/10.1016/0377-8398(93)90034-U).
- Lipps, J.H., Valentine, J.W., 1970. The role of foraminifera in the trophic structure of marine communities. *Lethaia* 3, 279–286. <https://doi.org/10.1111/j.1502-3931.1970.tb01271.x>.
- López Correa, M., Montagna, P., Joseph, N., Rüggeberg, A., Fietzke, J., Flögel, S., Dorschel, B., Goldstein, S.L., Wheeler, A.J., Freiwald, A., 2012. Preboreal onset of cold-water coral growth beyond the Arctic circle revealed by coupled radiocarbon and U-series dating and neodymium isotopes. *Quat. Sci. Rev.* 34, 24–43. <https://doi.org/10.1016/j.quascirev.2011.12.005>.
- Loubere, P.W., 1991. Deep sea benthic foraminiferal assemblage response to a Surface Ocean productivity gradient: a test. *Paleoceanography* 6, 193–204. <https://doi.org/10.1029/90PA02612>.
- Loubere, P.W., 1998. The impact of seasonality on the benthos as reflected in the assemblages of deep-sea foraminifera. *Deep-Sea Res. I Oceanogr. Res. Pap.* 45, 409–432. [https://doi.org/10.1016/S0967-0637\(97\)00092-7](https://doi.org/10.1016/S0967-0637(97)00092-7).
- Lutze, G.F., Thiel, H., 1989. Epibenthic foraminifera from elevated microhabitats; Cibicidoides Wuellerstorfi and Planulina Ariminensis. *J. Foraminif. Res.* 19, 153–158. <https://doi.org/10.2113/gsfjr.19.2.153>.
- Mackensen, A., Sejrup, H.P., Jansen, E., 1985. The distribution of living benthic foraminifera on the continental slope and rise off Southwest Norway. *Mar. Micropaleontol.* 9, 275–306. [https://doi.org/10.1016/0377-8398\(85\)90001-5](https://doi.org/10.1016/0377-8398(85)90001-5).



- Mackensen, A., Schmiedl, G., Harloff, J., Giese, M., 1995. Deep-sea foraminifera in the South Atlantic Ocean; ecology and assemblage generation. *Micropaleontology* 41, 342–358. <https://doi.org/10.2307/1485808>.
- Margreth, S., 2010. *Benthic Foraminifera Associated to Cold-Water Coral Ecosystems*. PhD. University of Fribourg, Switzerland.
- Margreth, S., Rüggeberg, A., Spezzaferri, S., 2009. Benthic foraminifera as bioindicator for cold-water coral reef ecosystems along the Irish margin. *Deep-Sea Res. I Oceanogr. Res. Pap.* 56, 2216–2234. <https://doi.org/10.1016/j.dsr.2009.07.009>.
- Margreth, S., Gennari, G., Rüggeberg, A., Comas, M., Pinheiro, L.C., Spezzaferri, S., 2011. Growth and demise of cold-water coral ecosystems on mud volcanoes in the west Alboran Sea: the messages from the planktonic and benthic foraminifera. *Mar. Geol.* 282, 26–39. <https://doi.org/10.1016/j.margeo.2011.02.006>.
- Martins, V.A., Jouanneau, J.M., Weber, O., Rocha, F., 2006. Tracing the Late Holocene evolution of the NW Iberian upwelling system. *Mar. Micropaleontol.* 59, 35–55. <https://doi.org/10.1016/j.marmicro.2005.12.002>.
- Matero, I.S.O., Gregoire, L.J., Ivanovic, R.F., Tindall, J.C., Haywood, A.M., 2017. The 8.2 Ka cooling event caused by Laurentide ice saddle collapse. *Earth Planet. Sci. Lett.* 473, 205–214. <https://doi.org/10.1016/j.epsl.2017.06.011>.
- Mazzini, A., Akhmetzhanov, A., Monteys, X., Ivanov, M., 2011. The porcupine Bank canyon coral mounds: oceanographic and topographic steering of deep-water carbonate mound development and associated phosphatic deposition. *Geo-Mar. Lett.* 32, 205–225. <https://doi.org/10.1007/s00367-011-0257-8>.
- Mcardle, B., Anderson, M.J., 2001. Fitting multivariate models to community data: a comment on distance based redundancy analysis. *Ecology* 82, 290–297. [https://doi.org/10.1890/0012-9658\(2001\)082%5B0290:FMMTCD%5D2.0.CO;2](https://doi.org/10.1890/0012-9658(2001)082%5B0290:FMMTCD%5D2.0.CO;2).
- McCave, N., Andrews, J., 2019. Distinguishing current effects in sediments delivered to the ocean by ice. II. Glacial to Holocene changes in high latitude north atlantic upper ocean flows. *Quat. Sci. Rev.* 223, 105902.
- Mccave, I.N., Manighetti, B., Robinson, S.G., 1995. Sortable silt and fine sediments size/composition slicing: parameters for Paleocurrent speed and paleoceanography. *Paleoceanography* 10, 593–610. <https://doi.org/10.1029/94PA03039>.
- Mienis, F., Van Weering, T.C.E., De Haas, H., De Stigter, H.C., Huvenne, V., Wheeler, A. J., 2006. Carbonate mound development at the Sw Rockall trough margin based on high resolution Tobi and seismic recording. *Mar. Geol.* 233, 1–19. <https://doi.org/10.1016/j.margeo.2006.08.003>.
- Mienis, F., De Stigter, H.C., White, M., Duineveld, G., De Haas, H., Van Weering, T.C.E., 2007. Hydrodynamic controls on cold-water coral growth and carbonate-mound development at the Sw and se Rockall trough margin, ne Atlantic Ocean. *Deep-Sea Res. I Oceanogr. Res. Pap.* 54, 1655–1674. <https://doi.org/10.1016/j.dsr.2007.05.013>.
- Mienis, F., Van Der Land, C., De Stigter, H.C., Van De Vorstenbosch, M., De Haas, H., Richter, T.O., Van Weering, T.C.E., 2009. Sediment accumulation on a cold-water carbonate mound at the southwest Rockall trough margin. *Mar. Geol.* 265, 40–50. <https://doi.org/10.1016/j.margeo.2009.06.014>.
- Mienis, F., Duineveld, G., Davies, A.J., Lavaley, M.S.S., Ross, S.W., Seim, H., Bane, J.M., Haren, H.V., Bergman, M.J.N., Haas, H.D., Brooke, S.D., Weering, T.C.E.V., 2013. Cold-water coral growth under extreme environmental conditions, the Cape Lookout area, Nw Atlantic. *Biogeosciences* 11, 2543–2560. <https://doi.org/10.5194/bg-11-2543-2014>.
- Mohn, C., Rengstorf, A., White, M., Duineveld, G., Mienis, F., Soetaert, K., Grehan, A., 2014. Linking benthic hydrodynamics and cold-water coral occurrences: a high-resolution model study at three cold-water coral provinces in the Ne Atlantic. *Prog. Oceanogr.* 122, 92–104. <https://doi.org/10.1016/j.pocean.2013.12.003>.
- Mojtahid, M., Schweizer, M., Douarin, M., Gabriel, J., Colin, C., Tisnérat-Laborde, N., Elliot, M., 2021. From glacial times to Late Holocene: benthic foraminiferal assemblages from cold water coral habitats off Northwest Scotland. *Mar. Geol.* 440, 106581 <https://doi.org/10.1016/j.margeo.2021.106581>.
- Morigi, C., Jorissen, F.J., Gervais, A., Guichard, S., Borsetti, A.M., 2001. Benthic foraminiferal faunas in surface sediments off ne Africa: relationship with organic flux to the ocean floor. *J. Foraminifer. Res.* 31, 350–368. <https://doi.org/10.2113/0310350>.
- Morigi, C., Sabbatini, A., Vitale, G., Pancotti, I., Gooday, A.J., Duineveld, G., Stigter, H.C.D., Danovaro, R., Negri, A., 2012. Foraminiferal biodiversity associated with cold-water coral carbonate mounds and open slope of se Rockall Bank (Irish continental margin ne Atlantic). *Deep-Sea Res. I Oceanogr. Res. Pap.* 59, 54–71. <https://doi.org/10.1016/j.dsr.2011.10.004>.
- Morrill, C., Anderson, D.M., Bauer, B.A., Buckner, R., Gille, E.P., Gross, W.S., Hartman, M., Shah, A., 2013. Proxy benchmarks for Intercomparison of 8.2 Ka simulations. *Clim. Past* 9, 423–432. <https://doi.org/10.5194/cp-9-423-2013>.
- Morris, K.J., Tyler, P.A., Masson, D.G., Huvenne, V., a. I. & Rogers, A., 2013. Distribution of cold-water corals in the Whittard canyon, Ne Atlantic Ocean. *Deep-Sea Res. Part II* 92, 136–144. <https://doi.org/10.1016/j.dsr2.2013.03.036>.
- Mueller, C., Larsson, A.I., Veuger, B., Middelburg, J., Van Oevelen, D., 2014. Opportunistic feeding on various organic food sources by the cold-water coral *Lophelia Pertusa*. *Biogeosciences* 11, 123–133. <https://doi.org/10.5194/bg-11-123-2014>.
- Murray, J.W., 2006a. *Ecology and Applications of Benthic Foraminifera*. Cambridge University Press.
- Murray, J.W., 2006b. *Ecology and Applications of Benthic Foraminifera*.
- Oksanen, J., Guillaume Blanchet, F.G., Friendly, M., Kindt, R., Legendre, P., Mcglinn, D., Minchin, P.R., O'Hara, R.B., Simpson, G.L., Solyomos, P., Stevens, H.H., Szoecs, E., Wagner, H., 2020. Package Version 2.5–7. <https://CRAN.R-project.org/packege=vegan>.
- Oliveira, A., Santos, A., Rodrigues, A., Vitorino, J., 2007. Sedimentary particle distribution and dynamics on the Nazaré canyon system and adjacent shelf (Portugal). *Mar. Geol.* 246, 105–122. <https://doi.org/10.1016/j.margeo.2007.04.017>.
- de Oliveira, L.M., Lim, A., Conti, L.A., Wheeler, A.J., 2021. 3D classification of cold-water coral reefs: A comparison of classification techniques for 3D reconstructions of cold-water coral reefs and seabed. *Front. Mar. Sci.* <https://doi.org/10.3389/fmars.2021.640713>.
- O'Reilly, B., Readman, P.W., Shannon, P.M., 2004. Cold water coral mounds: evidence for Early Holocene climate change and slope failure. *Geophys. Res. Lett.* 31 <https://doi.org/10.1029/2003GL018619>.
- O'Reilly, L., Lim, A., Titschack, J., Moore, N., O'Connor, O.J., Appah, J., Fentimen, R., Butschek, F., Harris, K., Venemenn, T., Wheeler, A., 2022. Using Novel Methods to Track British and Irish Ice Sheet Dynamics since the Late Pleistocene, Along the West Porcupine Bank, NE Atlantic. *Quaternary Science Reviews.* <https://doi.org/10.1016/j.quascirev.2022.107463>.
- Øvrebø, L.K., Haughton, P.D.W., Shannon, P.M., 2006. A record of fluctuating bottom currents on the slopes west of the porcupine Bank, offshore Ireland; implications for Late Quaternary climate forcing. *Mar. Geol.* 225, 279–309. <https://doi.org/10.1016/j.margeo.2005.06.034>.
- Palanques, A., Garcia-Ladona, E., Gomis, D., Martín, J., Marcos, M., Pascual, A., Puig, P., Gili, J.M., Emelianov, M., Monserrat, S., Guillén, J., Tintoré, J., Segura, M., Jordi, A., Ruiz, S., Basterretxea, G., Font, J., Blasco, D., Pagés, F., 2005. General patterns of circulation, sediment fluxes and ecology of the Palamos (La Fonera) submarine canyon, northwestern Mediterranean. *Prog. Oceanogr.* 66, 89–119. <https://doi.org/10.1016/j.pocean.2004.07.016>.
- Pirlet, H., Colin, C., Thierens, M., Latruwe, K., Van Rooij, D., Foubert, A., Frank, N., Blamart, D., Huvenne, V.A., Swennen, R., 2011. The importance of the terrigenous fraction within a cold-water coral mound: A case study. *Mar. Geol.* 282, 13–25. <https://doi.org/10.1016/j.margeo.2010.05.008>.
- Phleger, F.B., Soutar, A., 1973. Production of benthic foraminifera in three East Pacific oxygen minima. *Micropaleontology* 19, 110–115. <https://doi.org/10.2307/1484973>.
- Pollard, R.T., Griffiths, M.J., Cunningham, S.A., Read, J.F., Perez, F.F., Rioz, A.F., 1996. Vivaldi 1991 - a study of the formation, circulation and ventilation of eastern North Atlantic waters. *Prog. Oceanogr.* 37, 167–192. [https://doi.org/10.1016/S0079-6611\(96\)00008-0](https://doi.org/10.1016/S0079-6611(96)00008-0).
- Pomar, L., 2001. Ecological control of sedimentary accommodation: evolution from a carbonate ramp to rimmed shelf, Upper Miocene, Balearic Islands. *Palaeogeogr. Palaeoclimatol. Palaeoecol.* 175, 249–272. [https://doi.org/10.1016/S0031-0182\(01\)00375-3](https://doi.org/10.1016/S0031-0182(01)00375-3).
- Pratson, L.F., Nittrouer, C.A., Wiberg, P.L., Steckler, M.S., Swenson, J.B., Cacchione, D. A., Karson, J.A., Murray, A.B., Wolinsky, M.A., Gerber, T.P.D., Mullenbach, B.L., Spinelli, G.A., Fulthorpe, C.S., O'Grady, D.B., Parker, G., Driscoll, N., Burger, R.L., Paola, C., Orange, D.L., Field, M.E., Friedrichs, C.T., Fedele, J., 2009. Seascapes Evolution on Clastic Continental Shelves and Slopes.
- Price, D.M., Robert, K., Callaway, A., Lo Lacono, C., Hall, R.A., Huvenne, V., a. I., 2019. Using 3d photogrammetry from Rov video to quantify cold-water coral reef structural complexity and investigate its influence on biodiversity and community assemblage. *Coral Reefs* 38, 1007–1021. <https://doi.org/10.1007/s00338-019-01827-3>.
- Puig, P., Planques, A., Martín, J., 2014. Contemporary sediment-transport processes in submarine canyons. *Annu. Rev. Mar. Sci.* 6, 53–77. <https://doi.org/10.1146/annurev-marine-010213-135037>.
- Quaresma, L., Vitorino, J., Oliveira, A., Silva, J.E., 2007. Evidence of sediment resuspension by nonlinear internal waves on the Western Portuguese mid-shelf. *Mar. Geol.* 246, 123–143. <https://doi.org/10.1016/j.margeo.2007.04.019>.
- Qvale, G., Weering, T.C.E.V., 1985. Relationship of surface sediments and benthic foraminiferal distribution patterns in the Norwegian Channel (northern North Sea). *Mar. Micropaleontol.* 9, 469–488. [https://doi.org/10.1016/0377-8398\(85\)90014-3](https://doi.org/10.1016/0377-8398(85)90014-3).
- Ratmeyer, V., Belling, R., Bergenthal, M., Beuck, L., Brakel, C., Buhmann, S., Dodds, L.A., Dorschel, B., Engemann, G., Foubert, A.T.G., Gault, J., Grehan, A.J., Hayn, C., Jurkiw, A.L., Kahl, G., Kaiser, J., Klar, S., Lutz, M., Noë, S., Papstein, H., Rüggeberg, A., Ruhland, G., Schewe, F., Schmidt, W., Schröder, M., Seiter, C., Truscheit, T., Wienberg, C., 2006. Cruise Report Meteor Leg M61–3 Cork, Ireland - Ponta Delgada, Azores 04.06–21.06.2004. <https://media.suub.uni-bremen.de/bitstream/elib/4103/1/00010679.pdf>.
- Reimer, P.J., Austin, W.E.N., Bard, E., Bayliss, A., Blackwell, P.G., Bronk Ramsey, C., Butzin, M., Cheng, H., Edwards, R.L., Friedrich, M., Grootes, P.M., Guilderson, T.P., Hajdas, I., Heaton, T.J., Hogg, A.G., Hughen, K.A., Kromer, B., Manning, S.W., Muscheler, R., Palmer, J.G., Pearson, C.L., Van Der Plicht, J., Reimer, R.W., Richards, D.A., Scott, E.M., Southon, J.R., Turney, C.S.M., Wacker, L., Adolphi, F., Büntgen, U., Capano, M., Fahrni, S.M., Fogtmann-Schulz, A., Friedrich, R., Köhler, P., Kudsk, S.G.K., Miyake, F., Olsen, J., Reinig, F., Sakamoto, M., Sookdeo, A., Talamo, S., 2020. The Intcal20 northern hemisphere radiocarbon age calibration curve (P 55 Cal Kbp). *Radiocarbon* 62, 725–757. <https://doi.org/10.1017/RDC.2020.41>.
- Roberts, J.M., Wheeler, A.J., Freiwald, A., 2006. Reefs of the deep: the biology and geology of cold-water coral ecosystems. *Science* 312, 543–547. <https://doi.org/10.1126/science.1119861>.
- Roberts, J.M., Long, L.-A.H.D., Hartley, J.P., 2008. Cold-water coral reef frameworks, Megafaunal communities and evidence for coral carbonate mounds on the Hatton Bank, north East Atlantic. *Facies* 54, 297–316. <https://doi.org/10.1007/s10347-008-0140-x>.
- Roberts, J.M., Wheeler, A.J., Cairns, S., Freiwald, A., 2009. *Cold-Water Corals: The Biology and Geology of Deep-Sea Coral Habitats*. Cambridge University Press.

- Rowe, G.T., Polloni, P.T., Haedrich, R.L., 1982. The deep-sea macrobenthos on the continental margin of the Northwest Atlantic Ocean. *Deep-Sea Res. Part A* 29, 257–278. [https://doi.org/10.1016/0198-0149\(82\)90113-3](https://doi.org/10.1016/0198-0149(82)90113-3).
- Rüggeberg, A., Dullo, W.-C., Dorschel, B., Hebbeln, D., 2007. Environmental changes and growth history of a cold-water carbonate mound (propeller mound, porcupine Seabight). *Int. J. Earth Sci.* 96, 57–72. <https://doi.org/10.1007/s00531-005-0504-1>.
- Ryan, J.P., Chavez, F.P., Bellingham, J.G., 2005. Physical-biological coupling in Monterey Bay, California: topographic influences on phytoplankton ecology. *Mar. Ecol. Prog. Ser.* 287, 23–32. <https://doi.org/10.3354/meps287023>.
- Sakai, S., Kano, A., Abe, K., 2009. Origin, glacial-interglacial responses, and controlling factors of a cold-water coral mound in Ne Atlantic. *Paleoceanography* 24. <https://doi.org/10.1029/2008PA001695>.
- Saldías, G.S., Allen, S.E., 2020. The influence of a submarine canyon on the circulation and cross-shore exchanges around an upwelling front. *J. Phys. Oceanogr.* 50, 1677–1698. <https://doi.org/10.1175/JPO-D-19-0130.1>.
- Schiebel, R., Hemleben, C., 2007. *Planktonic Foraminifers in the Modern Ocean*. Springer-Verlag GmbH, Berlin Heidelberg.
- Schlacher, T.A., Williams, A., Althaus, F., Schlacher-Hoenlinger, M.A., 2010. High-resolution seabed imagery as a tool for biodiversity conservation planning on continental margins. *Mar. Ecol.* 31, 200–221. <https://doi.org/10.1111/j.1439-0485.2009.00286.x>.
- Schmidl, G., Bovée, F.D., Buscail, R., Charrière, B., Hemleben, C., Medernach, L., Picon, P., 2000. Trophic control of benthic foraminiferal abundance and microhabitat in the bathyal gulf of lions, Western Mediterranean Sea. *Mar. Micropaleontol.* 40, 167–188. [https://doi.org/10.1016/S0377-8398\(00\)00038-4](https://doi.org/10.1016/S0377-8398(00)00038-4).
- Schnitker, D., 1980. Quaternary deep-sea benthic foraminifers and bottom water masses. *Annu. Rev. Earth Planet. Sci.* 8, 343–370. <https://doi.org/10.1146/annurev.ea.08.050180.002015>.
- Schönfeld, J., 1997. The impact of the Mediterranean outflow water (mow) on benthic foraminiferal assemblages and surface sediments at the southern Portuguese continental margin. *Mar. Micropaleontol.* 29, 211–236. [https://doi.org/10.1016/S0377-8398\(96\)00050-3](https://doi.org/10.1016/S0377-8398(96)00050-3).
- Schönfeld, J., 2002a. A new benthic foraminiferal proxy for near-bottom current velocities in the Gulf of Cadiz, northeastern Atlantic Ocean. *Deep-Sea Res. Part I* 49, 1853–1875. [https://doi.org/10.1016/S0967-0637\(02\)00088-2](https://doi.org/10.1016/S0967-0637(02)00088-2).
- Schönfeld, J., 2002b. Recent benthic foraminiferal assemblages in deep high-energy environments from the Gulf of Cadiz (Spain). *Mar. Micropaleontol.* 44, 141–162. [https://doi.org/10.1016/S0377-8398\(01\)00039-1](https://doi.org/10.1016/S0377-8398(01)00039-1).
- Schönfeld, J., Dullo, W.C., Pfannkuche, O., Freiwald, A., Rüggeberg, A., Schmidt, S., Weston, J.F., 2011. Recent benthic foraminiferal assemblages from cold-water coral mounds in the porcupine Seabight. *Facies* 57, 187–213. <https://doi.org/10.1007/s10347-010-0234-0>.
- Sejrup, H.P., Fjæran, T., Hald, M., Beck, L., Hagen, J., Miljeteig, I., Morvik, I., Norvik, O., 1981. Benthonic foraminifera in surface samples from the Norwegian continental margin between 62 degrees N and 65 degrees N. *J. Foraminif. Res.* 11, 277–295. <https://doi.org/10.2113/gsjfr.11.4.277>.
- Shannon, P.M., 1991. The development of Irish offshore sedimentary basins. *J. Geol. Soc. Lond.* 148, 181–189. <https://doi.org/10.1144/gsjgs.148.1.0181>.
- Shannon, P.M., McDonnell, A., Bailey, W.R., 2007. The evolution of the porcupine and Rockall basins, offshore Ireland: the geological template for carbonate mound development. *Int. J. Earth Sci.* 96, 21–35. <https://doi.org/10.1007/s00531-006-0081-y>.
- She, J., Klinck, J.M., 2000. Flow near submarine canyons driven by constant winds. *J. Geophys. Res.* 105, 28671–28694. <https://doi.org/10.1029/2000JC990126>.
- Shepard, F.P., 1981. Submarine canyons: multiple causes and Long-time persistence. *AAPG Bull.* 65, 1062–1077. <https://doi.org/10.1306/03B59459-16D1-11D7-8645000102C1865D>.
- Shepard, F.P., Marshall, N.F., Mcloughlin, P.A., 1974. "Internal waves" advancing along submarine canyons. *Science* 183, 195–198. <https://doi.org/10.1126/science.183.4121.195>.
- Singh, D.P., Saraswat, R., Nigam, R., 2021. Untangling the effect of organic matter and dissolved oxygen on living benthic foraminifera in the southeastern Arabian Sea. *Mar. Pollut. Bull.* 172, 112883. <https://doi.org/10.1016/j.marpolbul.2021.112883>.
- Smeulders, G., Koho, K.A., Stigter, H.C.D., Mienis, F., Haas, H.D., Weering, T.C.E.V., 2014. Cold-water coral habitats of Rockall and porcupine Bank, ne Atlantic Ocean: sedimentary Facies and benthic foraminiferal assemblages. *Deep-Sea Res. Part II* 99, 270–285. <https://doi.org/10.1016/j.dsr2.2013.10.001>.
- Spezzaferri, S., Coric, S., 2001. Ecology of Karpatian (Early Miocene) foraminifers and calcareous Nannoplankton from Laa an Der Thaya, Lower Austria: a statistical approach. *Geol. Carpath.* 52, 361–374.
- Spezzaferri, S., Rüggeberg, A., Stalder, C., Margreth, S., 2013. Benthic foraminifer assemblages from Norwegian cold-water coral reefs. *J. Foraminif. Res.* 43, 21–39. <https://doi.org/10.2113/gsjfr.43.1.21>.
- Spezzaferri, S., Rüggeberg, A., Stalder, C., 2015. *Atlas of Benthic Foraminifera from Cold-Water Coral Reefs*. Cushman Foundation for Foraminiferal Research Special Publication.
- Spötl, C., Venemann, T., 2003. Continuous-flow isotope ratio mass spectrometric analysis of carbonate minerals. *Rapid Commun. Mass Spectr.* 17, 1004–1006. <https://doi.org/10.1002/rcm.1010>.
- Stalder, C., Spezzaferri, S., Rüggeberg, A., Pirkenseer, C., Gennari, G., 2014. Late Weichselian deglaciation and Early Holocene development of a cold-water coral reef along the Lophhavet shelf (northern Norway) recorded by benthic foraminifera and Ostracoda. *Deep-Sea Res. II Top. Stud. Oceanogr.* 99, 249–269. <https://doi.org/10.1016/j.dsr2.2013.07.009>.
- Stalder, C., Vertino, A., Rosso, A., Rüggeberg, A., Pirkenseer, C., Spangenberg, J.E., Spezzaferri, S., Camozzi, O., Rappo, S., Hajdas, I., 2015. Microfossils, a key to unravel cold-water carbonate mound evolution through time: evidence from the eastern Alboran Sea. *PLoS One* 10, e0140223. <https://doi.org/10.1371/journal.pone.0140223>.
- Stalder, C., Kateb, A.E., Vertino, A., Rüggeberg, A., Camozzi, O., Pirkenseer, C.M., Spangenberg, J.E., Hajdas, I., Rooij, D.V., Spezzaferri, S., 2018. Large-scale paleoceanographic variations in the Western Mediterranean Sea during the last 34,000 years: from enhanced cold-water coral growth to declining mounds. *Mar. Micropaleontol.* 143, 46–62. <https://doi.org/10.1016/j.marmicro.2018.07.007>.
- Stalling, D., Westerhoff, M., Hege, H.-C., 2005. Version 2018.36. <http://amira.zib.de>.
- Stewart, H.A., Davies, J.S., Guinan, J., Howell, K.L., 2014. The Dangeard and explorer canyons, South Western approaches UK: geology, sedimentology and newly discovered cold-water coral mini-mounds. *Deep-Sea Res. II Top. Stud. Oceanogr.* 104, 230–244. <https://doi.org/10.1016/j.dsr2.2013.08.018>.
- Streeter, S.S., Shackleton, N.J., 1979. Paleocirculation of the deep North Atlantic: 150,000-year record of benthic foraminifera and oxygen-18. *Science* 203, 168–171. <https://doi.org/10.1126/science.203.4376.168>.
- Suhr, S.B., Pond, D.W., Gooday, A.J., Smith, C.R., 2003. Selective feeding by benthic foraminifera on phytodetritus on the Western Antarctic peninsula shelf: evidence from fatty acid biomarker analysis. *Mar. Ecol. Prog. Ser.* 262, 153–162. <https://doi.org/10.3354/meps262153>.
- Team, R.C., 2021. <https://www.R-project.org/>.
- Thierens, M., Browning, E.L., Prilet, H., Loutre, M.-F., Dorschel, B., Huvenne, V., Titschack, J., Colin, C., Foubert, A.T.G., Wheeler, A.J., 2013. Cold-water coral carbonate mounds as unique palaeo-archives: the Plio-Pleistocene challenger mound record (ne Atlantic). *Quat. Sci. Rev.* 73, 14–30. <https://doi.org/10.1016/j.quascirev.2013.05.006>.
- Thomas, E.R., Wolff, E.W., Mulvaney, R., Steffensen, J.P., Johnsen, S.S.J., Arrowsmith, C., White, J.W.C., Vaughn, B.H., Popp, T.J., 2007. The 8.2 Ka event from Greenland ice cores. *Quat. Sci. Rev.* 26, 70–81. <https://doi.org/10.1016/j.quascirev.2006.07.017>.
- Titschack, J., Thierens, M., Dorschel, B., Schulbert, C., Freiwald, A., Kano, A., Takashima, C., Kawagoe, N., Li, X., 2009. Carbonate budget of a cold-water coral mound (challenger mound, Iodp Exp. 307). *Mar. Geol.* 259, 36–46. <https://doi.org/10.1016/j.margeo.2008.12.007>.
- Titschack, J., Baum, D., De Pol-Holz, R., López Correa, M., Forster, N., Flögel, S., Hebbeln, D., Freiwald, A., 2015. Aggradation and carbonate accumulation of Holocene Norwegian cold-water coral reefs. *Sedimentology* 62, 1873–1898. <https://doi.org/10.1111/sed.12206>.
- Titschack, J., Fink, H.G., Baum, D., Wienberg, C., Hebbeln, D., Freiwald, A., 2016. Mediterranean cold-water corals – an important regional carbonate factory? *Deposit. Rec.* 2, 74–96. <https://doi.org/10.1002/dep2.14>.
- Van Den Beld, I.M.J., Bourillet, J.F., Arnaud-Haond, S., De Chambure, L., Davies, J.S., Guillaumont, B., Olu, K., Menot, L., 2017. Cold-water coral habitats in submarine canyons of the Bay of Biscay. *Front. Mar. Sci.* 4, 1–30. <https://doi.org/10.3389/fmars.2017.00118>.
- Van Der Zwaan, G.J., 1982. *Paleoecology of Late Miocene Mediterranean Foraminifera*. PhD. University Utrecht.
- Vetter, E.W., Smith, C.R., Léo, F.C.D., 2010. Hawaiian hotspots: enhanced Megafaunal abundance and diversity in submarine canyons on the Oceanic Islands of Hawaii. *Mar. Ecol. Prog. Ser.* 413, 183–199. <https://doi.org/10.1111/j.1439-0485.2009.00351.x>.
- Wagner, A.J., Morrill, C., Otto Bliessen, B.L., Rosenbloom, N.A., Watkins, K.R., 2013. Model support for forcing of the 8.2 ka event by meltwater from the Hudson Bay ice dome. *Clim. Dyn.* 41, 2855–2873. <https://doi.org/10.1007/s00382-013-1706-z>.
- Wang, H., Lo Iacono, C., Wienberg, C., Titschack, J., Hebbeln, D., 2019. Cold-water coral mounds in the southern Alboran Sea (Western Mediterranean Sea): internal waves as an important driver for mound formation since the last deglaciation. *Mar. Geol.* 412, 1–18. <https://doi.org/10.1016/j.margeo.2019.02.007>.
- Wang, H., Titschack, J., Wienberg, C., Korpanty, C.A., Hebbeln, D., 2021. The importance of ecological accommodation space and sediment supply for cold-water coral mound formation, a case study from the Western Mediterranean Sea. *Front. Mar. Sci.* 8. <https://doi.org/10.3389/fmars.2021.760909>.
- Wheeler, A.J., Beyer, A., Freiwald, A., De Haas, H., Huvenne, V., Kozachenko, M., Olu-Le Roy, K., Opderbecke, J., 2007. Morphology and environment of cold-water coral carbonate mounds on the Nw European margin. *Int. J. Earth Sci.* 96, 37–56. <https://doi.org/10.1007/s00531-006-0130-6>.
- Wheeler, A., Lim, A., Peters, J., Sacchetti, F., Mcgrath, M., Browne, M., El Kateb, A., Ní Fhaoiláin, F., Renken, S., Schiele, K., Vertino, A., Officers & Crew of the Rv Celtic Explorer, 2014. West of Ireland coring Programme (Wicpro). In: *Rv Celtic Explorer. Cork – Killybegs. 6th March to 18th March 2014*. <https://www.ucc.ie/en/media/research/marinegeo/mgpdfs/WICPro-Cruise-Report-CE14014.pdf>.
- Wheeler, A.J., Capocci, R., Crippa, L., Connolly, N., Hogan, R., Lim, A., McCarthy, E., Mconigle, C., O'Donnell, E., O'Sullivan, K., Power, K., Ryan, G., Vertino, A., Holland I Rov Technical Team & Officers and Crew of the Rv Celtic Explorer, 2015. *Cruise Report: Quantifying Environmental Controls on Cold-Water Coral Reef Growth (Querci)*. [https://www.ucc.ie/en/media/research/marinegeo/mgpdfs/CruiseReport\\_QuERCi\\_FINAL.pdf](https://www.ucc.ie/en/media/research/marinegeo/mgpdfs/CruiseReport_QuERCi_FINAL.pdf).
- Wheeler, A., Connolly, N., Conti, L., Hogan, R., Lim, A., Massironi, C., Mullins, M., Murphy, P., Pinfield, R., Power, K., Toth, Z., Holland I Rov Technical Team & the Officers and Crew of the Rv Celtic Explorer, 2016. *Quantifying Environmental Controls on Cold-Water Coral Reef Growth: Part 2 file:///C:/Users/Kimberley/Downloads/CruiseReport\_QuERCi\_Final.pdf*.
- Wheeler, A., Burke, S., Griffin, B., Lim, A., Ní Fhaoiláin, F., O'Reilly, L., Summers, G., Holland I Rov Technical Team, Officers and Crew of the Rv Celtic Explorer, 2017. *Controls of Cold-Water Coral Habitats in Submarine Canyons (Cocohaca)*. [https://www.ucc.ie/en/media/research/marinegeo/mgpdfs/Cruise-Report\\_Final\\_CoCohaca.pdf](https://www.ucc.ie/en/media/research/marinegeo/mgpdfs/Cruise-Report_Final_CoCohaca.pdf).

- Wheeler, A., Lim, A., Butschek, F., O'Reilly, L., O'Driscoll, P., 2021. The "little MonSta" deep-sea benthic, precision deployable, multi-sensor and sampling lander array. *Sensors* 21, 3355. <https://doi.org/10.3390/s21103355>.
- White, M., 2007. Benthic dynamics at the carbonate mound regions of the Porcupine Sea bight continental margin. *Int. J. Earth Sci.* 96, 1–9. <https://doi.org/10.1007/s00531-006-0099-1>.
- White, M., Bowyer, P., 1997. The shelf-edge current north-west of Ireland. *Ann. Geophys.* 15, 1076–1083. <https://doi.org/10.1007/s00585-997-1076-0>.
- Wienberg, C., Wintersteller, P., Beuck, L., Hebbeln, D., 2013. Coral patch seamount (ne Atlantic) – a sedimentological and megafaunal reconnaissance based on video and hydroacoustic surveys. *Biogeosciences* 10, 3421–3443. <https://doi.org/10.5194/bg-10-3421-2013>.
- Wienberg, C., Titschack, J., Freiwald, A., Frank, N., Lundälv, T., Taviani, M., Beuck, L., Schröder-Ritzrau, A., Krenzel, T., Hebbeln, D., 2018. The Giant Mauritanian cold-water coral Mound Province: oxygen control on coral mound formation. *Quat. Sci. Rev.* 185, 135–152. <https://doi.org/10.1016/j.quascirev.2018.02.012>.
- Wienberg, C., Titschack, J., Frank, N., Pol-Holz, R.D., Fietzke, J., Eisele, M., Kremer, A., Hebbeln, D., 2020. Deglacial upslope shift of ne Atlantic intermediate waters controlled slope Erosion and cold-water coral mound formation (porcupine Seabight, Irish margin). *Quat. Sci. Rev.* 237, 106310 <https://doi.org/10.1016/j.quascirev.2020.106310>.
- Williamson, M.A., Keen, C.E., Mudie, P.J., 1984. Foraminiferal distribution on the continental margin off Nova Scotia. *Mar. Micropaleontol.* 9, 219–239. [https://doi.org/10.1016/0377-8398\(84\)90014-8](https://doi.org/10.1016/0377-8398(84)90014-8).
- Wilson, A.M., Raine, R., Mohn, C., White, M., 2015. Nepheloid layer distribution in the Whittard canyon, Ne Atlantic margin. *Mar. Geol.* 367, 130–142. <https://doi.org/10.1016/j.margeo.2015.06.002>.
- Woodruff, F., Douglas, R.G., 1981. Response of deep-sea benthic foraminifera to miocene paleoclimatic events, Dsdp site 289. *Mar. Micropaleontol.* 6, 617–632. [https://doi.org/10.1016/0377-8398\(81\)90024-4](https://doi.org/10.1016/0377-8398(81)90024-4).

### Further readings

- Gooday, A.J., 1986. Meiofaunal Foraminiferans from the bathyal porcupine Seabight (Northeast Atlantic): size structure, standing stock, taxonomic composition, species diversity and vertical distribution in the sediment. *Deep-Sea Res Part A* 33, 1345–1373. [https://doi.org/10.1016/0198-0149\(86\)90040-3](https://doi.org/10.1016/0198-0149(86)90040-3).
- Jorissen, F.J., Fontanier, C., Thomas, E., Hillaire-Marcel, C., De Vernal, A., 2007. Paleooceanographical proxies based on deep-sea benthic foraminiferal assemblage characteristics. In: *Proxies in Late Cenozoic Paleooceanography*. Elsevier.
- Lutze, G.F., Coulbourn, W.T., 1984. Recent benthic foraminifera from the continental margin of Northwest Africa: community structure and distribution. *Mar. Micropaleontol.* 8, 361–401. [https://doi.org/10.1016/0377-8398\(84\)90002-1](https://doi.org/10.1016/0377-8398(84)90002-1).
- Schlacher, T.A., Schlacher-Hoenlinger, M.A., Williams, A., Althaus, F., Hooper, J.N.A., Kloser, R.J., 2007. Richness and distribution of sponge Megabenthos in continental margin canyons off southeastern Australia. *Mar. Ecol. Prog. Ser.* 340, 73–88. <https://doi.org/10.3354/meps340073>.
- Thornalley, D.J.R., Elderfield, H., Mccave, I.N., 2009. Holocene oscillations in temperature and salinity of the surface subpolar North Atlantic. *Nature* 457, 711–714. <https://doi.org/10.1038/nature07717>.
- Voelker, A.H.L., Salgueiro, E., Rodrigues, T., Jiménez-Espejo, F.J., Bahr, A., Alberto, A., Loureiro, I.M., Padilha, M., Rebotim, A., Röhl, U., 2015. Mediterranean outflow and surface water variability off southern Portugal during the Early Pleistocene: a snapshot at marine isotope stages 29 to 34 (1020–1135 Ka). *Glob. Planet. Chang.* 133, 223–237. <https://doi.org/10.1016/j.gloplacha.2015.08.015>.